

WASM: Minerals, Energy, and Chemical Engineering

**Numerical Simulation Study of Wettability Impact on
Injectivity Remediation and Storage Capacity
in Underground CO₂ Storage**

Egi Adrian Pratama

0000-0002-6529-9715

This thesis is presented for the Degree of

Master of Philosophy

of

Curtin University

January 2024

Declaration

To the best of my knowledge and belief, this thesis contains no material previously published by any other person except where due acknowledgement has been made.

This thesis contains no material which has been accepted for the award of any other degree or diploma in any university.

Signature :(Egi Adrian Pratama)

Date: 10th January 2024

Acknowledgement

First and foremost, my praise goes to Allah Swt., the Greatest God who makes everything easier for me conducting this Master of Philosophy Research. I am grateful to Him for the good health and wellbeing that were essential to complete this thesis. I would also like to thank my thesis advisor, Associate Prof. Ali Saeedi. The door to his office was always open whenever I was stuck with the analysis or had a question regarding this work. He consistently allowed this paper to be my original work, though steered me in the right direction whenever he thought I needed it. My great appreciation is also directed to Dr. Matthew Myers as my co-supervisor. He has made a lot of efforts to improve the analysis of my research and upgrade my writing task to be published in a reputable journal. Thankfulness should also go to Prof. Reza Rezaee and all faculty staffs in Department of Petroleum Engineering, Curtin University for the whole insight they gave during my milestone presentations.

I could not have undertaken this journey without a full scholarship from the Indonesia's Endowment Fund for Education (read: *Lembaga Pengelola Dana Pendidikan*). I owe that much to Indonesian society and the Government of Indonesia that has been actively sending the young generation for study abroad in order to develop Indonesia in the future.

Finally, I must express my very profound gratitude to my parents and to my spouse and little kid for providing me with unfailing support and continuous encouragement throughout my years of study and through the process of researching and writing this thesis. This accomplishment would not have been possible without them. My time with my two princesses, Ezi and Hafla, was frequently sacrificed during the study duration. They never showed their disappointment. However, I do understand that they felt uncomfortable sometime. They deserve for the delight I reach through this accomplishment and the future greater time with me. Special thanks to Prof. Asep Kurnia Permadi and Dr. Andri Luthfi for the intangible support. I'd also like to recognize Iqro Center and other friends from Indonesian community in Perth, and Perth City Musallah Assoc. Inc. which I cannot write each of their name in this short page. Thank you.

Abstract

Deep saline aquifers are often favourable for underground CO₂ sequestration due to their large capacity and relatively low likelihood of resource conflicts. However, some possible issues can arise during CO₂ injection into aquifers. Often aquifers have a significant salinity level (hence they present minimal resource conflict issues), and as such, salt precipitation near the injection wellbore can be problematic. The salt precipitation can be exacerbated due to large amounts of water remaining trapped near the wellbore due to the water blockage phenomenon. Altering the rock wettability towards less water-wet can alleviate water blockage and, in turn, reduce the likelihood or severity of salt precipitation. Previous lab experiments have shown that supercritical CO₂ (sc-CO₂)-based silylation can effectively functionalise rock surfaces with hydrophobic silanes. The experimental and numerical simulation studies conducted to date have shown that rock wettability also has a strong control over the multiphase flow behaviour (e.g., relative permeability and residual CO₂ trapping) and plume migration in bulk of the storage medium.

In the first phase of this study, numerical models were constructed to evaluate the combined effects of multi-phase fluid flow, water evaporation and salt precipitation, under varying wettability (thus impacting the relative permeability characteristics of the reservoir). The change in wettability is assumed to have been caused by the silylation process reported in the relevant literature. The ultimate aim of this investigation was to evaluate the efficiency of this chemical treatment in addressing the earlier mentioned near-wellbore salt precipitation. As expected, the simulation results indicate that a decrease in injectivity due to salt precipitation is more significant when water blockage is also present. Injectivity deteriorates prominently in high salinity reservoirs since water evaporation into the injected CO₂ will cause significant salt precipitation. In a representative formation, the injectivity decline is worse (up to 68.6 % relative injectivity change (RIC)) when both salt precipitation and water blockage are considered. With hydrophobic silylation, the combined effects of salt precipitation and water blockage on RIC are decreased on an absolute basis by up to 7%. Depending on techno-economic considerations, implementation of this remedial method is encouraged as early as possible during a CO₂ injection program to minimise salt accumulation from the outset.

The second phase of this research evaluated the impact of reservoir rock wettability on the CO₂ storage performance of sandstone reservoirs using numerical simulation. Rock wettability, as an important factor characterising rock-fluid interactions, controls trapping mechanisms and, in turn, the CO₂ storage capacity of an aquifer. To date, limited studies have attempted to evaluate the impact of wettability variation on multiphase flow in a porous media, residual trapping, and storage performance during CO₂ storage, most of which have used

assumed or hypothetical datasets. An important feature of the current work differentiating it from other similar studies is the use of published representative experimental data instead of assumed/hypothetical datasets. In achieving this important objective, a detailed critical review of available literature was conducted to acquire representative values for various parameters of interest. An attempt was made to qualitatively classify the Land trapping coefficient for different wettability states. The findings indicated that a general outcrop sandstone sample composed of mostly quartz (i.e., water-wet), such as Berea and Bentheimer, would show a typical low Land coefficient in a range of 0.7-2. Surprisingly, the trapping coefficient for some limestones also lies in the same range. Other sandstone samples drilled from representative subsurface formations were found to have coefficients slightly larger in the range of 2.8-4.1, characterising mixed-wet rocks. Besides, the fact that mineral composition and grain packing may affect the results has been considered in the current study. In the case of discovering contradictive results in the literature, suitable data were selected after a comprehensive critical review. The final outcomes of the literature review were incorporated into a homogeneous box model for a comparative study of CO₂ storage under varying wettability states. A faster advancing vertical plume migration was seen in the water-wet case resulting in a shorter time for CO₂ to reach the caprock. A less pronounced difference was found in the lateral spreading of the plume around the injection point due to a slight deviation in the relative permeability curvature of each case. Due to less residually trapped CO₂, both intermediate and CO₂ wet cases resulted in a large mobile CO₂ volume reaching the top of the storage medium and spreading over a wider lateral distance under the caprock.

Publication by Author

1. **Pratama, Egi A.**, Matthew Myers, Asep K. Permadi, Ali Saeedi. 2023. “Simulation Study of sc-CO₂ Based Silylation for Decreasing Severity of Water Blockage and Salt Precipitation during Geological CO₂ Storage in Deep Saline Aquifers”. *Transport in Porous Media*, 150, 131–155 (2023). <https://doi.org/10.1007/s11242-023-02002-7>
2. **Pratama, Egi A.**, Matthew Myers, Asep K. Permadi, Ali Saeedi. “Wettability Impacts on Multiphase Flow and Capillary Residual Trapping in Underground CO₂ Storage: Review and Simulations”. Under preparation for a publication.

I have obtained permission from the copyright owners to use any third-party copyright material reproduced in the thesis, or to use any of my own published work in which the copyright is held by another party.

Table of Content

Declaration	i
Acknowledgement	ii
Abstract	iii
Publication by Author	v
Table of Content	vi
List of Figures	viii
List of Tables	xi
Abbreviations/Symbols.....	xii
Chapter 1 Background and Problem Description.....	1
1.1. Introduction	1
1.2. Background and Problem Description.....	1
1.3. Research Objective	2
1.4. Organization of Thesis.....	3
Chapter 2 Literature Review	4
2.1. Introduction	4
2.2. Underground CO ₂ Storage	4
2.2.1. Trapping Mechanisms	6
2.2.2. Containment Efficiency.....	10
2.2.3. Well Injectivity.....	12
2.3. Impact of Rock-Fluid Properties on Underground CO ₂ Storage	17
2.3.1. Porosity.....	17
2.3.2. Absolute and Relative Permeabilities.....	18
2.3.3. Brine Salinity.....	19
2.3.4. Formation Wettability	20
2.3.5. Wettability Alteration.....	22
2.4. Numerical Simulation of CO ₂ Storage in Saline Aquifer	24
2.4.1. Evaluation of Storage Capacity	25
2.4.2. Prediction of Deposited Salt.....	27
Chapter 3 Injectivity Issues Remediation in CO ₂ Geo-sequestration by Implementing Wettability Alteration	29

3.1. Introduction	29
3.2. Numerical Simulation Model	32
3.2.1. Component Transport Equations.....	32
3.2.2. Fluids and Mechanistic Models.....	33
3.2.3. Radial Single Well Model	40
3.3. Results & Discussion.....	42
3.3.1. Scaling-up Well Injectivity Issues Simulation	42
3.3.2. Simulation of Cases Applying Silylation	48
3.4. Conclusions	52
Chapter 4 Wettability Impact on CO ₂ Storage Capacity and Plume Migration.....	54
4.1. Introduction	54
4.2. Multiphase Flow of Gas/Supercritical CO ₂ -Brine System under Different Wettabilities	58
4.3. Capillary Residual Trapping under Different Wettabilities.....	61
4.4. Numerical Simulation.....	65
4.4.1. Aquifer Grid and Multiphase Flow Model.....	65
4.4.2. CO ₂ Trapping Model.....	66
4.4.3. Simulation Results & Discussion	69
4.5. Conclusions	71
Chapter 5 Conclusions, Recommendations, and Future Work	73
5.1. Conclusions	73
5.2. Recommendations and Future Works.....	74
References	76
Appendix A Official Permissions and Copyrights	95
Appendix B Attribution of Co-authors.....	96

List of Figures

Figure 1. Underground CO ₂ storage options (Ali et al., 2022)	5
Figure 2. Gas saturation for case of present and absent of hysteresis model (Nghiem et al., 2009)	7
Figure 3. A typical relative permeability curves indication a hysteresis process from drainage-imbibition process (Burnside & Naylor, 2014).....	8
Figure 4. Illustration of CO ₂ trapping mechanisms depicting the convective flow under CO ₂ dissolution process (Riaz and Cinar, 2014)	9
Figure 5. Brine properties by which CO ₂ is controlled whether stored as ion or mineral (Rackley, 2017).....	9
Figure 6. Schematic of drainage process in which CO ₂ (non-wetting phase) flows through the pores when the capillary pressure exceeds the entry pressure (Hildenbrand et al., 2002)	11
Figure 7. Possible pathways for CO ₂ leakage in response to geomechanics change within formation due to pressure build up and/or seismic activity (Rutqvist, 2012)	12
Figure 8. Productivity index profile under different flow regimes (Ahmed, 2001).....	13
Figure 9. Schematic of salt precipitation and water evaporation within pores during CO ₂ injection (Ott et al., 2015)	15
Figure 10. Concentration of dissolved CO ₂ in pure water (left) and 200 g/l brine (right) derived from model proposed by Duan and Sun (2003) (Gaus et al., 2008)	19
Figure 11. (a) advancing angle when the drop is inflated and (b) receding angle when the drop is deflated (de Gennes et al., 2004).....	21
Figure 12. Illustration of measured contact angle for different wettability characteristics in scCO ₂ -water-mineral system (Iglauer et al., 2015a)	21
Figure 13. Grid model employed in this work representing the core used by Ott et al. (2015)	36
Figure 14. a) Salt concentration yielded from simulation and b) salt saturation in the simulation results (–) compared to that in the experimental results (◊◊) which the data taken from work conducted by Ott et al. (2015).....	36
Figure 15. Pressure difference obtained in the simulation results (–) compared to that in experimental results (●).....	37

Figure 16. Permeability reduction model between reference study (●) which the data taken from work conducted by Ott et al. (2015) and this work (–)	37
Figure 17. Relative permeability of a) the zone affected by water blockage (RT-1) and b) original condition (RT-2).....	38
Figure 18. Relative permeability of pre- (impacted by water blockage, RT-1) and post-treatment of silylation. Modified from results obtained by Arjomand et al. (2020b)	40
Figure 19. Schematic of radial single well model and the rock properties. Colour scale is referred to Fig. 20.	41
Figure 20. Cross-section of radial single well model.....	41
Figure 21. Schematic of zone affected by water blockage where silylation takes place (RT-1; blue coloured zone) and original characteristics (RT-2; red coloured zone)	41
Figure 22. Injection pressure for base case (–), case 1: water blockage exists (–o–), case 2: salt precipitation exists (–□–), and case 3: both issues exist (–Δ–).....	44
Figure 23. Distribution of water saturation at the end of simulation which shown in full scale model for a) case 1: water blockage exists and b) base case	44
Figure 24. Injectivity index for base case (–), case 1: water blockage exists (–o–), case 2: salt precipitation exists (–□–), and case 3: both issues exist (–Δ–).....	45
Figure 25. Distribution of solid saturation for a) Case 2: salt precipitation exists and b) Case 3: water blockage and salt precipitation exist, at the end of simulation.....	46
Figure 26. Resistance factor applied on a) Case 2: salt precipitation exists and b) Case 3: water blockage and salt precipitation exist, at the end of simulation	46
Figure 27. k_{r,CO_2} at the end of simulation of Case 3: water blockage and salt precipitation exist	47
Figure 28. Injection pressure for Case 1: water blockage exists (–o–), Case 3: water blockage and salt precipitation exist (–Δ–), Case 4: silane treats Case 1 (–●–), and Case 5: silane treats Case 3 (–▲–) in the early period.....	48
Figure 29. Injectivity Index for Case 1: water blockage exists (–o–), Case 3: water blockage and salt precipitation exist (–Δ–), Case 4: silane treats Case 1 (–●–), and Case 5: silane treats Case 3 (–▲–).....	49

Figure 30. Distribution of salt precipitation in (a) case 3: water blockage and salt precipitation exist, at day 90, (b) case 5: silane treats Case 3, at day 90, and (c) case 3 and (d) case 5 at the end of simulation	50
Figure 31. Solid saturation profiles at the middle of perforation after 90 days of injection forecast.....	50
Figure 32. Schematic of injection pressure in case of salt precipitation and water blockage taking place at the same system	52
Figure 33. Schematic of injection pressure in case of sc-CO ₂ based silylation depressing negative impact of salt precipitation and water blockage	52
Figure 34. Typical initial-residual (IR) saturation relationship of non-wetting phase (S_{nwi} vs S_{nwr}) plot showing different C-constants from Land's (1968) empirical model ..	57
Figure 35. Irreducible water saturation (S_{wir}) summary for generated case study on wettability states.....	61
Figure 36. Initial-residual (IR) saturation relationship of non-wetting phase (S_{nwi} vs S_{nwr}) after classification based on wettability states, i.e., strong water-wet (— and ■) and less water-wet (— and ■). Variable “C” refers to trapping coefficient in Land's (1968) empirical model.	63
Figure 37. Aquifer model geometry and injection well location	66
Figure 38. Illustration of residual trapping occurring in a relative permeability vs. brine saturation (k_r vs. S_w) curve in both drainage (-●-) and imbibition (—) processes.	68
Figure 39. Plume migration for all case studies in 10 years of injection, end of injection (year 25), and 80 years of storage. Red arrows assist the comparison of lateral and vertical plume movement. White arrows with dashed line indicate the furthest plume position.....	70
Figure 40. CO ₂ storage capacities in percentage presenting each trapping mechanisms for all wettability case study	71
Figure 41. CO ₂ molality in the aqueous phase after 80 years of storage.	71

List of Tables

Table 1. Parameters used in the simulation describing the salt precipitation modeling based on the experiment conducted by Ott et al. (2015)	35
Table 2. Basic properties of silane reagent used in the experiment performed by Arjomand et al. (2020a).....	39
Table 3. The properties of Core GB.4 used in the experiment performed by Arjomand et al. (2020b)	39
Table 4. <i>Details of case studies developed in this study.</i>	42
Table 5. Summary of relative injectivity change for all studied cases.....	51
Table 6. Core samples properties being compared and endpoints of drainage coreflooding results.....	59
Table 7. Rock typing of original cores from compared studies by using hydraulic flow unit method (Amaefule et al., 1993)	59
Table 8. Sigmund & McCaffery's relative permeability model for each case study	66

Abbreviations/Symbols

A	Cross-sectional area
B	Fluid formation volume factor
C	Land trapping coefficient
Ca ²⁺	Calcium ion
CCS	Carbon, Capture, and Storage
CCUS	Carbon, Capture, Utilisation, and Storage
cm ³	Cubic centimetre
CO ₂	Carbon dioxide
CO ₃ ²⁻	Carbonate ion
CPTS	(3-chloropropyl)triethoxysilane
c _{H₂O,e/H₂O}	Concentration factor of H ₂ O at equilibrium/anytime in CO ₂ phase
c _{salt,max}	Maximum salt precipitation within the pore volume
c _{sil/salt}	The moles of adsorbed silane/salt within the pore volume
DECC	Department of Energy & Climate Change
DMAPTS	N,N-dimethylaminopropyl)trimethoxysilane
EGR	Enhanced Gas Recovery
EOR	Enhanced Oil Recovery
Fe ³⁺	Ferrum ion
f	Specific factor for evaporation rate constant Fluid fugacity
ft	feet
f _w	fractional flow of water/brine
g	Gravity constant
GB	Grey Berea Sandstone
Gt	Gigaton
H	Henry's law constant
H ⁺	Hydrogen ion
H ₂ O	Pure water
HCO ₃ ⁻	Bicarbonate ion
hr	hours
IFT	Interfacial tension
IR	Initial-Residual relationship for residual trapping
ISO	International Standard Organization
J	Injectivity index
k	Absolute/effective permeability
kg	kilogram
kmol	kilomol
k _r	Relative permeability
k _{rg} ^{d/i}	Relative permeability observed in drainage/imbibition process
k _{rg/w}	Gas/water relative permeability
k _{rg/w} '	Endpoint of gas/water relative permeability
k _v	Vertical permeability

k'	Reaction rate constant
k'_{ref}	Reaction rate constant at reference velocity
L	Length of a porous media Reservoir thickness
m	Metre Constant for velocity dependent reaction rate
m^2	Square metre
m^3	Cubic metre
MBO	Modified Black Oil
mD	Millidarcy
Mg^{2+}	Magnesium ion
min	Minutes
MPa	Megapascal
NASA	National Aeronautics and Space Administration
$n_{g/w}$	Exponent for gas/water
nm^2	Square nanometre
N/m	Newton/metre
pH	A scale used to specify the acidity or basicity of an aqueous solution
p_c	Capillary pressure
PI	Productivity Index
p_r	Average reservoir pressure
psi	Pounds per square inch
PSS	Pseudo-steady state
p_{wf}	Bottom-hole flowing pressure
p-T	Pressure-temperature
q	Fluid flow rate
r	Pore radius Evaporation rate
R	Ideal gas constant
r_e	Formation radius
R_f	Resistance factor
RIC	Relative Injectivity Change
R_nSiX_{4-n}	One of general formulas for alkoxysilane
rrf	Resistance factor constant
r_{salt}	Volumetric rate of salt formation
RT	Rock type
r_w	Well radius
$ScCO_2$	Supercritical carbon dioxide
SCF	Standard cubic feet
$S_{CO_2c/i/r}$	Critical/initial/residual saturation of CO_2
SI	International system of unit
SPE	Society of Petroleum Engineers
STB	Stock tank (standard) barrel
S_w	Water/brine saturation

S_{wc}	Water connate saturation
S_{wirr}	Irreducible water saturation
S_w^*	Normalized water saturation
t_{mix}	The mixing time for CO ₂ -brine dissolution
u_w	Darcy velocity of water/brine
v	Current velocity of water
V	Grid block volume
\bar{v}	Partial molar volume
v_{crit}	Critical velocity of water
v_{ref}	Reference velocity of water
WAG	Water Alternating Gas
w_i	Mole fraction of component-i in aqueous phase
wt. %	Weight percent
y_i	Mole fraction of component-i in gas phase
α	Conversion constant in PSS flow equation
γ	Interfacial tension
θ	Contact angle
μ	Fluid viscosity
$\lambda_{g/w}$	Gas/water mobility
Δp	Pressure difference
$\Delta \rho$	Density difference
Δx	Discrete length in a porous media
δ	Fluids density ratio
θ_A	Advancing contact angle
θ_R	Receding contact angle
ρ	Phase molar density
ϕ_v	Void porosity
ϕ_f	fluids-contained porosity
°C	Degree Celsius
μ CT	Micro-computed tomograph

Chapter 1 Background and Problem Description

1.1. Introduction

This research includes several numerical simulation studies performed to evaluate the impact of wettability (and its alteration) on several critical aspects of underground CO₂ storage, including well injectivity and storage performance. To achieve this primary goal, several simulation cases have been performed to assess the implementation of wettability alteration in overcoming two of the injectivity issues of water blockage and salt precipitation. The sought wettability alteration is supposed to take place through supercritical CO₂ (scCO₂) based silylation due to its effectiveness and less treatment time required. The impact of wettability on the storage performance of a storage site has also been evaluated using the dynamic rock properties as directly measured using experiments instead of the hypothetically generated data used in other similar studies.

This is a very short chapter that aims to provide a brief background to the research, present a short description of the problem at hand, list the fundamental objectives pursued, and finally present a brief overview of how this thesis is organized.

1.2. Background and Problem Description

Underground CO₂ storage is part of activities supporting the carbon capture utilization and storage (CCUS) scheme pursued by many countries and organizations to cut back on global CO₂ emissions. CCUS means capturing the greenhouse gas, i.e., CO₂ in this research, from its emitting sources and then optimizing the use of the gas instead of releasing it into the atmosphere. The optimizing actions can be in terms of “utilization” or “storage” in which CO₂ is (re-)used for enhancing oil recovery (EOR) or injected into an underground geological structure for safe permanent sequestration. CO₂ geo-sequestration has been encouraged by the Paris Agreement 2015 whose goal is to limit the global temperature rise below 2 °C compared to that of pre-industrial level. The implementation of CCUS has also been growing since 2017 as a response to the commitment made by United States and Europe while related projects are also being planned in Australia, China, Middle East, etc.

Among several types of geological sites considered for underground CO₂ storage, deep saline aquifers have been found to present the largest capacity for CO₂ storage. However, many studies have listed multiple challenges associated with underground geological structures that can be broadly classified as political, cross-chain, economic, and technical (Muslemeni, et al., 2020). The particular technical issues to consider while evaluating CO₂ storage in such structures, including saline aquifers, are well injectivity, containment and storage capacity.

The above-stated factors are often strongly impacted by the static and dynamic properties of the subsurface fluid-rock system.

One of the prominent properties of the system that controls the viability of a geological site for CO₂ storage is rock wettability. The wettability impacts the CO₂ plume propagation and the amount of CO₂ stored under the structural, solubility, and residual trapping. Due to the lack of available experimental data, studies conducted to date have often opted to use hypothetical data characterizing relative permeability, capillary pressure, etc. under varying wettability states in their numerical simulations (Al-Khdheawi et al. 2017a; 2017b; 2018). Wettability also plays a key role in controlling some of the injectivity issues encountered during CO₂ injection, particularly in deep saline aquifers. For instance, a strong water-wet condition may cause water blockage around the wellbore, which deteriorates the well injectivity. The pronounced entrapment of brine in the near wellbore region also causes another injectivity problem by promoting salt precipitation. The situation can get even worse under capillary-driven brine backflow into the strongly water-wet pore space leading to even more severe injectivity deterioration. As a remedy, several attempts have been made to alter the rock wettability toward less water-wet conditions, one of which is the injection of supercritical CO₂ (scCO₂) based silylation as reported by Arjomand et al. (2020a; 2020b). The work was conducted using Gray Berea sandstone cores to represent the condition of a deep saline aquifer.

In this study, the experimental results generated in recent years by Arjomand et al. (2020b) are upscaled to a larger scale to evaluate the impact of wettability on storage capacity and well injectivity through sets of numerical simulation cases. The simulations have been done to forecast the storage capacity and CO₂ plume propagation under two different wettabilities of the aquifer rock. Additionally, the same experimental results have also been utilized to simulate the wettability alteration by silane treatment in terms of remediating the water blockage and salt precipitation.

1.3. Research Objective

The main objectives of this research are as follows:

1. To develop integrated kinetics processes with the conventional fluid-fluid and fluid-rock models that can simulate the evaporation process while addressing the salting-out phenomenon.
2. To forecast the severity of the corresponding injectivity issues and the role of scCO₂ based silylation in remediating the water blockage and alleviating the severity of salt precipitation in the presence of water blockage.

3. To evaluate the capacity of CO₂ storage and the CO₂ plume propagation in a deep saline aquifer under different wettabilities using available representative experimental data.

1.4. Organization of Thesis

This thesis is prepared following a hybrid format. It uses a standard thesis structure in which some chapters constitute published manuscripts (e.g., Chapter 3 in its entirety has been published in the journal of *Transport in Porous Media* (full citation of the manuscript is provided on page v under “Publication by Author” heading)).

Fitting into the above-described thesis format, Chapter 1 is a short chapter that sets the scene by providing a very brief background to the research and stating the problem at hand. It also includes a list of research objectives and sets out the outline of the thesis. Subsequently, a comprehensive literature review is presented in Chapter 2 that forms the basis of this research. This chapter provides a detailed technical description of relevant aspects of underground CO₂ storage including trapping mechanisms, containment efficiency, and well injectivity. It also provides a description of how rock and fluid properties impact the CO₂ injection and storage process with a particular focus on rock wettability which is of main concern in this work. The Chapter ends with a detailed review of the relevant numerical simulation studies with the main aim of describing the existing knowledge gap and elaborating on how the current study helps to bridge the identified gap.

Chapter 3 contains the first publication by the author. This chapter covers the numerical simulation study done on the remediation of injectivity issues during CO₂ geo-sequestration by wettability alteration, i.e., supercritical CO₂-based silylation. The chapter consists of a published manuscript in its entirety. Therefore, its Introduction section may have overlaps with the information already included in Chapter 2. Chapter 4 is based on another manuscript under preparation for publication. This chapter presents a detailed technical review of the wettability impact on CO₂ storage capacity and plume migration complemented by an improved numerical simulation study that addresses some of the identified deficiencies in previous similar studies.

Lastly, Chapter 5 is another short chapter that presents a summary of the main findings of this study. It also includes a list of recommendations for potential future work that may be based on the current research.

Chapter 2 Literature Review

2.1. Introduction

This chapter provides a comprehensive background to this research program and present a detailed review of the relevant literature. Initially, a brief technical description of underground CO₂ storage is presented with a specific focus placed on deep saline aquifers which are the primary storage medium explored in this work. Subsequently, the chapter will provide a detailed discussion of the various properties of the subsurface fluid-rock system that control the main technical aspects of a storage site namely storage capacity, containment and injectivity. The last part of the chapter will focus on those aspects specific to the current study, which is the numerical study of CO₂ storage in deep saline aquifers evaluating storage capacity and injectivity-related issues, primarily salt precipitation.

2.2. Underground CO₂ Storage

Underground CO₂ storage has been prioritized by many countries and international agencies as a way of lowering CO₂ emissions. Without such measures, the ever-increasing emissions will keep intensifying the global warming through the well-known “greenhouse effect” (MacDowell et al., 2010). A rise of 1 °C of mean earth temperature has occurred since pre-industrial age (mid-1800s) up to 2021 during which the concentration of CO₂ in the atmosphere has doubled (NASA, 2023). Other environmental indications have also emerged such as a rise in the mean sea level, warmer oceans, melting glaciers, etc. As encouraged by the Paris Agreement 2015, the signatory nations have agreed to keep the global temperature rise below 2 °C compared to that of the pre-industrial level. Underground CO₂ storage is expected to make a measurable contribution by up to 20% reduction in emissions (DECC, 2012). The advantages of this sequestration method are large storage capacity, long term isolation of the unwanted gas with order of hundreds to thousands of years, reasonable cost, and relatively well understood and developed subsurface technologies adopted from the oil and gas industries (Bachu, 2000; Voormeij and Simandl, 2002; Yamasaki, 2003).

Before the process of storing CO₂ in an underground site, the gas is extracted from its emitting sources, which is referred to as the “capture” phase in CCUS. The concept is to prevent the release of CO₂ into the atmosphere. CO₂ should be taken out, for example, from the flue gas in a power plant or pre-flared gas in a producing hydrocarbon field. The separation process is basically the main costly action that requires some modification or additional technologies i.e., chemical adsorption, membrane separation, pre- and oxy-fuel combustions, cryogenic distillation, hydrate-based separation, etc. (Ghiat and Al Ansari, 2021). The separated CO₂ is usually compressed and then directed to the next stage by either ISO-tank

delivery or pipeline transfer depending on the distance between the capture and the storage sites. The next stage can be the “utilization” or “storage” or both in which CO₂ is (re-)used for EOR/EGR or injected into an underground geological site for safe permanent sequestration. Doing so will make CO₂ to be either circulated in the reservoir-well-pipeline network or trapped within the formation/bed. Based on the report conducted by Global CCS Institute (2022), there are 29 active CCUS projects worldwide which consist of 20 CO₂-EOR activities and 9 sites for dedicated geological storage. Alternatively, the captured CO₂ can be utilized by converting it into value-added chemicals such as ethanol, urea, etc.

As graphically depicted in Figure 1, to date, several different types of geological sites have been identified as potential candidates for CO₂ storage, including deep saline aquifers, depleted oil and gas reservoirs, CO₂-EOR targeted formations, unmineable coal seams or coalbed methane, organic rich shales, and salt caverns (Voormeij and Simandl, 2002; Aminu et al., 2017; Al Hameli et al., 2022). In general, each type of storage site has its own capacity to store CO₂ based on the trapping processes involved within the pores and the matrix. However, in addition to storage capacity, there are other important aspects needed to be assessed before deciding whether the corresponding site is feasible for CO₂ sequestration including containment efficiency, and injectivity (Miri and Hallevang, 2016).

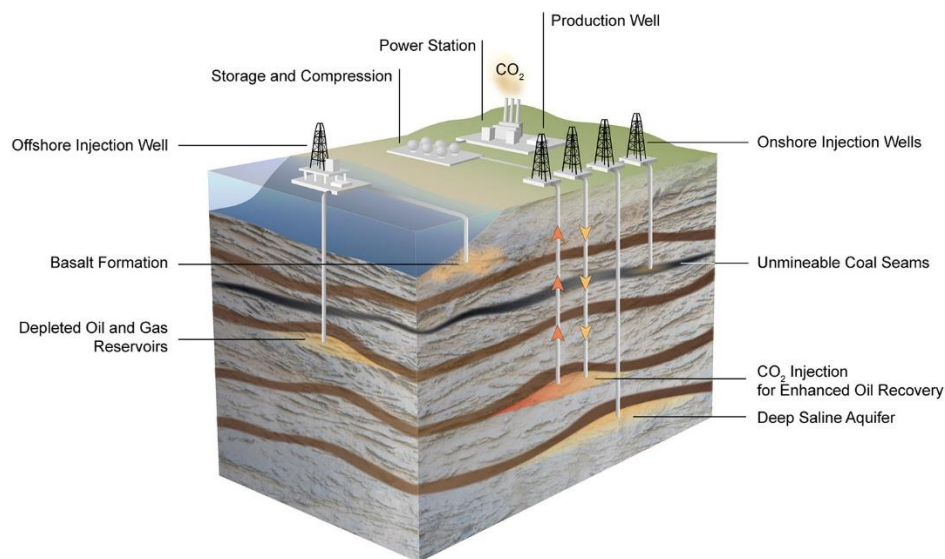


Figure 1. Underground CO₂ storage options (Ali et al., 2022)

The largest storage capacity is offered by deep saline aquifers which can store up to 10,000 billion tons (gigaton, Gt) of CO₂, followed by depleted hydrocarbon reservoirs with a capacity up to 1,000 Gt (Herzog and Golomb, 2004). That storage capacity is supported by four trapping mechanisms involved, namely structural, solubility, residual, and mineral trapping. These trapping mechanisms will be explained in detail in Section 2.2.1.

As a deep saline aquifer contains a large amount of brine, the ability of CO₂ to dissolve in the aqueous phase is a major advantage. Besides that, a large amount of CO₂ will be stored under capillary restraint within the pores once the brine returns imbibing into the zone swept by CO₂. As another advantage, saline aquifers with adequate permeability also require few injection wells. However, most deep saline aquifers are often located in areas with less developed infrastructure for subsurface injection which may raise the transport, compression and injection cost. In contrast to saline aquifers, depleted hydrocarbon reservoirs require less extended capital and operational costs as the existing infrastructures may be adopted for the transfer and injection of CO₂ (Aycaguer et al., 2001). In addition to technical uncertainties, CO₂ storage in deep saline aquifers may require addressing environmental issues and public perception (Bachu, 2000). Also, saline aquifers may suffer from several potential injectivity issues such as water blockage, salt precipitation, and fines migration contributing to further rise in the future operational costs. Thus, a detailed characterisation and numerical simulation are essential for the feasibility study of CO₂ storage in deep saline aquifers.

2.2.1. Trapping Mechanisms

The injected CO₂ can be trapped in many ways based on the characteristics of the targeted geological structure. For instance, an abandoned gas reservoir that has produced under volumetric depletion may reach more than 80% of recoverable volumes in-place by which there is also a large capacity for storing free CO₂. Supporting by structural trapping under the caprock, the fill-up of CO₂ may re-pressurize the reservoir near to its original pressure (Bachu et al., 2000). Also, a unique trapping mechanism is active in a coal seam. The ability of coal to adsorb CO₂ within its matrix while releasing methane contributes to another way of storing CO₂, namely adsorption trapping.

Generally, CO₂ flows within a geological formation and displaces the original fluids. The flow path is dominantly controlled by viscous and gravity forces. Thus, the CO₂ plume generally forms a “V”-shape in the vertical cross-section during injection. Commonly, CO₂ is less dense than the original resident fluid, such as brine in the deep saline aquifer. Consequently, CO₂ rises through the permeable formation due to the buoyancy effect. A caprock lying above the porous formation behaves as a barrier to isolate the free CO₂ preventing further upward migration and making it accumulate at the top of the structure. That process is the basic trapping mechanism for all sedimentary underground storages, called structural trapping (Iglauer et al., 2015a). The upward flow is halted due to high capillary entry pressure presented by ultra-low permeability traps (Wollenweber et al., 2010). The caprocks/traps are mainly composed of anhydrite, halite, muscovite, kaolinite, calcite, and other minerals (Chiquet et al., 2007; Iglauer et al., 2015b). The ability of the cap rock to keep the supercritical CO₂ trapped must be guaranteed for considerably long periods (Jiang, 2011).

However, as CO₂ is stored in the form of a free supercritical phase, it may still enter the traps due to slow diffusion, unsealed faults, or exceeding the capillary entry pressure (Meng and Jiang, 2014). Structural trapping was the first mechanism identified and characterised by researchers (Iglauer et al., 2015b; Arif et al., 2016).

Residual trapping, also known as capillary trapping, takes place when displaced brine re-imbibing the CO₂ swept zone after the end of injection which restrains a certain amount of CO₂ trapped within the pores of the rock formation. The capillarity of the rock governs these whole processes (Ali et al., 2022). It demonstrates the same outcome as that of drainage-imbibition scheme in a petroleum system, giving rise to what is known as the hysteresis effect. Under this scheme, migrating hydrocarbon (the non-wetting phase) displaces the resident brine (the wetting phase) via the so-called drainage displacement. While the reservoir is producing, hydrocarbon is withdrawn leaving an amount of residual hydrocarbon within the pores behind the brine front during an imbibition process. The drainage and imbibition processes during CO₂ storage in a deep saline aquifer are represented by the displacement of brine by CO₂ and then reintroduction of the displaced brine once the injection has stopped, respectively. Figure 2 shows the impact of hysteresis on CO₂ trapping as simulated by Nghiem et al. (2009). Lack of hysteresis model fails to show residual trapping as CO₂ relative permeability curve acts reversibly (de Gennes et al., 2004; Juanes et al., 2006). The trapping phenomenon can be easily understood through a set of relative permeability curves representing hysteresis process as shown by Figure 3.

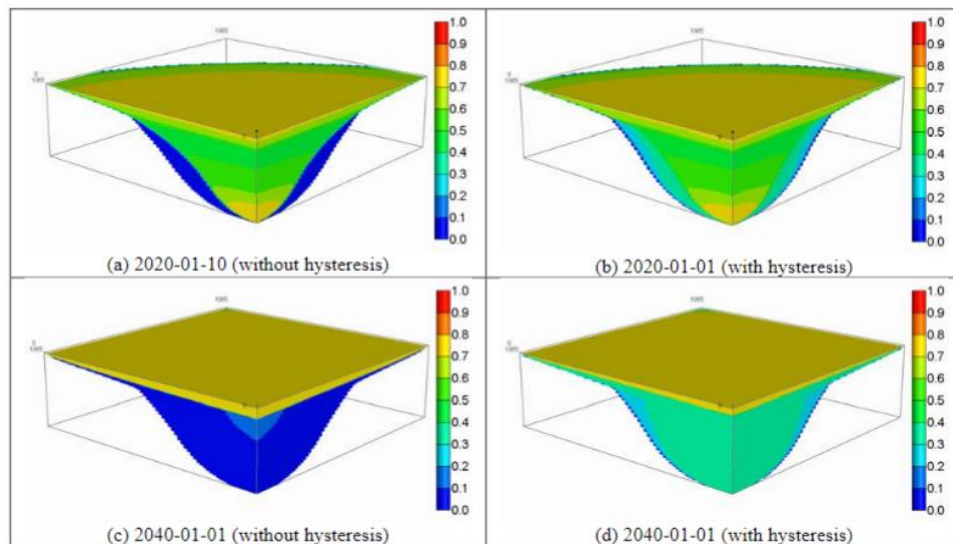


Figure 2. Gas saturation for case of present and absent of hysteresis model (Nghiem et al., 2009)

Residual trapping sequesters a considerable amount of CO₂ that will remain immobile within the pores even in the existence of leakage pathway through faults or wells (Burnside

and Naylor, 2014). Unlike the structural trapping that behaves as a barrier for movable CO₂ phase, residual trapping is considered much safer as it breaks the connection of some upward-flowing CO₂ when the brine re-imbibes. Thus, the rock capillarity locks CO₂ as a series of isolated droplets (Nghiem et al., 2009; Burnside and Naylor, 2014). It is worth noting that injecting CO₂ and brine alternately can actually help increasing the amount of CO₂ trapped as residual phase since the injected brine gives rise to forced imbibition (Juanes et al., 2006).

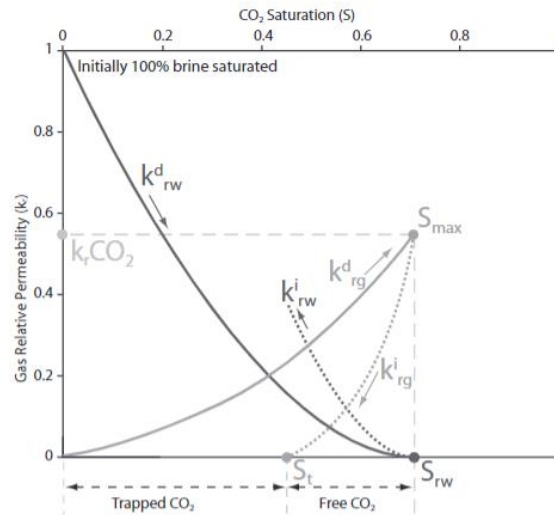


Figure 3. A typical relative permeability curves indication a hysteresis process from drainage-imbibition process (Burnside & Naylor, 2014)

Solubility trapping is another trapping mechanism active during CO₂ storage in deep saline aquifers. This mechanism refers to the storage of CO₂ in the aqueous phase due to its ability to dissolve in water forming bicarbonate ion (HCO₃⁻) (Ajayi et al., 2019). The dissolution process is induced by molecular diffusion in the contact of brine and free CO₂ (Ali et al., 2022). The ionic reaction proceeds slowly and may require thousands of years to completely dissolve in the aquifer brine (Lindeberg and Wessel-Berg, 1997). Dissolution of CO₂ turns the brine slightly denser and drives downward movement of the CO₂-saturated brine. This negative buoyant plume assures permanent and safe storage of CO₂ since the stored CO₂ does not appear as a distinctive phase in the system and actually moves downward and would not cause any caprock integrity concerns. Also, during this convective sinking of CO₂ fresh brine rises to contact the remaining free CO₂ providing continuous CO₂ dissolution (Riaz et al., 2006). The sketch depicted in Figure 4 (Riaz and Cinar, 2014) explains the convective flow occurred during solubility trapping. The solubility of CO₂ in aqueous phase is a function of pressure, temperature, and brine salinity (Chang et al., 1996; Ji et al., 2005). Increase in temperature and salinity reduces the solubility of CO₂ while increase in pressure having opposite effect.

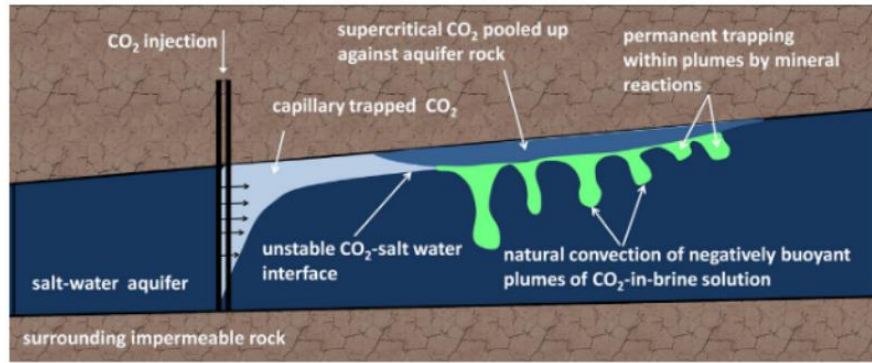


Figure 4. Illustration of CO₂ trapping mechanisms depicting the convective flow under CO₂ dissolution process (Riaz and Cinar, 2014)

Lastly, mineral trapping acts as the safest process for CO₂ storage during which aqueous CO₂ (bicarbonate ion) forms a new carbonate mineral, i.e., calcite, muscovite, etc., as a result of the reaction between the dissolved CO₂ and minerals and organic materials in aquifer rock (Al Hameli et al., 2022). In detail, the dissolution of CO₂ in an aqueous phase lowers the pH of brine. This induces a dissolution of in-situ minerals forming free cations to neutralize the acidic state (pH less than 7). The reaction between cations, i.e., Ca²⁺, Mg²⁺, Fe³⁺, etc., and the bicarbonate ion forms new carbonaceous minerals leading to permanent CO₂ storage. Consequently, there could be variations of rock porosity and permeability after this solid precipitation has been established. Such a process is controlled by the structure, mineralogy, and hydrogeology of existing lithologies (Rochelle et al., 2004). Mineral trapping is an extension of solubility trapping which is governed by the concentration of cations within brine and the brine pH as depicted in Figure 5 (Rackley, 2017). As the dissolution of CO₂ into a brine takes a long time, the formation of carbonaceous mineral trapping requires even more time to happen (Bachu et al., 1994). Based on known kinetic rates in several published literature, the formation of the carbonaceous minerals may take up to thousands of years to complete (White et al., 2005).

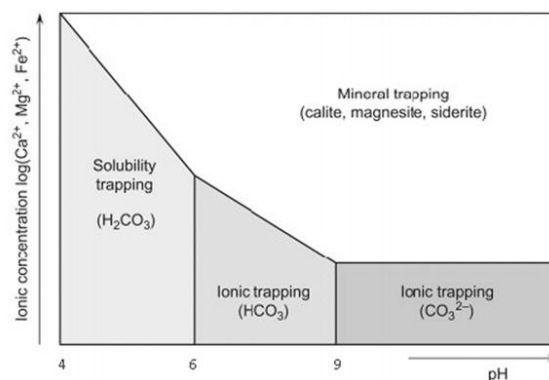


Figure 5. Brine properties by which CO₂ is controlled whether stored as ion or mineral (Rackley, 2017)

2.2.2. Containment Efficiency

Containment efficiency refers to the ability of a geological formation (deep saline aquifers in this study) to keep CO₂ unescaped in competition with the buoyancy effect. In an ideal condition, free CO₂ will be permanently isolated in its host formation for a long time under the earlier described structural trapping. In other words, a caprock acts as a barrier to the upward flow of CO₂ to prevent leakage of CO₂ toward upper beds or even back into the atmosphere. This represents the primary sequestration mechanism during the first decade of CO₂ storage implementation (Wollenweber et al., 2010; Iglauer et al., 2015b). The integrity of caprock is essential for the structural trapping of CO₂. Poor caprock integrity facilitates CO₂ flowing upward which reduces the storage capacity of the host formation. The flow through a low permeability caprock will not take place as long as the CO₂ fluid pressure is less than the capillary entry pressure of the caprock, as shown in Figure 6 (Hildenbrand et al., 2002). Since there is no fluid withdrawal during CO₂ injection in deep saline aquifers, increase in pore pressure is expected during CO₂ injection. The increase must be kept lower than the capillary entry pressure to keep free CO₂ confined within the structure. Also, there are several leakage pathways that allow CO₂ to reach the upper zone beyond the targeted formation, such as unsealed faults/fracture networks, poorly cemented wells, and diffusion through water-saturated caprocks (Aminu et al., 2017). Those phenomena affect the containment efficiency of a storage site.

The capillary sealing capacity of a caprock is expressed as a minimum required pressure of a non-wetting fluid to displace a wetting phase in a specific pore geometry. Assuming a cylindrical pore geometry, the threshold pressure can be expressed as basic formula of capillary pressure as follow:

$$p_c = \frac{2\gamma \cos \theta}{r} \quad (1)$$

where γ is interfacial tension (IFT, N/m) between the wetting (brine) and the non-wetting (CO₂) fluids and θ designates the contact angle between the wetting fluid and the rock surface. Also, r denotes the pore radius (m). According to the equation, a low permeability caprock that has a small pore radius provides a high capillary entry pressure.

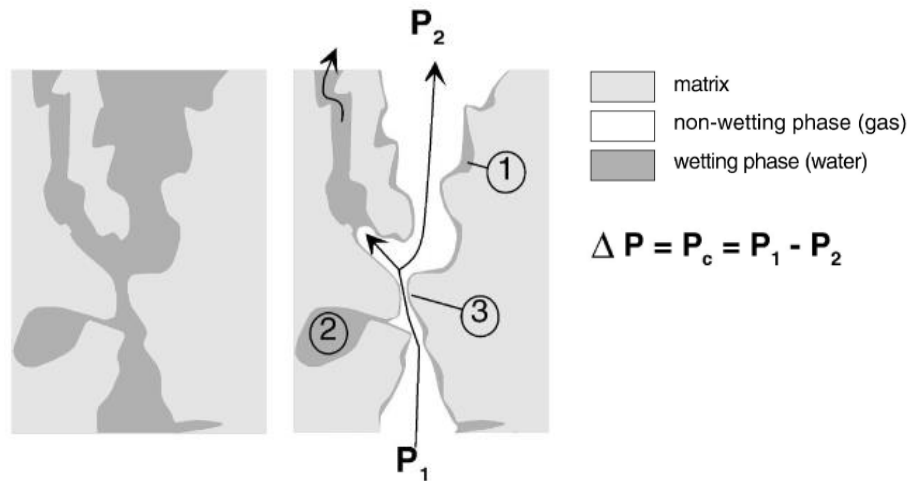


Figure 6. Schematic of drainage process in which CO₂ (non-wetting phase) flows through the pores when the capillary pressure exceeds the entry pressure (Hildenbrand et al., 2002)

CO₂ leakage through caprock pores can also be induced by an alteration of the caprock properties which leads to a reduction of the capillary entry pressure. In addition to the pore radius, this threshold pressure is controlled by wettability (will be explained in Section 2.3.4), and fluids IFT (Downey, 1984). The dissolution of CO₂ into aqueous phase triggers the low pH condition and consumes some reactive minerals. Mineral dissolution opens the pores (the radius becomes larger) which leads to lower the capillary entry pressure of the caprock. In the experimental work performed by Canal et al. (2013), injection of CO₂ to a sandstone core collected in Spain reveals an increase of porosity and permeability by 10.5% and a factor of 4, respectively, due to the dissolution of minerals. The sample was mostly composed of quartz (92.1 vol%) and much lesser amounts Mg-calcite (0.3 vol%), while more clays are expected in common caprock which, in turn, high impact on mineral dissolution may be induced. Hildenbrand et al. (2004) reported that IFT between CO₂-brine in the pressures range of 6-20 MPa and temperatures below 71 °C was half that of hydrocarbon-brine at the same p-T conditions. The water-wet caprock in hydrocarbon-brine system was also altered to intermediate-wet in case of CO₂-brine fluids due to the lower interfacial tension and contact angle (Chiquet et al., 2007). These findings lead to less sealing capacity of a caprock in response to the low capillary entry pressure due to the lower IFT between CO₂-brine. Thus, caution is needed in ruling that a reservoir caprock sealing hydrocarbon would provide the same sealing ability toward CO₂ (Li et al. 2006). Less water wet caprock has also been proven reducing the storage capacity and the confinement efficiency (Chiquet et al., 2007; Iglauer et al., 2015b; Al-Khdheawi et al., 2017a; Aminu et al., 2017).

As indicated earlier, leakage pathways may form because of poor cementing and existing unsealed fault and fracture network in the host formation (Figure 7). Poor cement can

be caused by an improper cementing job or a cement degradation. A CO₂-rich brine induces an acidic condition which may react with the alkaline borehole cement. This process degenerates the cement and shorten the cement lifetime. Based on Connell et al. (2015), the cement degradation takes place in two main stages: first stage is when acidic brine reacts with calcium hydroxide phases in the cements forming a carbonate mineral; second stage is when the precipitated carbonate mineral dissolves into the undersaturated brine. The second stage requires two other processes: 1) the brine is under solubility shortage of calcium and carbonate ions, and 2) there is always fresh brine flowing to the cement continuously. On the other hand, pre-existing fault and fracture network may allow a considerable CO₂ leakage out of the host formation. Besides any induced seismic activity, the fault and the fracture network leakage can be stimulated by the dissolution of mineral in the fault/fracture which gives a considerable permeability for CO₂ to flow. Also, cracks can be created on caprocks, fault and fracture due to a buildup pressure during CO₂ injection. The occurrence of many of these events is influenced by the distance to the point of CO₂ injection. Therefore, placement of injection wells requires comprehensive geological investigation, seismic activity assessment around the site, seismic monitoring, surface and soil gas monitoring, and proper modelling of pressure buildup and fluids migration (Sminchak and Gupta, 2003; Beaubien et al., 2013).

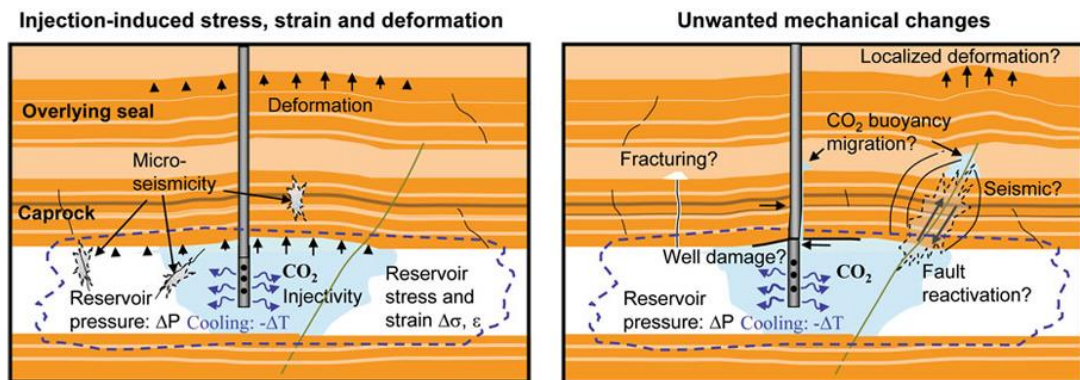


Figure 7. Possible pathways for CO₂ leakage in response to geomechanics change within formation due to pressure build up and/or seismic activity (Rutqvist, 2012)

2.2.3. Well Injectivity

Injectivity is usually evaluated through a parameter called injectivity index. Injectivity index (J) is similar to another term known as the productivity index (PI) mainly used in the oil and gas production activities. In case of injecting fluid to a geological formation, injectivity index is the proper term to identify the performance of a reservoir-well system. In oil and gas, productivity (or injectivity) index represents the capability of a well to produce fluid(s) from [to inject fluid(s) into] a permeable formation (Craft & Hawkins, 1991). Injectivity index is

expressed in $\text{m}^3/\text{hr.MPa}$ (STB/day.psi in Field Units) which is described by the following formula:

$$J = \frac{q}{p_{wf} - p_r} \quad (2)$$

where q is fluid flow rate (SI unit in m^3/hr ; field unit in STB/day or SCF/day), p_{wf} and p_r are well bottom-hole flowing and average reservoir pressures (MPa; psi), respectively. In the case of CO_2 underground storage, the flow rate is usually expressed in tonnes/hr.

To calculate J , the injected fluid should flow within a permeable formation for a considerably long time as it should reach the pseudo-steady state (PSS) period (Ahmed, 2001). Under this state, the change of pressure at every point in the reservoir $(\frac{\partial p}{\partial t}|_r)$ is constant. The calculation of J using data from other flowing periods leads to inaccurate outcomes. that is because J is still varied under the transient flow period as can be seen in Figure 8. In the case of the injectivity index, J curve increases in the transient flow period until it reaches constant under PSS (Valluri et al., 2021).

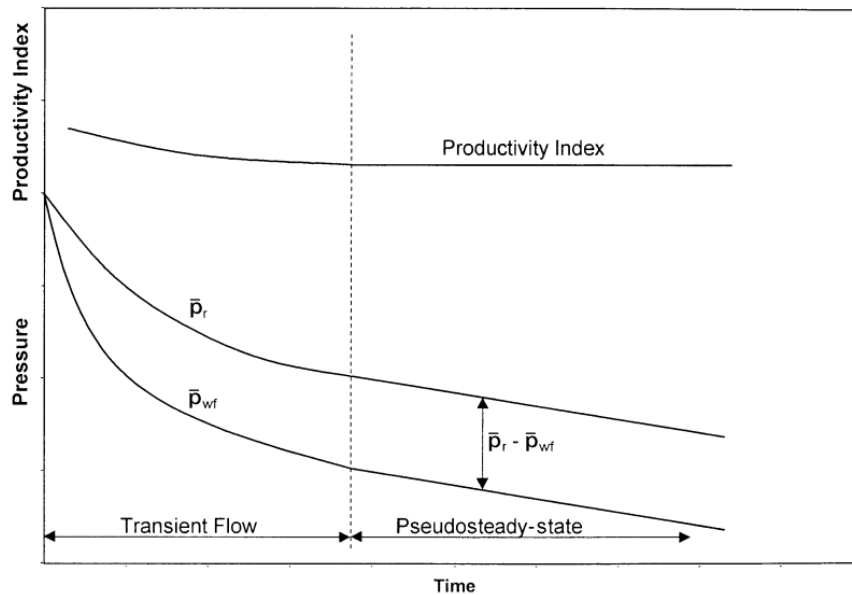


Figure 8. Productivity index profile under different flow regimes (Ahmed, 2001)

However, J may drop at a high production rate even once PSS period has been reached (Craft & Hawkins, 1991). In oil and gas reservoirs, this decline may be caused by (1) a turbulence flow within the well, (2) reduction of oil permeability due to the presence of free gas expelled from oil, (3) increased oil viscosity in case of system below bubble point pressure, and/or (4) permeability reduction due to compressibility (Craft & Hawkins, 1991). Even though this index is mainly used to represent well property, the number indeed changes as if

some of reservoir properties are altered. According to fluid flow equation in a radial porous media under PSS flow regime, J can be expressed as below:

$$J = \alpha \frac{kh}{\mu B [\ln(r_e/r_w) - 0.75]} \quad (3)$$

where α is a conversion constant, k and h are formation permeability (m²; mD) and formation thickness (m; ft), respectively, μ and B are fluid viscosity (Pa.s; cP) and fluid formation volume factor (unitless: reservoir state volume/standard state volume), respectively, r_e and r_w are radius of formation and well (m; ft), respectively. The above equation describes how J is controlled by the fluid and reservoir properties which tend to be varied during the exploitation, i.e., μ , B , and k . For multiphases flow, k refers to an effective fluid permeability which is described as $k \cdot k_r$, where k_r is a fluid relative permeability.

In case of CO₂ underground storage into deep saline aquifer, the same approach can be applied to evaluate injectivity. At a certain condition in which no turbulence is expected in the well, the only reason that causes decline of J is the variation of fluid and aquifer formation properties. CO₂ viscosity is considerably low for the whole period of injection and may not significantly affect J due to the pressure variation. Injection rate is mainly measured in unit of mass per hour, thus B is not considered anymore. However, aquifer permeability is more favorable to change due to geochemical processes during CO₂ injection which precipitates and dissolves minerals within the aquifer formations (Xu et al., 2007; Gaus, 2010; Shao et al., 2010; Hu et al., 2011). This affects injectant effective permeability, k , and thus impacts the injectivity index.

When CO₂ is injected into saline aquifers, evaporation of liquid water into CO₂ phase leads to a process where the dissolved salts precipitates (Figure 9). This phenomenon is broadly called “salting-out” effect and in this context, salts can precipitate in the wellbore vicinity and behind the drying-out front (Kleinitz et al., 2001; Lorenz and Müller, 2003; Peysson et al., 2011). The precipitated salt decreases the porosity and permeability resulting in a poor injectivity. The impact of salt precipitation is more prominent when a capillary-driven backflow is also present. Under this condition, the formation water (with dissolved salts) flows toward injection well due to a capillary suction. As the evaporation continues, further accumulation of localized salt precipitation near the wellbore takes place (Giorgis et al., 2007; Pruess & Müller, 2009; André et al., 2014).

The capillary-driven backflow can be easily understood by identifying the fractional flow of water/brine below:

$$u_w = f_w u_t + f_w \lambda_g \left(\frac{\partial p_c}{\partial S_w} \frac{\partial S_w}{\partial x} \right) + f_w \lambda_g [(\rho_w - \rho_g)g] \quad (4)$$

where u_w is Darcy velocity of water/brine, f_w is the fractional flow of water/brine $[\lambda_w/(\lambda_w + \lambda_g)]$, λ_g is gas mobility $[k k_{rg}/\mu_g]$, p_c is the capillary pressure, S_w is the water/brine saturation, and ρ_w and ρ_g are the density of water and gas, respectively. On the right-hand side, the first, second and third terms represents flow affected by viscous force, capillary gradient, and gravity forces, respectively. The gradient of capillary pressure described as $\partial p_c/\partial S_w$ is negative and becomes large when the water saturation is near the residual saturation. Capillary pressure curve near residual saturation usually forms asymptotic line which is much steeper. Considering the gradient of capillary pressure curve near residual saturation, the flow impacted by the second term may overcome the viscous force resulting in counter-current flow of water represented by the negativity of the gradient. As a consequence, dissolved salt follows the backflow toward the injection well. As the evaporation keeps on stage, there may be an accumulation of salt precipitated near the wellbore.

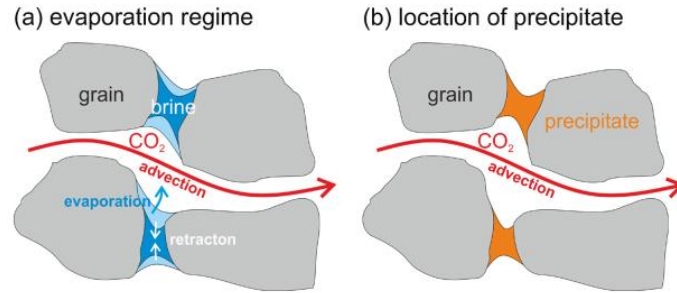


Figure 9. Schematic of salt precipitation and water evaporation within pores during CO₂ injection (Ott et al., 2015)

Other studies have found injectivity impairment insignificant in the presence of salt precipitation (Roels et al., 2014; Ott et al., 2015). In these experiments, precipitation formed homogeneously indicating the absence of the capillary-driven back flow. This causes CO₂ to flow essentially as a single phase when the porous media is virtually devoid of a water phase and the gas relative permeability increases to near unity. In other words, this overall mobility improvement is resulted from the increase in relative permeability despite the effects of salt precipitation on absolute permeability. This specific phenomenon occurs only when CO₂ injection rate exceeds a certain critical rate (André et al., 2014; Ott et al., 2015; Miri & Hellevang, 2016). Below the critical rate, local precipitation due to capillary backflow can occur and the impact on mobility is more significant. It worth noting that the researchers did not their study in low permeability samples in which formation of solid is expected to affect

the permeability significantly. Ott et al. (2021) conducted studies in a multi-porosity rock (i.e., dolomite) as opposed to Berea in their previous study showing that salt precipitation in this case strongly affects permeability.

In another study, Ott et al. (2015) identified that evaporation may take place weakly during the viscous force displacement until the brine is immobile within the pores. After a couple of hours of injection, brine saturation changes only slightly. After a longer period of time where the water saturation remains constant, salt precipitation begins to dominate suggesting that evaporation is strong. Based on this study, solid saturation should not exceed irreducible water saturation even though capillary driven backflow takes place.

As another injectivity impairment mechanism, water blockage can also take place when CO₂ is stored in deep saline aquifers. Water blockage occurs when the formation water (wetting phase) forms a thin film on the rock surface and occupies a range of pores leaving limited pore space for CO₂ to flow necessitating high injection pressure. In other words, water blockage reduces the gas relative permeability (Mahadevan and Sharma, 2003; Arjomand et al., 2020b; Lopez et al., 2021). The issue is common under strong-water-wet conditions (i.e., in sandstone reservoirs where rocks composed predominantly by quartz) with invading fluids introduced during drilling, completion, and fracturing activities (Holditch, 1979; Bennion et al., 1996; Al-Anazi et al., 2003). Those activities may use water-based fluids and considering that water is strongly wetting toward sandstone an increase in irreducible water saturation near the perforation can occur. This issue is not usually detected during normal experimental work as core analysis in laboratory may show low connate water saturation. In fact, the core sample may have been cleaned/restored which diminishes the observed impact of operating fluids during drilling, completion or hydraulic fracturing activities. Not surprisingly, the impact of water blockage increases significantly for low permeability reservoirs and aquifers (Bennion, 2002).

Several remediation methods have been proposed to overcome the above-mentioned injectivity issues. Salt precipitation can be handled temporarily by pre-injecting low salinity water into the well reducing brine salinity around the wellbore (Pruess & Müller, 2009). However, this method may only temporarily solve the problem by delaying or moving the location of the precipitation. As evaporation keeps taking place, immobile brine will exist causing salt precipitation albeit a bit later. Also, injecting low salinity water can induce clay mineral activity causing other forms of damage (i.e., fines migration, and clay swelling). Another technique recently proposed and tested at the Quest CCS facility located in Alberta, Canada (Smith et al., 2022) used a water-based fluid to dissolve precipitated salts near the wellbore. This method succeeded in repairing the injectivity index to twice of the pre-treatment value. However, there is no further evaluation regarding possibility of water blockage

following the treatment and a fines migration induced by the water injection into the formation. It is also worth noting that CO₂ has the ability to vaporize trapped brine which, in turn, reduces the water blockage issue (Bennion et al., 1996). However, injectivity remains worse as salt will be precipitated following the evaporation (Zuluaga & Monsalve, 2003). High drawdown pressure remedies this issue in some cases, while others show ineffective results (Bennion et al., 1996). Another approach is to use a chemical treatment to change the rock wettability and hence permanently eliminate the occurrence of water blockage. For example, it has been proposed in the literature to inject the supercritical CO₂ with an organo-alkoxysilane component (i.e., sc-CO₂-based silylation) to change the formation wettability toward less water-wet thereby addressing water blockage (Arjomand et al., 2020b). Detail explanation about this technique is discussed in Section 2.3.5 regarding wettability alteration.

2.3. Impact of Rock-Fluid Properties on Underground CO₂ Storage

As explained in earlier sections of this chapter, storage capacity, confinement, and injectivity, are essential for a successful CO₂ storage by a targeted geological formation. The properties of the subsurface fluid-rock system play an important role in impacting the above mentioned three requirements and determining the suitability of a geological formation for CO₂ sequestration. As this study specifically focuses on storage capacity and injectivity, their relationships with various system properties are elaborated in the following sections.

2.3.1. Porosity

The capacity of an aquifer for CO₂ storage is largely controlled by the formation porosity. Porosity is the fraction of void volume over the bulk rock volume. CO₂ is trapped in the void space in the form of free gas/supercritical phase under the structural trapping and in immobile phase under the residual trapping. According to Chadwick et al. (2008), a porosity greater than 0.2 is favorable for CO₂ storage while values less than 0.1 need careful consideration. In terms of mineral trapping, the size of pores plays important role in determining the reaction process. As studied by Emmanuel et al. (2010), large pore size promotes readily space for the mineralization while smaller pores suppress the growth of mineral. Reaction rate is restrained due to interfacial energy effect provided by the smaller pores.

Porosity on its own has no direct relationship with the injectivity. However, porosity-permeability is strongly correlated, thereby injectivity will be affected due to the change of porosity. Mineral precipitation decreases pore size and in turn, permeability drops. Permeability reduction, thus reduced injectivity, induced by the growth of mineral in pore space has been well studied by numerous researchers including Giorgis et al. (2007), Pruess and Müller (2009), Peysson et al. (2011), Roels et al., (2014), André et al. (2014), Ott et al.

(2015), Jeddizahed and Rostami (2016), Cui et al. (2018), Ho and Tsai (2020), Ott et al. (2021) and many more. Most of them utilized porosity-permeability relationship proposed by Verma and Pruess (1988). Another old technique to correlate the permeability reduction with change of porosity is Kozeny-Carman's correlation (Carman, 1997). However, Kozeny-Carman correlation usually overestimates the permeability evolution due to the change of porosity, especially in the case of high tortuosity and less connected pores (Mostaghimi et al., 2013).

2.3.2. Absolute and Relative Permeabilities

Absolute permeability represents the ability of a rock formation to facilitate the flow of fluids within its pores. The magnitude of permeability can be described as how easily the fluids pass through porous media (Abidoeye et al., 2015). Based on Darcy's law, permeability (k) of a porous media is mathematically formulated as:

$$k = \frac{q\mu L}{A\Delta p} \quad (5)$$

The formula defines the permeability as the constant of proportionality in the above equation when an incompressible fluid with viscosity of μ and flow rate q passes through a porous media with the length of L and cross-sectional area of A , imposing a pressure difference of Δp across the medium.

During the CO₂ geo-sequestration, the original rock permeability may be altered in response to geochemical reactions taking place within the pores. The reactions may either dissolve feldspar minerals or precipitate carbonate minerals and clay which, in turn, increases or decreases the original permeability, respectively (Gaus, 2010). However, most of the reactions occur in many years after the injection of CO₂ as related to the mineral trapping mechanism. The earliest precipitant encountered during the injection which can deteriorate injectivity is salt (mostly halite) due to the drying-out and the salting-out processes.

Having CO₂ and brine in deep saline aquifer leads to the concept of two-phase flow. While absolute permeability describes intrinsic property of a porous media, relative permeability poses the inter-relationship of fluids and the porous rock. It describes how each fluid's flow is restrained by another one. The concept of relative permeability may be integrated into the original Darcy equation, resulting in the following equation:

$$q_i = \left(\frac{kk_{ri}}{\mu_i} \right) \frac{\Delta p_i}{\Delta x} \quad (6)$$

where q_i , k_{ri} , Δp_i , and μ_i denote the flow rate, relative permeability, pressure drop, and viscosity, respectively, for phase- i . The term $\left(\frac{kk_{ri}}{\mu_i} \right)$ describes mobility of phase- i . The

mobility ratio between CO₂ and brine dictates the propagation and the speed of CO₂ plume. On the other hand, the phenomenon of two-phase flow causes some amount of residual saturation of each fluid during drainage and imbibition processes. Strong hysteresis phenomenon in relative permeability renders a certain amount of CO₂ plume immobilized which promotes large residual trapping behind the buoyant flow of free CO₂. The fundamental aspect of hysteresis can be explained by the concept of wettability (Section 2.3.4). Another obvious conclusion from Equation 6 is that permeability and mobility of a phase have strong control over its injectivity by controlling pressure buildup.

2.3.3. Brine Salinity

Brine salinity affects the CO₂ solubility in aqueous phase. The more saline the aquifer is, the less soluble the CO₂ can be. Figure 10 below shows the comparison of CO₂ solubility in pure water and 200 g/l brine. This dissolution gives rise to solubility trapping and will determine the amount of remaining free CO₂ trapped under the caprock. As indicated earlier, the circulation of fresh brine moving upward and denser CO₂-rich brine flowing down will take place following the dissolution of CO₂ into aqueous phase. Over time, free CO₂ under structural trapping can therefore reduce and diminish. The time required to fully dissolve free CO₂ into brine is controlled by vertical permeability and the density difference between fresh and saturated brines. Based on Ennis-King and Paterson (2005), the mixing time (t_{mix}) can be estimated as:

$$t_{mix} \approx \frac{\delta L \mu}{k_v \Delta \rho g} \quad (7)$$

where δ is density ratio of CO₂ in gas phase and CO₂ as dissolved in aqueous phase, L is the reservoir thickness, μ is brine viscosity, k_v is vertical permeability of the formation, and $\Delta \rho$ is the density difference between fresh and saturated brines. The processing time can be in the range of 1,600 to 16,000 years.

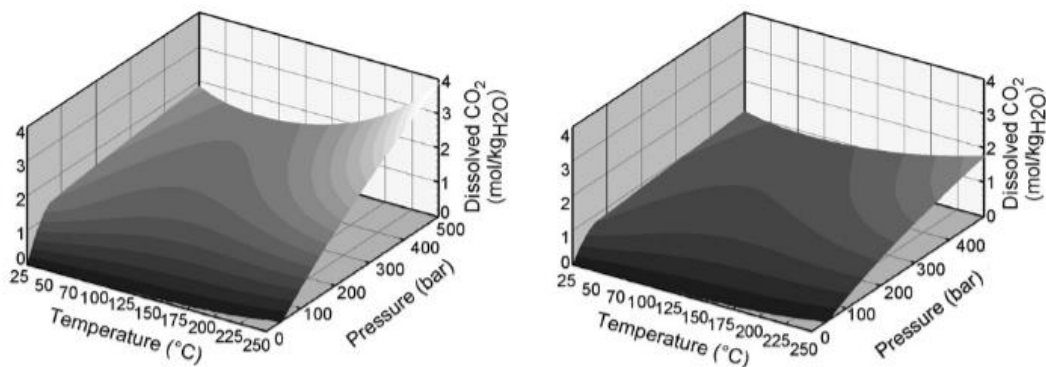


Figure 10. Concentration of dissolved CO₂ in pure water (left) and 200 g/l brine (right) derived from model proposed by Duan and Sun (2003) (Gaus et al., 2008)

Getting back to the earliest period of CO₂ injection, the build-up of salt near the wellbore is the consequence of the brine salinity which has passed the salt solubility in aqueous phase. The portion of solid salt filling the pores is aligned with the degree of salinity of the original brine. In short, simple mass balance can predict the solid saturation based on the brine salinity if the evaporation is assumed to occur on the brine at residual saturation. The precipitation only gets worst in the presence of the capillary-driven backflow which transports salt to the injection source. A local precipitation may appear when the drying-out front meets the counter flow of brine.

2.3.4. Formation Wettability

Rock wettability is related to the behavior of two immiscible fluids, CO₂ and formation brine in this case, in terms of adhering on the rock surface due to intermolecular interactions. The behavior can be either a tendency of a fluid to be in contact with and spread on solid/rock surface as dominated by adhesive forces or a prevention of a fluid to be attached on the solid/rock surface due to cohesive forces (Abidoye et al., 2015; Iglauer et al., 2015a). The definition, basically, sounds simple, however, the property is very complex due to the strong influence by a wide variety of factors including rock minerals, formation heterogeneity, accessible surface area, surface roughness, and to some extent the composition or salinity of original brine. A comprehensive understanding of wettability has been well established in hydrocarbon sector, specifically in oil industry, where the system is mainly composed of oil-brine system. Hydrocarbon gas is commonly considered as a non-wetting phase in every condition, while oil may act as a wetting phase such that in carbonate reservoir (Chilingar and Yen, 1983) and altered-wettability sandstone reservoir due to asphaltene precipitation (Yan et al., 1997; Al-Maamari and Buckley, 2003; Amin et al., 2010). The same approach can be used in CO₂-brine-rock system by switching oil-wet to CO₂-wet.

The measurement of wettability is obtained through a contact angle formed by a denser-fluid droplet placed on a solid/rock surface which is surrounded by the lighter fluid. There are two types of contact angles that explains drainage and imbibition processes. Advancing angle (θ_A) is measured when the drop is inflated (Figure 11a) which describes the process of wetting phase displacing non-wetting phase, called imbibition. On the other hand, receding angle (θ_R) is the angle measured when the drop is deflated representing the drainage process (de Gennes et al., 2004). Hysteresis is partially caused by the difference between these two angles measured during the above phenomena. Higher advancing angle prevents full reversal displacement of non-wetting phase (CO₂) by wetting phase (brine) during imbibition process resulting in a portion of a trapped non-wetting phase (CO₂) within the pores. Wettability is of importance in evaluation of p_c - S - k_r (capillary pressure, saturation history, and relative

permeability, respectively) relationship which dictates the vertical-horizontal migration of CO₂ and the residual trapping capacity.

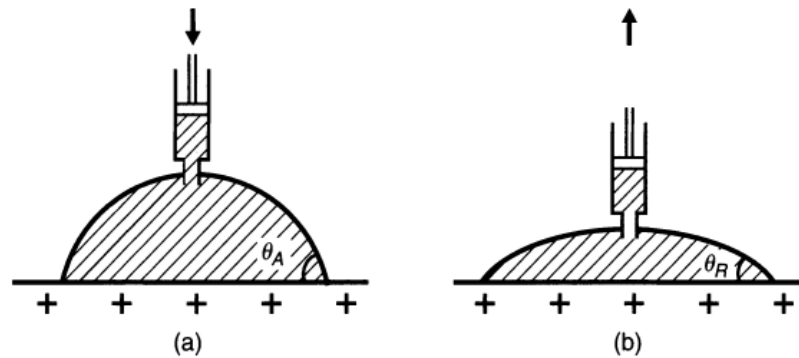


Figure 11. (a) advancing angle when the drop is inflated and (b) receding angle when the drop is deflated (de Gennes et al., 2004)

Figure 12 depicts three levels of wettability based on the measured contact angle with the smaller the angle, the more water-wet the rock is. Less water wet caprock is usually related to a less efficient structural trapping performed by a geological formation (Iglauer et al., 2015b; Al-Khdheawi et al., 2017a). However, less water wet sandstone formation improves residual trapping of CO₂ compared to that of water wet formation (Al-Khdheawi et al., 2017b). For the sake of safe storage, strong water wet formation is preferable preventing unwanted CO₂ migration beyond the targeted formation.

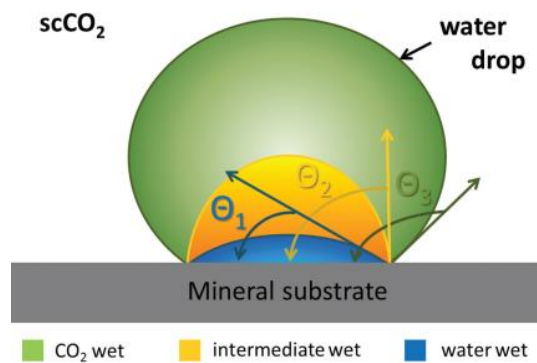


Figure 12. Illustration of measured contact angle for different wettability characteristics in scCO₂-water-mineral system (Iglauer et al., 2015a)

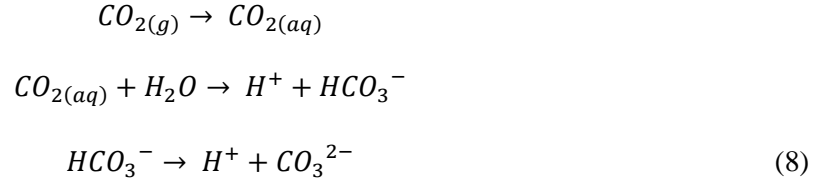
Wettability also affects the injectivity of an injection well. As explained/ in Section 2.2.3, water blockage comes up due to the strong water wet conditions. A relatively large amount of water trapped is mainly caused by the minerals composing the rock formation which

is characterized as hydrophilic such as quartz, clays, chlorite, and feldspar. This makes water to adhere to the pore surface and in turn, forming a water film. The access for CO₂ is limited due to the trapped brine film and to some extent requires higher injection pressure for CO₂. Also, as large amount of water trapped in water-wet formation, the severity of salt precipitation increases.

Wettability has been proven affecting the evaporation process and permeability impairment due to salt deposition (Rufai and Crawshaw, 2018). Rufai and Crawshaw performed experimental work of CO₂ flow in a micromodel consisting of fracture (high permeable channel) and matrix (low permeable channel). The porous micromodel was characterized as water-wetting. Subsequently, the wettability alteration of micromodel was achieved by injecting silicone solution composed of silicone caulk and dodecane. Based on their results, in case of using brine occupying the pores, fracture permeability impairment of water-wet condition is more significant than that of oil-wet condition. This is affected by the hydraulic disconnection from matrix to fracture system promoted by oil-wet condition. Such a situation suppresses the evaporating surface area and causes evaporation taking place shortly in a limited area. Furthermore, capillary flow of brine, that provides more salt to be deposited in fracture channel, is halted. Mixed-wet case shows a typical impact on the evaporation process and the permeability impairment as done by water-wet. Study conducted by Bergstad and Shokri (2016) found that increasing hydrophobic grains does not significantly impact the evaporative flux. However, pore surface covered by salt precipitation in mixed-wet sample is less than that in water-wet sample. They concluded that patchy salt precipitation resulted in mixed-wet is porous that pushes up the brine to evaporative area in the fracture channel. That may be the reason why evaporation process in mixed-wet can balance the cons of the hydraulic disconnection.

2.3.5. Wettability Alteration

Wettability has been traditionally assumed not to change in hydrocarbon systems. However, numerous studies have found that rock wettability may be altered from its original condition when CO₂ invades the rock formation. For example, as indicated earlier, this alteration can impact the caprock wettability which affects its containment capacity. Although the binary CO₂ system is inert to dry rock minerals, rock wettability is altered due to geochemical reactions taking place between rock minerals and brine containing dissolved CO₂. The reactions induce pH reduction because H⁺ is released as a product of CO₂ dissolution into brine:



The conditions generated by the above process e.g., low pH, presence of bicarbonate ion, etc., lead to the dissolution of susceptible minerals which, in turn, decreases the capillary entry pressure of the caprock (Schaefer and McGrail, 2005; Liu et al., 2012; Armitage et al., 2013; Sigfusson et al., 2015; Rezaee et al., 2017). In other words, changes in surface mineral composition and surface roughness within the pores lead to a change in wettability as evaluated through contact angle measurements of the CO₂-brine-rock system (Ali et al., 2021).

Although the above-described change in caprock wettability is considered highly undesirable, favorable artificial wettability alteration has been assessed by many studies as a way of remediating issues encountered during CO₂ underground storage. Caprock wettability reversal was studied by Ali et al. (2021) using an alumina nanofluid. They found that the presence of organic molecules can alter rock wettability to a less water wet. The alteration negatively impacts the caprock integrity. An alumina nanofluid was proposed to reverse the caprock wettability to reinstate the containment security of the storage site and safeguard the structural trapping.

Water blockage is another possible injectivity issue that can be alleviated by the concept of wettability alteration. A traditional method previously used to address water blockage is implementing a high-pressure drawdown in the wellbore area that can lead to the removal of trapped water. Given the temporary effect of such techniques, researchers attempted to mitigate water blockage chemically for a more permanent alleviation approach. Injecting supercritical CO₂ with an organo-alkoxysilane component (sc-CO₂ based silylation) is one of many attempts made and has been proven in the laboratory to change the wettability of sandstone formations toward less water-wet addressing water blockage (Arjomand et al., 2020b). This technique even outperforms conventional silylation using liquid solvents in terms of accelerating the kinetic reaction rates, i.e., the sc-CO₂ based accomplishes the reaction within 30 minutes compared to 24 hours taken using the conventional liquid solvent-based method (Sánchez-Vicente et al., 2014).

The silane reagent has the general formula of R_nSiX_{4-n}, where “R” signifies the non-hydrolysable organic group and “X” represents the hydrolysable groups. During the silylation process, organo-alkoxysilane modifies the rock surface by reacting with the hydroxyl group of adsorbed water on the rock surface (hydrolysis) and forming siloxane or strong covalent bond of hydrolyzed silane with the hydroxyl group on the rock surface (condensation).

Siloxane polishes the rock surface leading to the displacement of some immobile water. Due to limited water within the system, polymerization of siloxane growing vertically with respect to the flow direction, which may clog the pores, can be avoided (Loste et al., 2004). The treatment will increase the mobility of CO₂ and formation water, thus resolving poor injectivity. Since no water is expected to exist in the pore space after the treatment, no salt precipitation is expected to take place as well. However, silylation relies on the accessibility of the pore space and the reactivity of surface minerals with silane. Considering that sandstone, in addition to the dominant quartz, includes other minerals, silane may not react and cover all the surfaces within the pore space. Several studies performed using the sc-CO₂ based silylation on mesoporous silica found that silane reaches up to 1.6 molecules/nm² of covered surface, the so-called bonding density (Staroverov & Fadeev, 1991; Cao et al., 2001; López-Aranguren et al., 2012). A recent study used N,N-dimethylaminopropyl)trimethoxysilane (DMAPTS) to perform sc-CO₂ based silylation to a mesoporous silica system and could reach a bonding density of 2.5 molecules/nm² (Sánchez-Vicente et al., 2014). It is worth noting that the complexity of a rock formation mineralogy often leads to difficulty in the measurement of bonding density.

2.4. Numerical Simulation of CO₂ Storage in Saline Aquifer

Simulation is the best way to understand and predict the evolution of CO₂ being injected into the deep saline aquifer for underground storage before the injection is commenced. Several techniques have been developed to simulate CO₂ migration within the porous media and the trapping mechanisms, i.e., analytical method (Nordbotten et al., 2005; Zhou et al., 2008), streamline simulations (Obi and Blunt, 2006; Qi et al., 2009), inversion percolation technique (Cavanagh and Ringrose, 2011; Cavanagh and Haszeldine, 2014), and conventional 3D grid-based simulations as the modern technique used nowadays. The latter technique uses the typical numerical equations used in oil and gas sector combined with a range of physical phenomena such as geomechanics and geochemistry to address the specific behaviours exhibited by CO₂ flow within the deep saline aquifer formation system. Several simulator packages are available with adequate capabilities to model CO₂ storage in deep saline aquifers, among them are Computer Modelling Group (CMG) with GEM-GHG Module (Nghiem et al., 2004; 2009), ECLIPSE 100 and 300 (Schlumberger) with CO2STORE Module (Pickup et al., 2011; 2012), Automatic Differentiation General Purpose Reservoir Simulator (AD_GPRS) by Stanford University (Fan, 2006; Benson et al., 2013), Multiphase Flow Transport and Energy Model on Unstructured Grids (MUFTE-UG) developed by University of Stuttgart and University of Heidelberg (Ebigbo et al., 2006), TOUGH and TOUGH2 by the National Laboratories in USA (Pruess et al., 2002), and many others as listed by Ajayi et al. (2019).

2.4.1. Evaluation of Storage Capacity

CO₂ plume migration initially became the focus of simulation studies of CO₂ underground storage. Theoretical models were developed to estimate the distribution of CO₂ plume and immobile CO₂ in the form of trapped and dissolved phases (Farcas and Woods, 2008; Juanes et al., 2010; Nordbotten and Dahle, 2011). The findings from analytical models were confirmed by simulation studies, which found capillarity to be significant in controlling the plume distribution and the amount of residually trapped CO₂. Incorporating capillarity effect, represented by the hysteresis phenomenon, led to the study of rock wettability impact on storage capacity of the deep saline aquifers.

Comprehensive multiphase flow modelling of CO₂ storage in deep saline aquifer coupled with the corresponding geochemical reactions were performed by Pruess et al. (2003) using TOUGHREACT (older version of TOUGH2), Doughty (2007) using TOUGH2, Nghiem et al. (2004 & 2009) and Kumar et al. (2005) using CMG-GEM module. Other comprehensive studies which disregard mineralization modelling were performed by Sifuentes et al. (2012) using ECLIPSE 100 (CO2STORE module) and Flett et al. (2007) using CHEARS (developed by Chevron). Normally, the residual and structural trapping evaluated through the migration of CO₂ plume and the distribution of gas saturation can be well simulated by using traditional hydrocarbon simulator incorporated with a hysteresis model as conducted by Juanes et al. (2006). However, CO₂ solubilization model is then required to essentially simulate trapped CO₂ in the aqueous phase similar to the studies conducted by Sifuentes et al. (2012) and Goater et al. (2013). The methods usually used for CO₂ solubility modelling are correlations from Chang et al. (1996), Spycher and Pruess (2005), and modified Henry's Law as function of brine salinity (Li and Nghiem, 1986). Lastly, the mineral trapping simulation requires geochemical reactions modelling to cater the interactions between CO₂-brine and CO₂-rich brine and rock forming carbonate minerals as performed by Nghiem et al. (2004 & 2009) and Pruess et al. (2003). Based on the previous simulation studies, running time of the simulation follows the long-term storage expectations of up to 500-10,000 years to give enough time for mineralization to occur.

Previous simulation studies have explained the significant impact of formation heterogeneities (i.e., porosity-permeability distribution, formation dip, mineralogy variety, rock characterisation) on the CO₂ storage mechanisms (Doughty, 2007; Bryant et al., 2008; Krevor et al., 2015). According to simulation performed by Ennis-King and Peterson (2002), low residual gas saturation in the imbibition stage leads to a high CO₂ dissolution rate since the CO₂ trapped under residual phase is slow to dissolve. A less vertical to horizontal permeability ratio leads to a wider lateral CO₂ plume propagation within the formation, and vice versa (Pruess et al., 2003). Similarly, high horizontal permeability improves the lateral

movement of CO₂ and, in turn, increases solubility and residual trapping (Sifuentes et al., 2012). Based on study by Flett et al. (2007), increasing shale content in the rock composition, or a decrease in rock quality, also promotes less upward movement of CO₂ due to the shale barriers. Thus, CO₂ lateral movement is enhanced. Although the rate of residual trapping is restrained by the formation with higher shale content, it gives longer time for the system to reach equilibrium and less mobile CO₂ accumulated under the caprock due to layered shales. This may be beneficial in terms of limiting the reliance on the high-risk structural trapping. The typical results were also explained by Goater et al. (2013) who compared the homogeneous and heterogeneous cases in a relatively low average permeability model, i.e., 11 md ($11 \times 10^{-15} \text{ m}^2$). In addition, localized pressure buildup due to low permeability regions was observed in a heterogeneous case leading to poor and uneconomical injectivity. However, in relatively moderate to high average permeability systems (i.e., 145×10^{-15} to $1 \times 10^{-12} \text{ m}^2$), heterogeneous case provides larger storage capacity compared to that of homogeneous case. Layered rock characteristics due to the presence of shale (low permeability) improves the lateral movement leading to an improved amount of CO₂ trapped by the residual and dissolution trapping mechanisms. Besides the formation heterogeneities, injection strategy such as water alternating gas (WAG) (Juanes et al., 2006) and mixed CO₂-brine injection (Qi et al., 2009) also plays a positive role to increase the portion of CO₂ trapped as the residual phase. Chased water is expected to boost the imbibition compared to the natural imbibition induced by buoyant effect, and thus, increasing the amount of CO₂ retained by residual trapping. Injecting the CO₂ as deep as possible, e.g., at the base of a formation, is suggested to provide large CO₂-brine interactions which can enhance the storage capacity (Kumar et al., 2005; Sifuentes et al., 2012).

As presented by the above review, so far, the impact of numerous factors on CO₂ storage capacity has been evaluated and documented. However, less attention has been given to the role of wettability in controlling the CO₂ plume movement and its impact on the amount of trapped CO₂. As one of the few studies conducted to date, a complex sensitivity study was done by Al-Khdheawi et al. (2017a & 2017b) on this topic. The authors considered five different wettabilities, i.e., strongly water-wet, weakly water-wet, intermediate-wet, weakly CO₂-wet, and strongly CO₂-wet, for their numerical simulation studies that used hypothetical input data in modelling different wettability characteristics. As reported by these researchers, strong water wet rock involves the lowest CO₂ plume propagation with less mobile CO₂ trapped under the caprock, the lowest amount of CO₂ dissolution trapping, and the greatest CO₂ residual trapping. Nevertheless, the lack of representative experimental data that can be incorporated in numerical simulation studies to objectively model different wettability

characteristic and their specific multi-phase flow behaviors is the main issue associated with such studies.

2.4.2. Prediction of Deposited Salt

The simulation of salt precipitation was initially conducted by Lorenz and Müller (2003) by modifying simulator TOUGH2 using EWASG module (Batistelli et al., 1997) to include NaCl as an additional component and the salt thermodynamic phase change. Before further use to simulate salt precipitation, modified codes were validated with traditional template in ECLIPSE to see its ability in mimicking the injection of gas into a porous media saturated by water. The bottomhole pressure predicted by the modified model showed good agreement and is only slightly deviated in shut-in period compared to that simulated using ECLIPSE due to lack of hysteresis feature. The salt saturation in the simulation results was also found to qualitatively agree with the reference experiments. Giorgis et al. (2007) generated TMGAS module, as a part in TOUGH2 family, to simulate a two-phase flow of a gas mixture with a sodium chloride brine, and to some extent the precipitation of halite. They performed simulations of 1D and 2D single-well dry CO₂ injection to a depleted gas reservoir model having a permeability of $400 \times 10^{-15} \text{ m}^2$, a porosity of 0.32, and a thickness of 10 m. They found that when saturation of aqueous phase is low, the solid salt saturation is independent from the injection rate as the immobility of aqueous phase cannot support further flow toward evaporation front. Also, the amount of salt precipitation increases following an increase in the injection rate up to a certain value, beyond which salt precipitation reduces because higher injection pressure depreciates capillary pressure gradient, reducing the brine back-flow toward injection well.

The impact of the capillary driven back-flow on enhancing localized salt precipitation during CO₂ injection into deep saline aquifer has been simulated in several studies such as Pruess and Müller (2009), Kim et al., (2012), and André et al. (2014). As reported by these studies, localized precipitation may not appear when injection rate is higher than a certain critical value (Giorgis et al., 2007; Kim et al., 2012; André et al., 2014; Ott et al., 2015). Under such a condition, the capillary pressure gradient is overwhelmed by a high viscous force from the high injection rate, denoted as evaporative regime (Miri and Hallevang, 2016). Beside TMGAS module, ECO2N module in TOUGH2 has been developed by Pruess (2005) to specifically model water-brine-CO₂ system in a deep geological formation including the molecular dissolution as used by Pruess and Müller (2009), Kim et al., (2012), and André et al. (2014). Guyant et al. (2015) also used TOUGH2/ECO2N to simulate single phase CO₂ injection for underground storage in a deep saline aquifer where the aim was to see the impact of different completion types on the salt distribution and the resultant pressure buildup with variation in permeability. Two types of completion (i.e., half and fully open) were assessed

and the results showed typical conclusions where localized salt precipitation was formed in high permeability zone, while less precipitation was formed in the low permeability zone.

Hurter et al. (2007) simulated a radial single well CO₂ injection for storage in deep saline aquifer using commercial simulator ECLIPSE 300. Specific codes to cater for drying-out and salting-out phenomena were incorporated into the traditional compositional simulator. Cui et al. (2018) built a radial single well model using CMG-GEM module to assess the impact of fluid-rock interactions on the reservoir properties and the injectivity. They enhanced the CCS modelling conducted by Nghiem et al. (2004) (which describes CCS simulation including geochemical reactions) by incorporating the codes to address the pH changes due to CO₂ solubility and the salt precipitation due to water evaporation. Sensitivity studies were done on parameters such injection rate, water salinity, initial porosity, initial permeability, capillary pressure, etc. Mutual solubility of H₂O and CO₂ were modelled following the thermodynamic equilibrium by using the equality of fugacity in both gas and aqueous phases. However, evaporation of water into CO₂ phase typically follows a kinetics approach instead of a local equilibrium partitioning. This approach was first investigated by Roels et al. (2014) in their study which coupled experimental results with numerical modeling. With a kinetics model, salt precipitation can be more accurately modelled both near the wellbore and further away from the well. However, the use of equilibrium phase partitioning may overpredict the localized salt precipitation occurring near the injection wellbore.

Chapter 3 Injectivity Issues Remediation in CO₂ Geo-sequestration by Implementing Wettability Alteration

This chapter comprises a published work titled: “Simulation Study of sc-CO₂ Based Silylation for Decreasing Severity of Water Blockage and Salt Precipitation during Geological CO₂ Storage in Deep Saline Aquifers” (Full citation: **Pratama, Egi A.**, Matthew Myers, Asep K. Permadi, Ali Saedi. 2023. “Simulation Study of sc-CO₂ Based Silylation for Decreasing Severity of Water Blockage and Salt Precipitation during Geological CO₂ Storage in Deep Saline Aquifers”. *Transport in Porous Media*, 150, 131–155 (2023). <https://doi.org/10.1007/s11242-023-02002-7>). The chapter uses the published manuscript in its entirety, as a result, parts of the Introduction sections may be repeats of the information already presented in Chapter 2.

3.1. Introduction

Carbon capture, utilization, and storage (CCUS) has been prioritized by many countries and international agencies as part of a strategy to lower CO₂ emissions and mitigate climate change effects. The aim of CCUS generally is to capture CO₂ from a variety of emitting sources and use it for many purposes (i.e., fuels, chemicals production, enhanced oil recovery, geological storage) to reduce atmospheric greenhouse gas emissions. Many studies have identified several challenges related to implementation of CCUS which can be classified broadly into political, cross-chain, economic, and technical issues (Muslemanni et al., 2020). Poor injectivity is one of the technical issues often encountered during CO₂ injection and storage in subsurface geological structures (Andre et al., 2014). Injectivity problems may be caused by a variety of reasons including asphaltene precipitation (Srivastava et al., 1999; Darabi et al., 2014; Cho et al., 2016), water blockage (Ford et al., 1988; Mahadevan & Sharma, 2003; Arjomand et al., 2020b), salt precipitation (Giorgis et al., 2007; Pruess & Müller, 2009; Andre et al., 2014; Ott et al., 2015) and fines migration (Sayegh et al., 1990; Mohamed et al., 2012; Iglauer et al., 2014; Yusof et al., 2022).

When CO₂ is injected into saline aquifers, evaporation of liquid water into the CO₂ phase leads to a process where the dissolved salts precipitate. This phenomenon is broadly called “salting-out”; in this context, salts can precipitate in the wellbore vicinity (Kleinitz et al., 2001; Lorenz & Müller, 2003; Peysson et al., 2011). The dissolution of CO₂ alone is not expected to cause a significant decrease in the solubility of sodium chloride in water at elevated pressure/temperature (Sawamura et al., 2007; Zhao et al., 2015). However, the solubility of other salts (e.g., calcium carbonate) are strongly related to pH resulting from CO₂ dissolution into an aqueous phase. Regardless, precipitated salts are predominantly a result of water

evaporation and cause a decrease in porosity resulting in potentially poor injectivity. The impact of salt precipitation is most prominent when capillary-driven backflow is also present. Under this condition, formation water (with dissolved salts) flows back toward the injection well due to capillary suction. As evaporation continues, further accumulation of localized salt precipitates near the wellbore takes place (Giorgis et al., 2007; Pruess & Müller, 2009; Andre et al., 2014).

However, other studies found that injectivity impairment was insignificant in the presence of salt precipitation (Roels et al., 2014; Ott et al., 2015). In these experiments, precipitation formed homogeneously indicating the absence of capillary-driven back flow. This causes CO₂ to flow essentially as a single-phase when the porous media is virtually devoid of a water phase and the gas relative permeability increases to near unity. In other words, this overall mobility improvement results from the increase in relative permeability despite the effects of salt precipitation on absolute permeability. This specific phenomenon occurs only when CO₂ injection rate exceeds a certain critical rate (Andre et al., 2014; Ott et al., 2015; Miri & Hellevang, 2016). Below this critical rate, local precipitation due to capillary backflow can occur and the impact on mobility is more deleterious. However, the authors did not observe the phenomena in low permeability samples in which the formation of solid is supposed to affect the permeability significantly. Ott et al. (2021) conducted studies in a multi-porosity rock (i.e., dolomite) as opposed to Berea in their previous study showing that salt precipitation in this case strongly affects permeability.

For numerical simulations, evaporation of water into the CO₂ phase is typically described as a kinetic phenomenon instead of local equilibrium partitioning. This kinetics approach was first investigated by Roels et al. (2014) in their study which coupled experimental results with numerical modelling. They found that using local equilibrium partitioning in a computational simulation for evaporation overestimated salt precipitation near the wellbore. With a kinetics model, the salt precipitation both near the well bore and further away from the well is more accurately simulated. On the other hand, Ott et al. (2015) identified that evaporation may take place weakly during viscous force displacement until the brine is immobile within the pores. After a couple of hours of injection, brine saturation changes only slightly. After a longer period where the water saturation remains constant, salt precipitation begins to dominate suggesting that evaporation is strong. Based on this study, solid saturation should not exceed irreducible water saturation even though capillary driven backflow takes place.

Though water blockage is more common in hydrocarbon reservoirs (particularly tight gas reservoirs (Bennion, 2002)), water blockage can also take place when CO₂ is stored in deep saline aquifers. Water blockage occurs when the formation water forms a thin film on the

rock surface and occupies smaller pores leaving limited pore space for CO₂ to flow necessitating a high injection pressure. In other words, water blockage reduces gas relative permeability (Mahadevan & Sharma, 2003; Arjomand et al., 2020b; Lopez et al., 2021). The issue is common under strongly water-wet conditions (i.e., rocks composed predominantly of quartz) in sandstone reservoirs with invaded fluids which are used during drilling, completion, and fracturing activities (Holditch, 1979; Bennion et al., 1996; Al-Anazi et al., 2003). Those activities may use water-based fluids and considering that water is strongly wetting toward sandstone an increase in irreducible water saturation near the perforation can occur. This issue is usually unpredicted as core analysis in laboratory may show low connate water saturation. In fact, the core sample may have been cleaned/restored which diminishes the observed impact of operating fluids during drilling, completion, or hydraulic fracturing activities.

Several remediation methods have been proposed to overcome the above-mentioned injectivity issues. Salt precipitation can be alleviated temporarily by pre-injecting low salinity water into the well reducing brine salinity around the wellbore (Pruess & Müller, 2009). However, this method may only temporarily solve the problem by delaying or moving the location of the precipitation. As evaporation keeps taking place, immobile brine will extend causing salt precipitation albeit a bit later. Furthermore, injecting low salinity water can induce clay mineral activity causing other forms of damage (i.e., fines migration, and clay swelling). Another effort recently proposed and tested at the Quest CCS facility located in Alberta, Canada (Smith et al., 2022) used a water-based fluid to dissolve precipitated salts near the wellbore. This method succeeded in repairing the injectivity index to twice the pre-treatment value. However, there is no further evaluation regarding the possibility of water blockage following the treatment and fines migration induced by the water injection into the formation.

Regardless, it is worth noting that injection of CO₂ could vaporize trapped brine (causing salt precipitation) as well as induce water blockage (Bennion et al., 1996). Generally, injectivity worsens with salt precipitation deteriorating the absolute permeability (Zuluaga & Monsalve, 2003). In some case, a high drawdown pressure remediates this issue (Bennion et al., 1996). Another approach is to use a chemical treatment to change the rock wettability and hence permanently impact the extent of water blockage. This includes injecting supercritical CO₂ with an organo-alkoxysilane component (i.e., sc-CO₂ based silylation) to chemically functionalize the rock surface and change the formation wettability toward less water wet thereby addressing water blockage (Arjomand et al., 2020b). This technique even outperforms conventional silylation using organic solvents by accelerating the kinetic reaction rate (i.e., the sc-CO₂ based accomplishes the reaction within 30 minutes compared to 24 hours for conventional method under otherwise similar conditions) (Sánchez-Vicente et al., 2014); a modest increase in coverage is also observed with this approach. Silane reagents have the

general chemical formula R_nSiX_{4-n} , where “R” represents a non-hydrolysable organic group and “X” represents hydrolysable groups (typically halides or alkoxy groups). During the silylation process, organo-alkoxysilane modifies the rock surface by reacting with the hydroxyl groups on the rock surface (through a hydrolysis/condensation process) to form covalent bonds. Several studies which performed sc-CO₂ based silylation on mesoporous silica found that silane reaches up to 1.6 molecules per nm² of surface (Staroverov & Fadeev, 1991; Cao et al., 2001; López-Aranguren et al., 2012). A recent study that used N,N-dimethylaminopropyltrimethoxysilane (DMAPTS) in a sc-CO₂ based method on mesoporous silica reached a bonding density of approximately 2.5 molecules/nm² (Sánchez-Vicente et al., 2014).

To date, there have been several studies coupling experimental data with numerical simulations to evaluate formation damage due to salt precipitation during CO₂ injection (Roels et al., 2014; Andre et al., 2014; Ott et al., 2015; Roels, et al., 2016; Ott et al., 2021). Also, water blockage has been observed frequently in gas reservoirs particularly with the development of low permeability gas reservoirs; the impact of CO₂ injection on water blockage has been examined as well (Ford et al., 1988; Bennion et al., 1996; Bennion, 2002; Mahadevan & Sharma, 2003; Arjomand et al., 2020b; Lopez et al., 2021; Lopez et al., 2023). However, such studies have only these issues on their own and not examined how they are coupled. This study attempts to simulate both water blockage and salt precipitation in a single numerical reservoir simulation and to analyse the impact of surface wettability (i.e., changes induced by the silylation process) when both take place in situ. The purpose of this study is to develop a deeper understanding of the corresponding phenomena during CO₂ underground storage and well preparation before the implementation of a chemical treatment.

3.2. Numerical Simulation Model

3.2.1. Component Transport Equations

This work uses the same conservation equations that were used by Kohse and Nghiem (2004) to model the deposition of solid asphaltene from crude oil within a reservoir. This includes the basic components flow, asphaltene deposition rate (in this study, replaced by salt precipitation rate), and a materials balance of the deposited solids with the asphaltene present in crude oil. We use a similar model here noting that supercritical CO₂ will be treated as the gas phase. Silane injection is simulated under miscible condition with CO₂. Silane then will be adsorbed on rock surface as an outcome of silylation process where it will have minimal impact on the porosity and assumed to only affect the wettability characteristics (i.e., the multi-phase relative permeability behaviour). As silane acts like polymer within a porous media, transport equation normally used in polymer enhanced oil recovery is applied in this work.

The accumulation terms of the flowing components and the adsorbed silane can be written as (Druetta and Picchioni 2019; CMG 2020):

$$\frac{\partial}{\partial t} [V\phi_f(\rho_g S_g y_i + \rho_w S_w w_i) + V\phi_v c_{sil}] \quad (9)$$

where V is the grid block volume, ρ and S are the phase molar density in mol/m³ and phase saturation, respectively, c_{sil} is the moles of adsorbed silane within the void pore volume in moles/m³, y_i and w_i are moles fraction of component- i – which are water, CO₂, and dissolved salt – in the gas and water phases, respectively. ϕ_v and ϕ_f are void porosity and fluids-contained porosity, respectively. The relationship between ϕ_v and ϕ_f are proposed to consider the presence of solid salt (denoted as “salt”) and/or adsorbed silane. They are related following this formula:

$$\phi_f = \phi_v [1 - (c_{sil}/\rho_{sil} + c_{salt}/\rho_{salt})] \quad (10)$$

where c and ρ are the moles of the component per void pore volume and their molar density. When there is no solid and/or adsorbed component, then $\phi_f = \phi_v$. In this simulation, the small concentration of silane used has an insignificant impact on porosity with salt precipitation being the only solid which appreciably affects porosity.

The conservation equation for solid salt formation is written below (Parvin et al., 2020; CMG, 2020):

$$\frac{\partial}{\partial t} (\phi_v c_{salt}) = r_{salt} \quad (11)$$

where r_{salt} is a volumetric rate of salt formation in moles/day.m³.

3.2.2. Fluids and Mechanistic Models

Salt Precipitation

For this study (and similar to prior studies), the aquifer brine is assumed to be composed of only halite (i.e., sodium chloride) and water. The effects of minor impurities on salt precipitation due to evaporation are not considered here. The modified black oil (MBO) fluid model within the reservoir simulator Computer Modelling Group (CMG) was used with the STARS module. This simulator can also implement the kinetics of the evaporation process.

Experimental results obtained by Ott et al. (2015) with a 20 wt.% NaCl aqueous solution and numerical simulations results by Roels et al. (2014) were used to generate the salt precipitation kinetic model. A non-equilibrium phase partitioning was applied for the

evaporation of water from the aqueous phase. This process results in an increase of salt precipitation which induces the precipitation. The mass transfer of water toward CO₂ phase was simulated with a closer match between experimental results of salt precipitation distribution and subsequent numerical simulations, using kinetic approach following the reaction rate as follow (Pinder & Celia, 2006; Roels et al., 2014):

$$r = k' \phi_v (c_{H_2O,e} - c_{H_2O}) \quad (12)$$

where r and k' are the evaporation rate (units of moles·day⁻¹·grid volume⁻¹) and reaction rate constant (units of day⁻¹ for a first order reaction), respectively. c_{H_2O} and $c_{H_2O,e}$ are the concentration factor (moles per void pore volume) of H₂O in the CO₂ phase at any time and its equilibrium concentration (moles per pore volume), respectively. Under these conditions, the maximum (or equilibrium) mole fraction of water in the CO₂ phase was set at 0.004 (Ji et al., 2005; Spycher & Pruess, 2005; Miri & Hallevang, 2016). CO₂ solubility in water is important during the CO₂ injection into saline aquifer as it is responsible for the solubility trapping mechanism. However, within this context, the role of dissolved CO₂ does not appreciably affect salt precipitation and as such is not considered in this work. Dissolved CO₂ may induce mineralization near the wellbore such as Calcite precipitation. However, the amount of Calcite precipitation is negligible compared to that of Halite precipitation as shown in simulation results by Cui et al. (2018). The STARS module in the CMG simulators uses a specific factor “ f ” designed to explain weak evaporation processes when viscous forces are dominant. This factor is a function of water velocity and governed by the following equations (CMG, 2020):

$$f = \left[\frac{v - v_{crit}}{v_{ref}} \right]^m \quad (13)$$

$$k' = k'_{ref} \cdot f \quad (14)$$

where v , v_{crit} , and v_{ref} are the current, critical and reference velocities of water, respectively (see Table 1). The constant m is set negative resulting in a smaller factor for larger water velocities. Due to a non-zero rule for v_{ref} , it was fixed at a very low water velocity. This number was obtained from the water velocity near the residual water saturation in a traditional coreflood simulation performed before defining onset of the evaporation process. Then, the reaction rate constant varies based on the velocity of water following Equation (5) and (6). k'_{ref} is the reaction rate constant at v_{ref} which is a fitting-parameter in this case. k'_{ref} is assumed to be the maximum reaction rate constant and is applied to trapped brine up to $v_{ref} + v_{crit}$.

Once salt saturation is reached in the aqueous phase, salt precipitation will commence. In fact, halite solubility in water is only moderately sensitive to temperature changes up to 80 °C and pressures up to 10 bar (Pinho & Macedo, 2005; Sawamura et al., 2007). As such, a constant salt solubility of 26.5 wt.% (or 0.1 mole fraction) was utilized to simplify the numerical simulation. During the evaporation process, once saturation is reached the solid salt is assumed to instantly form until the brine has been completely dried. For this simulation, however, the mass transfer of the salt from aqueous solution to solids uses a kinetic approach with a large rate constant as described by Equation (12). Kohse & Nghiem (2004) used a value of 50,000 day⁻¹ to represent the equilibrium process of a mass transfer for asphaltene deposition which is assumed to be very fast in their simulation; we use the same value here.

Table 1. Parameters used in the simulation describing the salt precipitation modelling based on the experiment conducted by Ott et al. (2015)

$v_{ref}=v_{crit}$	1.19 x 10 ⁻⁵ m/day
m	-0.95
k'_{ref}	3850 day ⁻¹

Permeability Reduction Model due to Salt Precipitation

Salt precipitation definitively reduces the porosity of the rock formation; with a strong positive correlation between permeability and porosity, the permeability is also expected to drop. A variable resistance factor (R_f) is introduced to quantify the permeability reduction induced by salt precipitation. The relationship is written by (CMG, 2020):

$$R_f = \frac{k_0}{k} \quad (15)$$

$$R_f = \max[1, g(c_{salt})] \quad (16)$$

where c_{salt} , k_0 and k is the moles of solid salt within the void pore volume, initial and salt deposition-induced permeability values, respectively. R_f will not be less than 1 and increase as the salt precipitation increases. The function $g(c_{salt})$ can be defined with any porosity-permeability relationship (e.g., Kozeny-Carman, Verma-Pruess or a regression model based on results from core flooding experiments). Higher incremental R_f over a change in porosity is supposed to be applied on low permeability formations as the change is very sensitive in this characteristic. Several studies utilized critical porosity, at which permeability drops to zero due to solid deposition, in a range of 85-90 % of the original porosity (Pruess & Müller, 2009;

Andre et al., 2014; Ott et al., 2015; Ott et al., 2021). Giorgis et al. (2007) performed a simulation study in relatively high permeability by using a critical porosity of 50% of the original porosity.

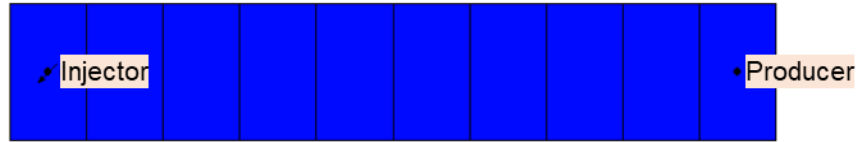


Figure 13. Grid model employed in this work representing the core used by Ott et al. (2015)

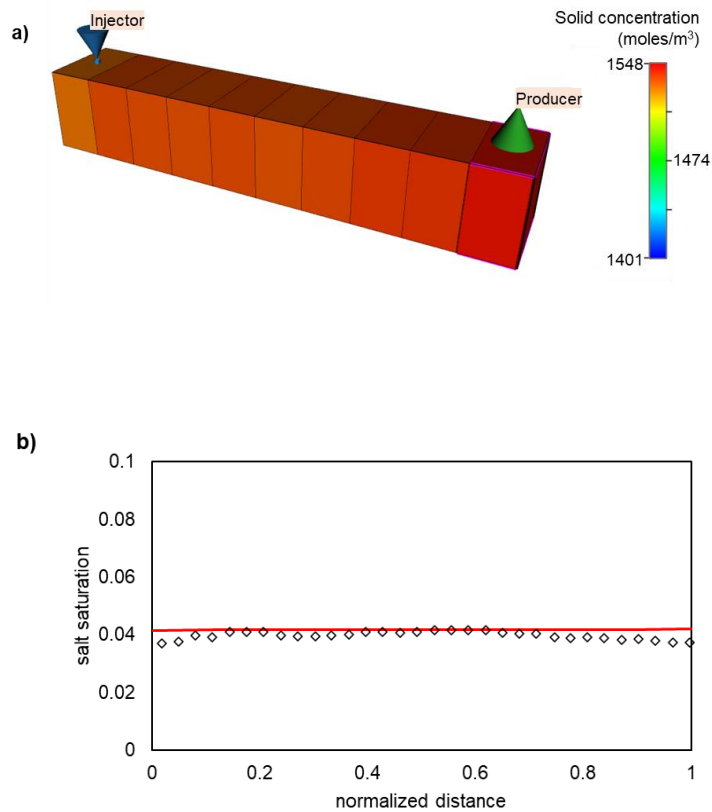


Figure 14. a) Salt concentration yielded from simulation and b) salt saturation in the simulation results (—) compared to that in the experimental results (◊◊) which the data taken from work conducted by Ott et al. (2015)

To determine the fitting parameters in Table 1 and an approximation to $g(c_{salt})$, a 1-D simulation (with the grid model shown in Figure 13, each cell has dimensions of 0.5 (length) x 1 (width) x 1 (thickness) cm) was performed based on the experiment results obtained by Ott et al., (2015). These fitting parameters were then used in the larger scale simulation for this study. CO₂ injection is simulated at a rate of 0.0062 m³/day (4.4 cm³/min) into a water-saturated model. It is assumed that $v_{ref}=v_{crit}$ to represent a low water velocity in which the evaporation rate is maximum. Salt saturation and differential pressure obtained in the

simulation show good agreement with the experimental results, as can be seen in Figure 14 and 15. Ott et al. (2015) used porosity-permeability relationship proposed by Verma & Pruess (1988) to describe these results as it has more flexible fitting parameters. The function $g(c_{salt})$ used in this work is described by Equation (17) (Wang & Liu, 2014; Choi et al., 2015; CMG, 2020) and the comparison with experimental data from Ott et al. (2015) is shown by Figure 16.

$$g(c_{salt}) = 1 + (rrf - 1) c_{salt} / c_{salt,max} \quad (17)$$

where rrf is a resistance factor constant and $c_{salt,max}$ is the maximum amount of salt expected present in a pore volume (moles/m³.pore volume). rrf is a fitting parameter and is adjusted to obtain a qualitative best-match of the porosity-permeability reduction relationship with the experimental data. In this work, 60 was used for the rrf . $c_{salt,max}$ is obtained from the maximum salt precipitation observed in the experiment. The maximum salt saturation is 0.4 which equates to 14,784moles/m³. The latter number was used in this simulation as $c_{salt,max}$.

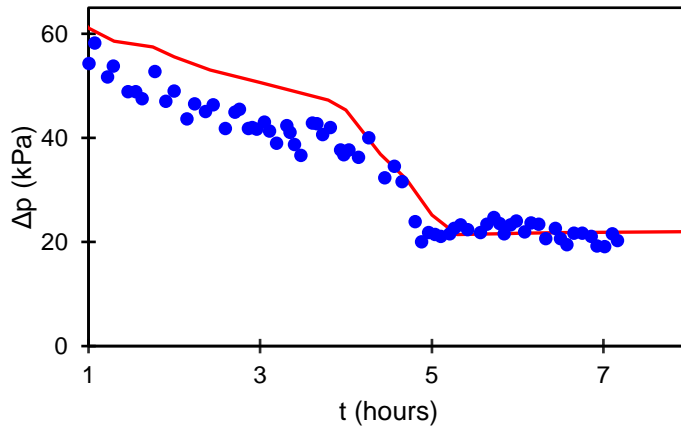


Figure 15. Pressure difference obtained in the simulation results (—) compared to that in experimental results (●)

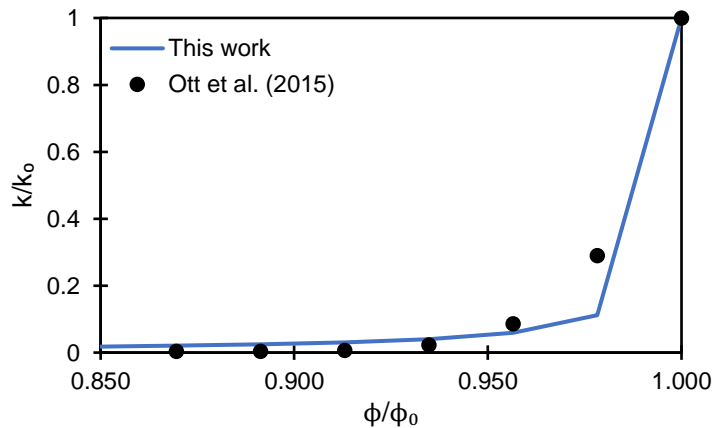


Figure 16. Permeability reduction model between reference study (●) which the data taken from work conducted by Ott et al. (2015) and this work (—)

Evaporation also decreases the trapped brine saturation causing an increase in the relative permeability for CO₂. When the formation becomes completely dry, CO₂ flows as a single phase. In this work, gas relative permeability beyond the connate water saturation (S_{wc}) was modelled linearly increasing from its endpoint at S_{wc} towards unity. This is also applied to cases where water blockage takes place. The relative permeability curves used in the simulation can be seen in Figure 21 and the extrapolation during drying-out is annotated as a dashed line in Figures 21 and 22.

Water blockage model

Water blockage is a severe decrease in the relative permeability of water due to a strongly water wet formation characteristic. This issue is particularly exacerbated in low permeability reservoirs and restricts the flow of CO₂ due to high amount of remaining brine within the pore space limiting the ability for CO₂ to flow (Bennion, 2002). Consequently, the impact of this issue decreases as water saturation reduces. Water blockage is most common after using water-based fluids or muds for drilling or completion activities; there will be an unusual condition characterizing the invaded zone near the wellbore. This is modelled by separating the invaded zone from the rest of the reservoir (see Figure 21). This zone should be very strongly water-wet compared to the original formation wettability with a higher S_{wc} and lower k_{rg} (gas/CO₂ relative permeability) at S_{wc} . Relative permeability curves used to represent the water blockage are shown by Figure 17a. The curve was constructed based on the flooding results from a core that exhibited water blockage issue as performed by Arjomand et al. (2020b) (as core GB.4). Figure 17b was synthetically constructed using the empirical correlations (Eq. 18-19) (Benson et al., 2013) for a typical sandstone formation which has $S_{wc} = 0.2$ (common value for Berea sandstone), exponents of 1.6 for n_g and 2.7 for n_w , k_{rw}' (water relative permeability end-point) = 1, and k_{rg}' (k_{rg} end-point) = 0.66 (Bennion & Bachu, 2008; Krause et al., 2011; Krevor et al., 2012).

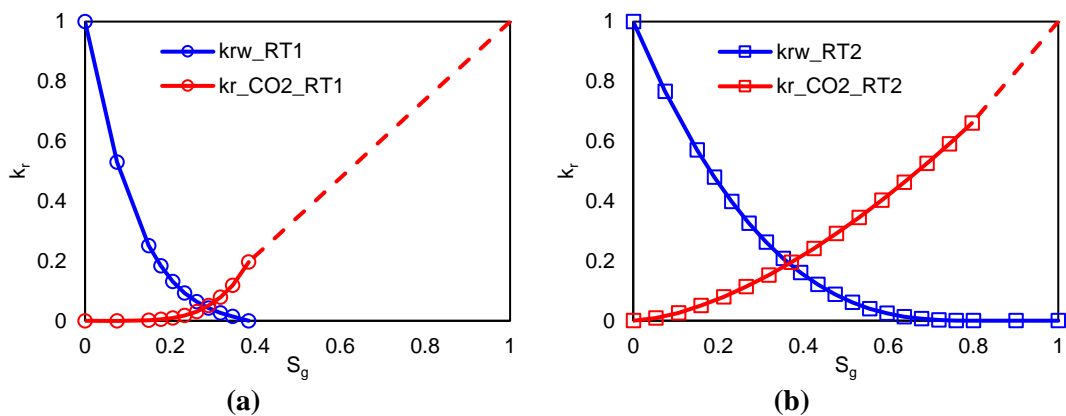


Figure 17. Relative permeability of a) the zone affected by water blockage (RT-1) and b) original condition (RT-2)

$$k_{rw} = k_{rw}' \left(\frac{S_w - S_{wc}}{1 - S_{wc}} \right)^{n_w} \quad (18)$$

$$k_{rg} = k_{rg}' \left(\frac{1 - S_w}{1 - S_{wc}} \right)^{n_g} \quad (19)$$

Silylation process model

The experimentally determined impacts of sc-CO₂ based silylation on the rock wettability (therefore relative permeability curves) was implemented to remediate water blockage. The type of silane used in this work has a formula of R₁SiX₃, where R is an unhydrolysable organic group and X is a hydrolysable group such as halogen, alkoxy, etc. (Combes et al., 1999). Experimental results obtained by Arjomand et al. (2020b) for core GB.4 using silane reagent of (3-chloropropyl)triethoxysilane (CPTS) were integrated into this study. Other properties of this chemical and core sample are listed in Table 2 and 3, respectively. The experiment was operated at 21 MPa and 60 °C.

Table 2. Basic properties of silane reagent used in the experiment performed by Arjomand et al. (2020a)

Chemical formula	C ₉ H ₂₁ ClO ₃ Si
Silane density at 25 °C	1,000 kg/m ³
Molecular weight	240.8 kg/kmol
Boiling point	221.15 °C
Cloud point at 60 °C	9.8 MPa

Table 3. The properties of Core GB.4 used in the experiment performed by Arjomand et al. (2020b)

Quartz content	63.9 wt%
Diameter	0.038 cm
Length	0.076 cm
Porosity	0.191
Permeability	2.02 x 10 ⁻¹³ m ²

In the simulation, CPTS is co-injected with CO₂ under a miscible state at the operating condition. Two processes are included for silylation process, i.e., hydrolysis and condensation. In fact, those processes are very sensitive depending on many conditions such as pH of brine, presence of catalyst, chemical properties of the silane, brine salinity, silane concentration, etc.

(Issa & Luyt, 2019). The kinetics of this process will be complicated to model at the field-scale of these numerical simulations. In this study, hydrolysis and condensation of CPTS were assumed to occur instantly once CPTS interacts with brine. This assumption was taken since silylation takes less than a day to complete which is very short compared to the whole simulation period. Considering the economic aspect, silane may not be injected continuously for long time. In this work, silane injection was simulated for 2 days from the beginning of injection to affect a wettability change in the near wellbore region most affected by water blockage.

Mechanistically, water is detached from the rock surface following the condensation leading to a more hydrophobic surface. However, this microscale process was simplified considering the wellbore-drainage-scale used in this work. The release of water component after condensation was coupled with wettability alteration triggered by silylation. In this work, once the silane invades the water blockage impacted zone, the relative permeability curves shift toward less water-wet instantly. This process infers the reduction of connate water saturation due to silylation as described in Figure 18.

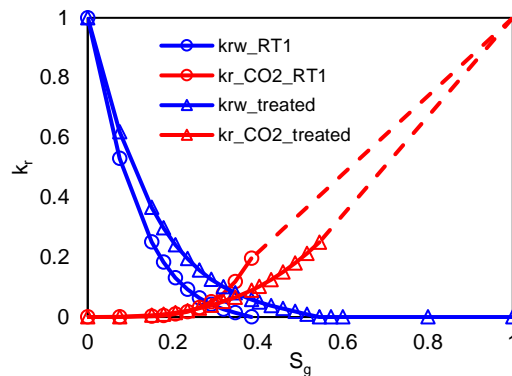


Figure 18. Relative permeability of pre- (impacted by water blockage, RT-1) and post-treatment of silylation. Modified from results obtained by Arjomand et al. (2020b)

3.2.3. Radial Single Well Model

The results obtained from the experiments are scaled up to a larger radial single-well model. The schematic and properties of the radial model can be seen in Figure 19. The grid size is increased logarithmically away from the injector towards the outer radius. The vertical layering is composed of 10 grids with identical thickness. The injector is perforated in the first-six grids (indicated by arrows, see Figure 20) from the formation top. The model edge was set to open flow to represent an infinite boundary. The top and bottom boundaries of the model were set closed (no-flow). A temperature and pressure of 58.9 °C and 16 MPa, respectively, were applied to represent a deep saline aquifer.

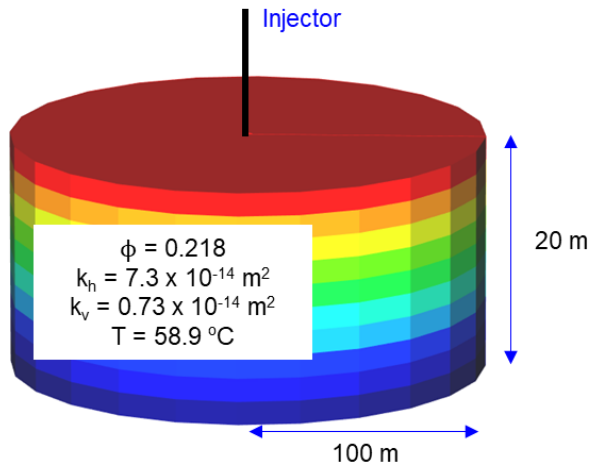


Figure 19. Schematic of radial single well model and the rock properties. Colour scale is referred to Fig. 20.

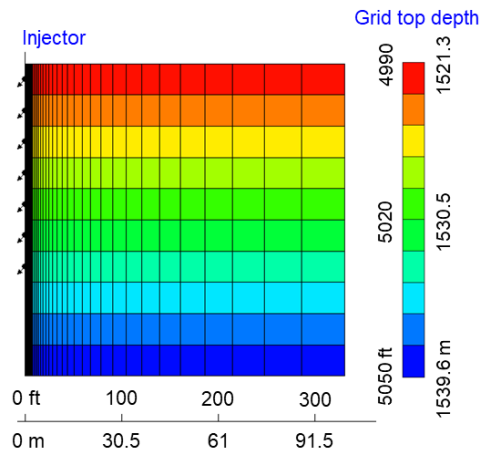


Figure 20. Cross-section of radial single well model

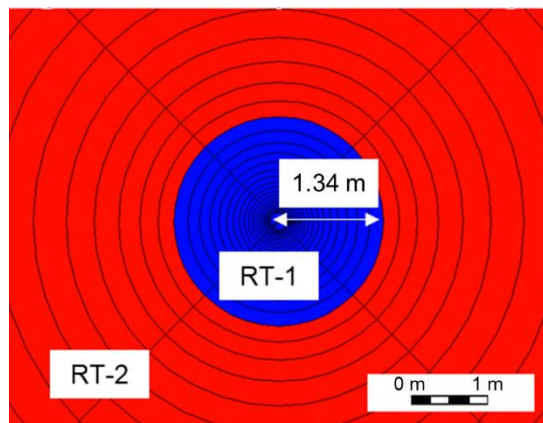


Figure 21. Schematic of zone affected by water blockage where silylation takes place (RT-1; blue coloured zone) and original characteristics (RT-2; red coloured zone)

In Figure 21, two rock types were assigned to represent an invaded zone (i.e., zone RT-1 which is characterized by water blockage). This zone extends to 1.34 m measured from the injector as shown by Figure 9. Figure 5 shows the different characteristics of both rock types in terms of relative permeability. Relative permeability of treated zone by silylation is provided in Figure 6. If silane invades RT-2, it is assumed to have no effect on the relative permeability characteristics.

Six cases including a base case were developed to elucidate the impacts of silylation on a reservoir impacted by water blockage/salt precipitation. Cases 1 to 3 are designed to observe the impacts of water blockage and salt precipitation both separately and simultaneously. Case 4 and 5 are designed to examine the role of silylation reducing the severity of injectivity loss caused by these issues. A similar constraint toward injection well is used for all cases, i.e., constant injection rate of 193.4 tonnes/day. The simulation ends after 455 days. The information summarizing the cases is shown in Table 4.

Table 4. Details of case studies developed in this study.

Case	Water blockage	Salt Precipitation	Silylation
Base case			
Case 1	√		
Case 2		√	
Case 3	√	√	
Case 4	√		√
Case 5	√	√	√

3.3. Results & Discussion

3.3.1. Scaling-up Well Injectivity Issues Simulation

The primary aim of this study is to elucidate qualitatively the efficacy of a silylation treatment (causing a wettability changes) to address the impacts of water blockage and salt precipitation on CO₂ injectivity. With that in mind, for the purposes of simulation scale-up, some adjustment regarding the process parameters needs to be considered. The simulation parameters used for salt precipitation were derived from experimental results obtained at a lower pressure and temperature (i.e., 10 MPa and 45 °C, respectively) compared to those which used for radial single-well simulation (i.e., 16 MPa and 58.9 °C, respectively) here. Increasing the temperature improves the solubility of water in the CO₂ phase leading to enhanced evaporation. On the other hand, the higher pressure slows the evaporation rate of water (Zuluaga & Monsalve, 2003). For the simulation in this study, the solubility (mole fraction)

of water in CO₂ is assumed to be 0.007 for the selected conditions (Ji et al., 2005; Spycher & Pruess, 2005; Miri & Hallevang, 2016). For the purposes of this qualitative assessment, no other parameters were adjusted. This work is considered as the worst case of precipitated salt while specific experimental work can be conducted to obtain representative parameters at higher pressure conditions. On the other hand, the water blockage model does not employ process parameters that are generally sensitive to pressure and temperature. Therefore, parameter adjustment is not necessary for this issue in terms of simulation scale-up from core-scale toward radial single-well.

Analysis is conducted toward injectivity index (J) (akin to permeability) of each case study. The injectivity index is defined as the amount of CO₂ which can be injected for a unit of pressure drop (i.e., $p_{injection} - p_{aquifer}$, as described in Equation 20). Injectivity loss as the impacts in the case studies are evaluated as the relative injectivity change (RIC) as represented by Equation 21 (Sokama-Neuyam et al., 2017; Yusof et al., 2022). Both parameters are mathematically defined as:

$$J = \frac{q_{inj}}{\Delta p} \quad (20)$$

$$RIC = 1 - \frac{J_i}{J_{bc}} \quad (21)$$

where q_{inj} and Δp are injection rate in tonnes/day and pressure drop in MPa, respectively. Subscripts -i and *bc* refer to case-*i* to which the results are evaluated and the base case, respectively. In this work, the CO₂ injection rate is the same and constant for all cases. Since the boundary is infinite, $p_{aquifer}$ is assumed unchanged during over the entirety of simulated time-period. For comparison purposes, the pressure at bottom of the well is used for these calculations.

Injection pressure in the early period (i.e., initial 10 days) of case 1 is up to 0.14 MPa higher than that of the base case as depicted in Figure 22. This is caused by the condition in which CO₂ remains static until gas saturation reaches 0.15 (the so-called critical gas saturation) as can be shown by Figure 17a. Gas mobility is also dropped due to high amount of immobile water around the vicinity of perforation. Limited space for gas flowing causes higher pressure during the injection. As shown by Figure 22, injection pressure of case 1 stays higher than that of base case throughout the first 10 days of the simulation. At the end of this period, a high amount of water is still trapped near the well bore area as shown in Figure 23a thus reducing CO₂ mobility.

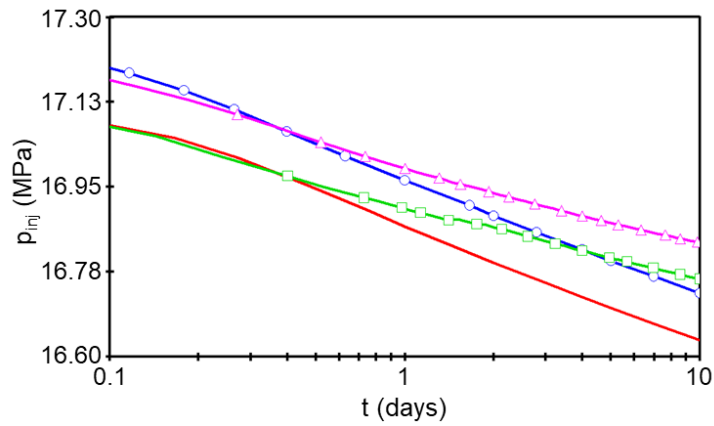


Figure 22. Injection pressure for base case (—), case 1: water blockage exists (—○—), case 2: salt precipitation exists (—□—), and case 3: both issues exist (—△—)

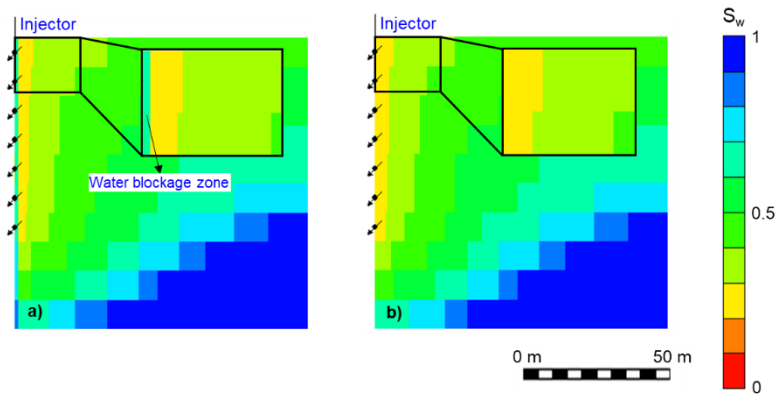


Figure 23. Distribution of water saturation at the end of simulation which shown in full scale model for a) case 1: water blockage exists and b) base case

Injection pressure of case 2 is noticeably higher than that of base case after a certain period of injection due to the initiation of salt precipitation. This indicates that the water has been displaced around the perforation close to the irreducible saturation. Under this condition, evaporation is at its maximum rate. However, water blockage (represented by case 1) deteriorates the well injectivity worse than that caused by salt precipitation (represented by case 2) during this early injection period. Over this period, salt precipitation continues causing an ever-increasing damage to the well injectivity (as indicated by a pressure difference between case 2 and the base case). Thus, the bottom-hole pressure of case 2 is higher than that of case 1 after 4 days of injection (see Figure 22).

Case 3 (which simulates the combined effects of water blockage and salt precipitation) yields higher injection pressure than those of base case, case 1 and case 2 at the early period of injection. The impacts of water blockage, which should be dominant during this period, are combined with the effects of evaporation which cause decreasing water saturation. The

injection pressure for case 3 becomes higher than those of other cases after the first day of injection. Since the amount of trapped brine in this case is higher than that of case 2, the resulting salt precipitation is also larger, resulting in a more severe impact on injectivity.

For the base case, the injectivity index continuously increases (with the rate of increase tapering with time) throughout the longer 455-day simulation (see Figure 24). For this case, the pseudo-steady state might have not been reached within this period. This is presumably caused by the open system used in this simulation to represent the infinite lateral boundary. Similar behaviour was observed by Meng et al. (2015) who studied the effect of boundaries affecting pressure profile buildup and salt precipitation distribution. From their study, for the case of an open boundary system, the pressure buildup near the wellbore keeps decreasing gently (i.e., inverse relationship to injectivity index) although salt has been precipitated. This pattern is also observed at the infinite-acting flow regime before pseudo-steady state takes place.

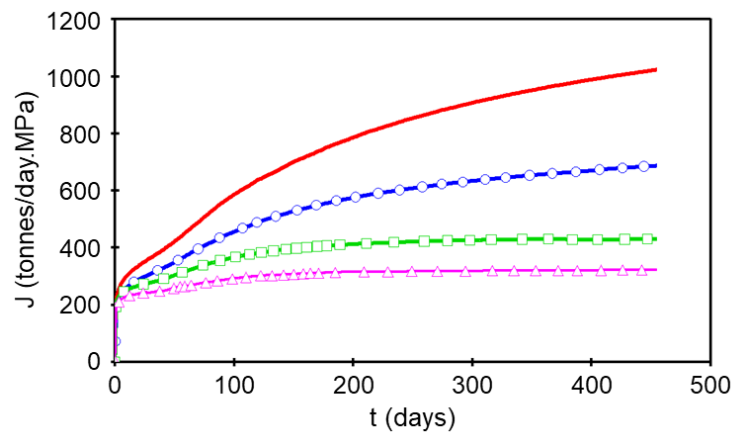


Figure 24. Injectivity index for base case (—), case 1: water blockage exists (—○—), case 2: salt precipitation exists (—□—), and case 3: both issues exist (—△—)

On the other hand, water blockage (case 1, which the simulation limits to a distance of less than 1.34 m from injector) deteriorates the injectivity up to 32.9% after 455 days of injection period, as shown by Table 5 and Figure 24. That considerable injectivity loss is caused by only a higher injection pressure required due to the large amount of water trapped near the wellbore. More severe damage is identified when salt precipitation takes place either in case 2 or 3 with an injectivity collapses up to 58% and 68.6% for cases 2 and 3, respectively.

The distribution of precipitated salt for case 2 at the end of the 455-day simulation is shown in Figure 25a with precipitated solid extending approximately 6.1 m from the well. A nearly identically affected distance is observed in case 3. However, as shown in Figure 25b, the solid saturation in the water blockage zone of case 3 lies between 0.06-0.18 while that in

case 2 lies between 0.03-0.05. A sharp decrease in the solid saturation in case 3 is identified between the invaded and uninvaded zones (see Figure 13b); the irreducible water saturations are substantially different as described by k_r curves in Figure 17a and 17b. This variation of immobile saturation provides different amounts of prospective salt which can then precipitate. However, the amount of solid deposited (i.e., very little) within the uninvaded zone in case 3 seems to be similar to that in case 2.

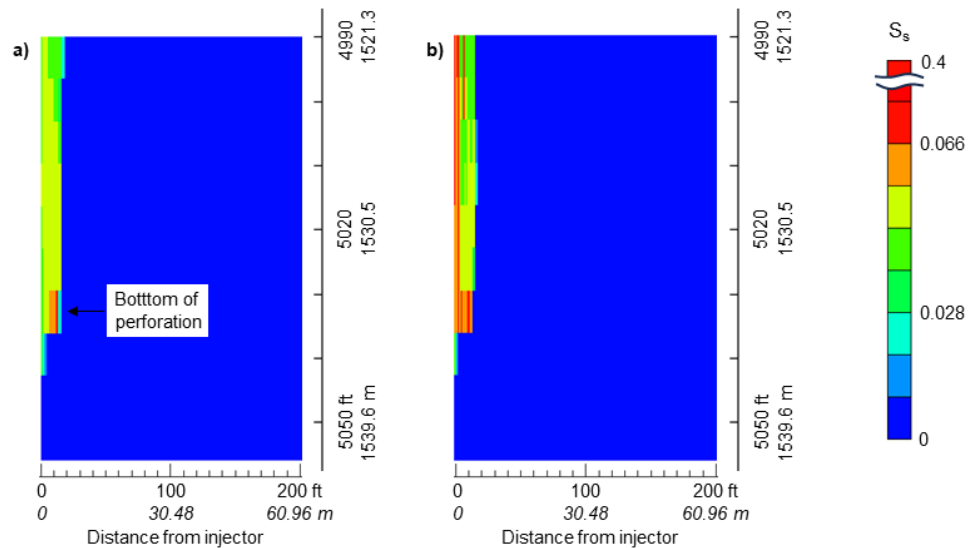


Figure 25. Distribution of solid saturation for a) Case 2: salt precipitation exists and b) Case 3: water blockage and salt precipitation exist, at the end of simulation

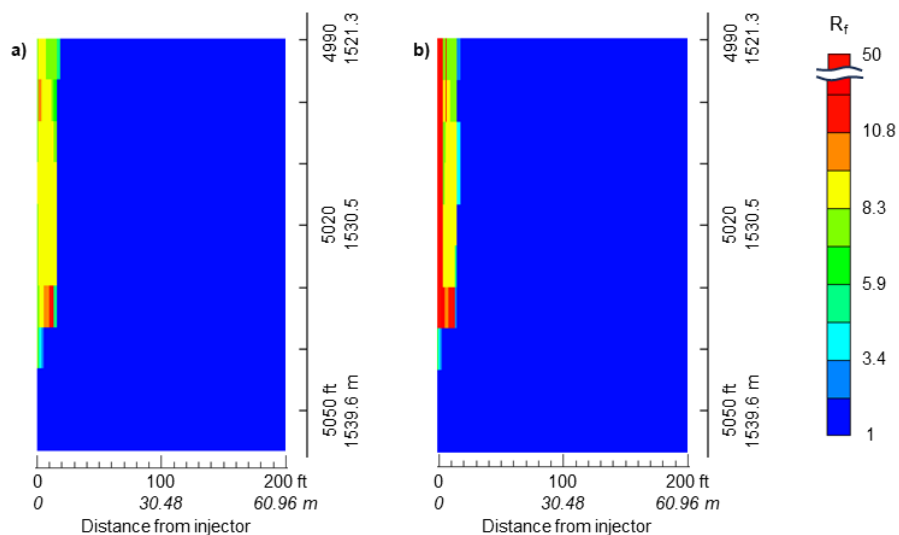


Figure 26. Resistance factor applied on a) Case 2: salt precipitation exists and b) Case 3: water blockage and salt precipitation exist, at the end of simulation

An accumulation of salt is captured at the bottom of the perforation in both cases. Capillary-driven backflow of brine, which was also modelled in the simulation, supported by buoyant effects causes the accumulation of salt at the bottom of perforation. Due to those processes, brine flows downward to the injection well direction. The resistance factor for case 2 varies from 6 to 11.5 (which means the permeability for case 2 is 8.7-16.7% of its original number in the base case) and indicative of the impact of solid salt precipitation on injectivity (see Figure 26a). The impact of salt combined with water blockage results in an increase in the resistance factor to between 10.7 to 50 (i.e., a permeability of 2-9.3% of the original permeability in the base case) (see Figure 26b).

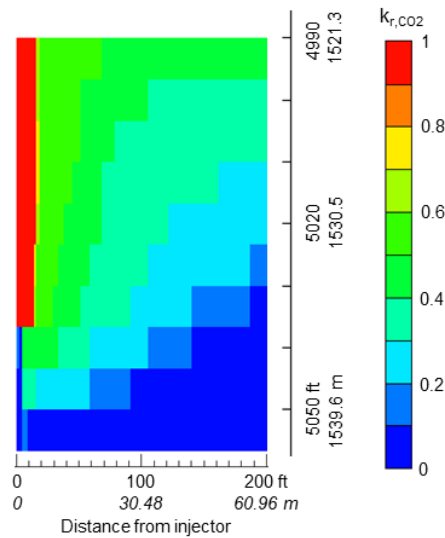


Figure 27. k_{r,CO_2} at the end of simulation of Case 3: water blockage and salt precipitation exist

As previously elaborated in Section 2, injecting CO_2 may help to alleviate water blockage as the water component within the invaded zone is evaporated by continuous stream of injected CO_2 . At the simulation end for case 3, the CO_2 relative permeability (see Figure 27) is near unity in the invaded zone showing that the pore space has been effectively dried completely (i.e., CO_2 flows as a single fluid within the pore space). Thus, the CO_2 relative permeability is increased under this condition where water blockage is insignificant. However, evaporated water turns the brine more saline; eventually, the solution becomes saturated resulting in precipitate formation with further evaporation. The damage to the injectivity for case 3 is even worse than that caused by either case 1 or 2. From this condition, the relationship between water blockage and salt saturation becomes clear. Water blockage diminishes when evaporation takes place; however, this also induces salt precipitation. In this strongly water wet formation, the zone impacted by water blockage exhibits enhanced salt precipitation. Furthermore, intensive salt precipitation occurs in the volume near the well perforation since

brine remains immobile behind the front and fresh CO₂ invades that zone rigorously. Below the well perforation, evaporation is minimal resulting in dramatically less salt precipitation in this zone (see Figure 25).

3.3.2. Simulation of Cases Applying Silylation

For this study, silylation is applied to remediate water blockage around the wellbore by changing the wettability characteristics. The injection pressure for case 4 (representing water blockage and silylation) is slightly decreased compared to case 1 (representing water blockage only) (see Figure 28). This may be due to some reasons. Basically, this results from the CO₂ relative permeability decreasing due to this treatment (see Figure 18). The CO₂ relative permeability for the post-treatment state remains lower than that of pre-treatment up to the original irreducible brine saturation. However, the injection pressure for case 4 is lower since some trapped brine near the wellbore has been displaced due to the treatment. As a consequence, the gas saturation enlarges which, in turn, increases the end-point CO₂ relative permeability. The effect of the silylation treatment is more noticeable for brine mobility as indicated by Arjomand et al. (2020b). Similar comparisons between cases 3 and 5 can be made.

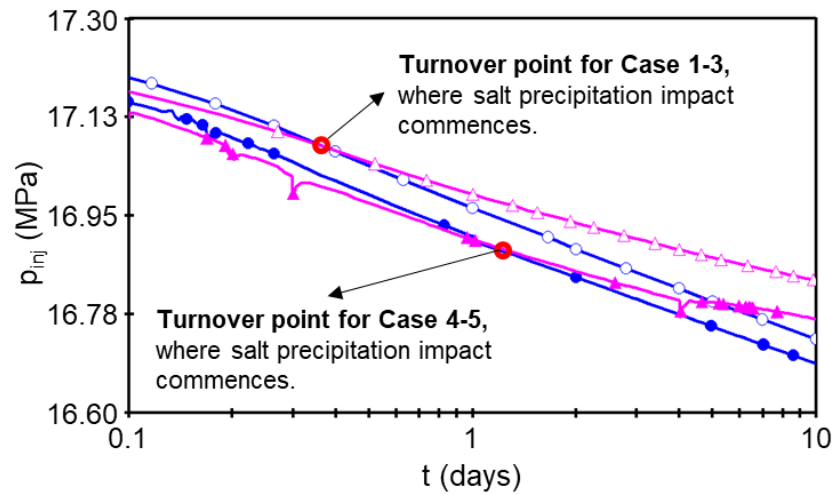


Figure 28. Injection pressure for Case 1: water blockage exists (—○—), Case 3: water blockage and salt precipitation exist (—△—), Case 4: silane treats Case 1 (—●—), and Case 5: silane treats Case 3 (—▲—) in the early period

Comparing cases 1 and 4 or cases 3 and 5, the application of alkoxysilane co-injected with sc-CO₂ decreases the severity of injection loss as shown by Figures 28 and 29. As the silylation is assumed to occur instantly over the simulation timescale, a lower injection pressure is observed from the beginning of the simulation. On an absolute basis, this method counteracts the injectivity index by approximately 5-7%. This number when silylation shifts the wettability represented by a decrease in irreducible water saturation from approximately

0.55 to 0.40 (see Figure 18). The improvement in injectivity seems unchanged beyond 90 days. The role is supposed to be more significant when dealing with strong water-wet and wider invaded zones in the targeted aquifer formation.

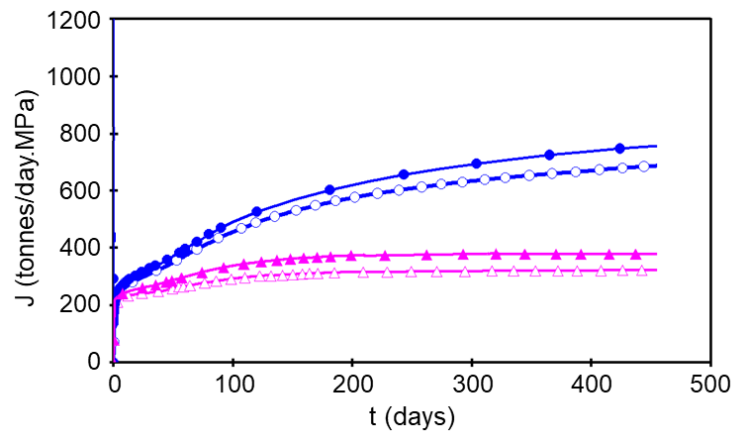


Figure 29. Injectivity Index for Case 1: water blockage exists (—○—), Case 3: water blockage and salt precipitation exist (—△—), Case 4: silane treats Case 1 (—●—), and Case 5: silane treats Case 3 (—▲—)

During the early period (i.e., up to 10 days), comparing case 5 with case 3, a reduction in the injection pressure is observed (see Figure 28). Comparing cases 4 and 5, the effects of salt precipitation on injection pressure are not evident until after 2 days (as indicated by nearly coincident lines); salt precipitation then acts dominantly after that period which is indicated by the lines becoming separated (see red circle symbols in Figure 16 indicating turnover point). Comparing cases 3 and 5 (see Figure 30), after both 90 days and 455 days, the silylation treatment decreases the salt precipitation immediately around the wellbore leading to precipitation further from the wellbore. After 90 days of injection in case 3, the invaded zone has been dried and 6-15% of pore has been filled by precipitated salt; following silylation, salt precipitation decreases to 5-7.5% of pore space albeit over a larger volume (see Figures 30a and 30b). Similar behaviour is observed at the simulation end (see Figures 30c and 30d).

Comparing salt distribution in the perforation middle for cases 3 and 5 (see Figure 31), silylation seems to decrease the severity of salt precipitation encouraged by water blockage. The salt saturation of case 5 in the invaded zone (representing a distance of 1.34 m from injector) is reduced compared to case 3 and nearly the same as in case 2. The salt accumulated in case 3 is slightly elevated just before the edge of the invaded zone (i.e., a distance of 0.6-1.22 m from the injector). This high localized precipitation is induced by early capillary suction which occurs at a high irreducible water saturation. Under this condition, the brine in uninvasion zone is still moveable. Some brine from the uninvasion zone flows back to the invaded zone providing more salt to be precipitated. A similar pattern is shown by case 5;

additionally, the brine previously trapped within invaded zone is displaced further into the uninvaded zone. In case 2, the salt precipitates homogenously as there is no water blockage (i.e., different relative permeability curves). This different capillary behaviour should be well noticed during the plan of full-field scale CO₂ storage in a saline aquifer.

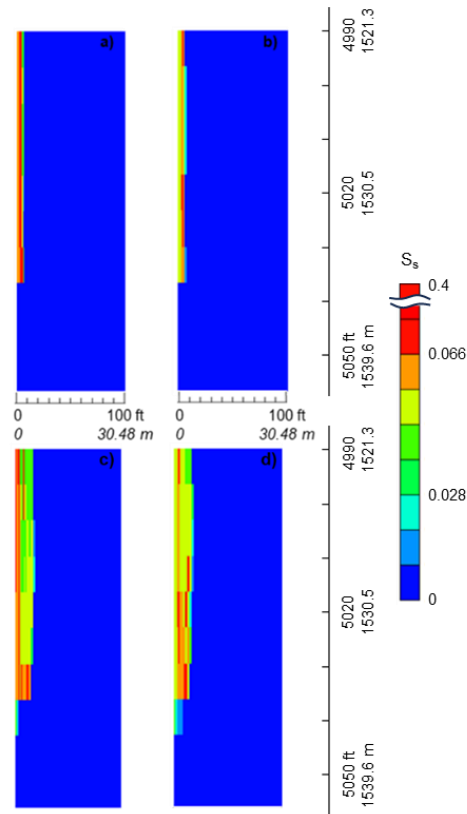


Figure 30. Distribution of salt precipitation in (a) case 3: water blockage and salt precipitation exist, at day 90, (b) case 5: silane treats Case 3, at day 90, and (c) case 3 and (d) case 5 at the end of simulation

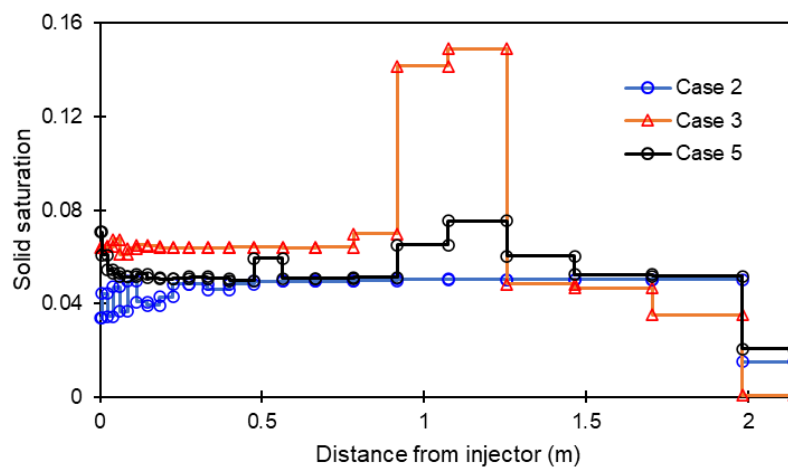


Figure 31. Solid saturation profiles at the middle of perforation after 90 days of injection forecast

Table 5. Summary of relative injectivity change for all studied cases

Case	RIC		
	10 days	90 days	455 days
Case 1	13.2%	21.4%	32.9%
Case 2	16.5%	36.1%	58.0%
Case 3	24.0%	48.7%	68.6%
Case 4	7.7%	15.1%	26.0%
Case 5	19.1%	40.9%	63.1%

Based on the simulation work, water blockage impact (red colour in Figure 32) decreases as salt forms within the pores (see top panels in Figure 32). When the maximum salt precipitation has been reached (blue colour), gas mobility is improved because it flows as a single phase. Silane co-injected with CO₂ has been simulated and it decreases the severity of both issues as indicated by a lower impact level compared to that without silane injection (see top panels in Figure 33). Wettability shift induced by silylation reduces the trapped water within the pores to alleviate water blockage negative impact. In the meantime, lower connate water saturation also depreciates the amount of salt that will be precipitated.

One thing should be noted that both case 3 and 5 are not in sequence (see Figures 32 and 33). Silylation must be applied as early as possible to reduce the severity of salt precipitation. The formation of solid salts covering the pore surface may halt the silylation process in altering wettability. Silane may fail to access quartz which is already covered by salt. This happens only when the aquifer has been injected for a certain period with pure CO₂. This phenomenon was recognized by Arjomand and his research team (Arjomand et al., 2020b) during their experiment. Under this condition, silane treatment may be ineffective. On the other hand, specific experiments are required to investigate the effects of evaporation and silylation when they take place simultaneously. The evaporation rate of water component in the presence of silane in CO₂ phase may not be the same as that in the pure CO₂ injection. There could be another wettability alteration taking place and needed to be modelled due to salt precipitation which has been investigated as a hydrophilic micro-porous crystal (Kim et al., 2013; Miri et al., 2015; Miri & Hallevang, 2016). The suction of brine toward evaporation front under capillary force may be stronger. This phenomenon can be a future simulation work in a larger scale as unconsidered in this work.

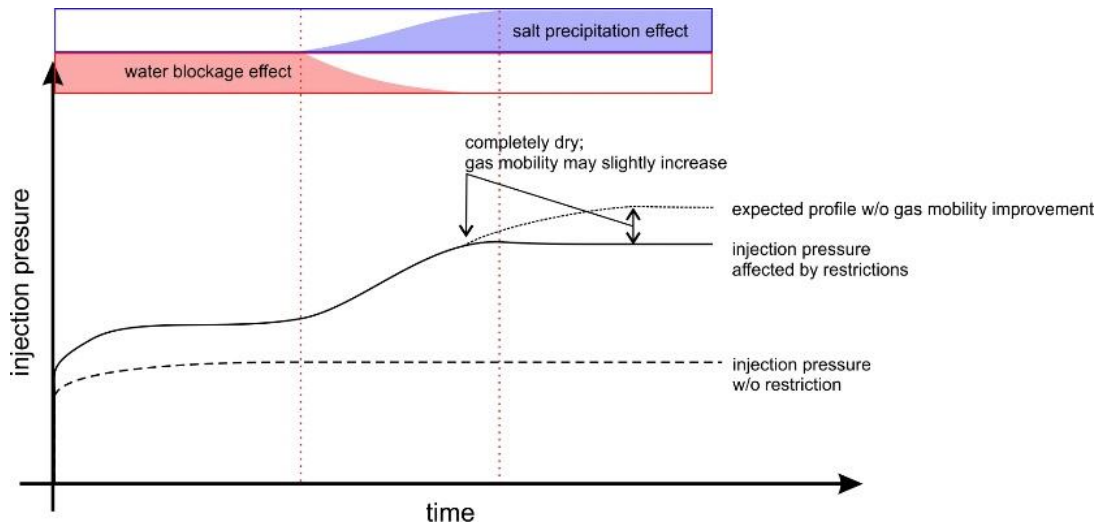


Figure 32. Schematic of injection pressure in case of salt precipitation and water blockage taking place at the same system

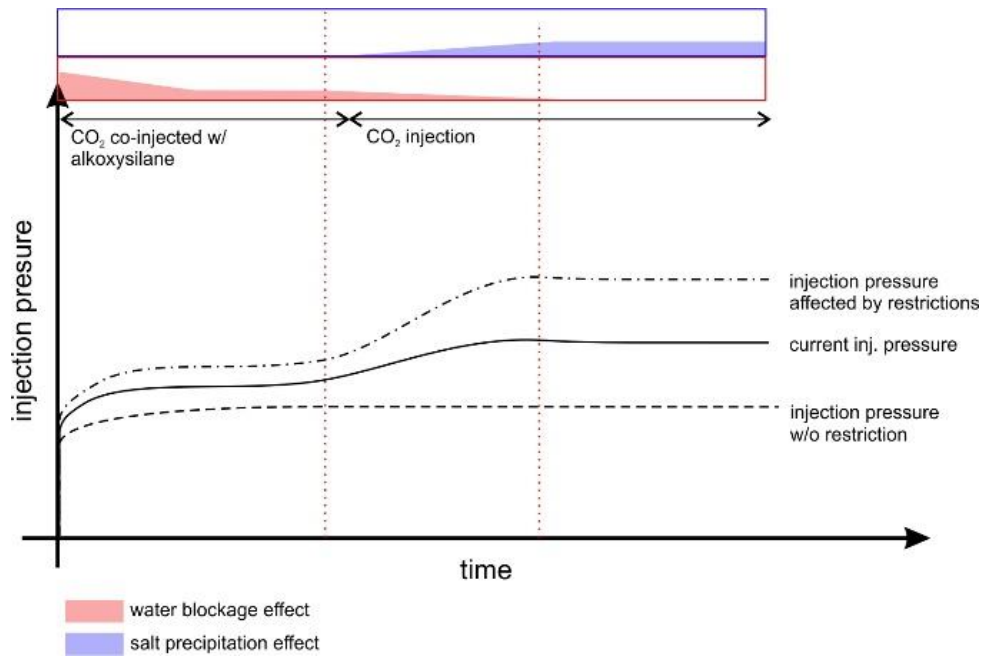


Figure 33. Schematic of injection pressure in case of sc-CO₂ based silylation depressing negative impact of salt precipitation and water blockage

3.4. Conclusions

According to the simulation result, a decrease in injectivity due to salt precipitation is more significant than that due to water blockage. Salt precipitation decreases pore space by forming additional solid in it, while water blockage affects the mobility of CO₂ due to relatively high irreducible water saturation. The negative impact of water blockage gradually diminishes (as the water evaporates) while salt starts growing within the pore space. With a

high level of trapped brine, the injectivity is deteriorated more severely (up to 68.6% of relative injectivity change (RIC)) when both salt precipitation and water blockage occur. Different capillary behaviour may induce localized precipitation considering the heterogeneity either caused by water blockage or naturally employed in the geological structure of a deep saline aquifer.

Beside the ability of sc-CO₂ based silylation in altering wettability, applying this method reduces the severity of salt precipitation indirectly. The alteration turns some trapped brine moveable and thus decreases irreducible water saturation. This phenomenon prevents large accumulation of salt near perforation of the injection well. In case of salt precipitation endorsed by water blockage, this method counteracted the injectivity around 5 to 7 % of RIC (absolute basis). In addition, this method is encouraged to be implemented before continuous CO₂ injection for the geological sequestration because the expected mechanism will not work when salt precipitation comes up covering the pore surface.

Chapter 4 Wettability Impact on CO₂ Storage Capacity and Plume Migration

This chapter has been developed for another journal publication entitled “Wettability Impacts on Multiphase Flow and Capillary Residual Trapping in Underground CO₂ Storage: Review and Simulations”. Similar to Chapter 3, this chapter uses the complete manuscript which may include some overlaps with the information contained in previous chapters.

4.1. Introduction

Geological CO₂ storage is one of many strategies to lower CO₂ emissions and mitigate increasing atmospheric CO₂ concentration. Without these being actively implemented, an increasing population and need to improve quality of life will lead to unabated emissions resulting in climate change which will ultimately negatively impact humanity, biodiversity and the environment (MacDowell et al., 2010). An approximately 1 °C increase in mean earth temperature has occurred since the pre-industrial age (i.e., mid-1800s) up to 2021 and this is largely attributed to the atmospheric CO₂ concentration increasing by 50% (NASA, 2023). Other impacts include higher sea level (caused by warmer oceans and melting ice) and more extreme weather events. The Paris Agreement 2015 sets a framework for limiting the global temperature rise below 2 °C compared to pre-industrial levels. Some assessments indicate that underground CO₂ storage alone could economically contribute to a 20 % reduction in overall greenhouse gas emissions (DECC, 2012). The advantages of this sequestration method include scalability to gigatonne storage capacities, good integration with large point-source emitters (i.e., fossil fuel industry and in particular the oil/gas sector), permanence (on the order of hundreds to thousands of years) and cost-effectiveness (depending on the circumstances) (Bachu, 2000; Voormeij & Simandl, 2002; Yamasaki, 2003).

Strategies for geological CO₂ storage include deep saline aquifers which have the potential to store up to approx. 10⁴ gigatonnes of CO₂ (Herzog & Golomb, 2004). This large capacity is predicated on four trapping mechanisms (i.e., structural, solubility, residual, and mineral trapping). However, most deep saline aquifers are associated with less developed infrastructure for subsurface CO₂ injection (compared to storage in depleted gas reservoirs) which may raise the transport cost. Many studies have also revealed several challenges when planning CO₂ injection into underground geological structures. An understanding of rock-fluid interaction is essential in order to evaluate CO₂ trapping mechanisms and the resulting storage capacity. In this regard, rock wettability characteristics have a significant impact on storage capacity, injectivity and CO₂ plume migration.

In this context, rock wettability is defined as the behaviour of two immiscible fluids (namely, CO₂ and formation brine) adhering onto the rock surface due to intermolecular interactions. The tendency of these fluids to wet the rock surfaces is dominated by a combination of fluid/rock adhesive forces and fluid cohesive forces (Abidoye et al., 2015; Iglauer et al., 2015a). The definition is relatively simple; however, the resulting characteristics are very complex due to a strong dependence on rock mineral type, formation heterogeneity, accessible surface area, surface roughness, chemical reactivity and to some extent the composition (or salinity) of the original formation brine. To date, the best way to measure wettability is contact angle measurements formed by a denser fluid droplet which is surrounded by a lighter fluid and is placed on a solid/rock surface. A comprehensive understanding of the impacts of wettability is well-established for the hydrocarbon/oil industry, where the dominant system is oil-brine interaction with formation rock. The same approach can be used to understand the CO₂-brine-rock system by switching from considering an oil-wet characteristic to a CO₂-wet characteristic.

Comprehensive multiphase flow modelling of CO₂ storage in deep saline aquifers coupled with the corresponding geochemical reactions caused by either CO₂ or CO₂-brine has been performed by others to evaluate plume migration and storage performance based on reservoir and fluid properties. According to simulation results by Ennis-King & Peterson (2002), a low residual gas saturation in the imbibition stage leads to a high CO₂ dissolution rate since the CO₂ trapped in the residual phase is slow to dissolve. A small vertical to horizontal permeability ratio leads to a broadened CO₂ plume propagation within the formation, and vice versa (Pruess et al., 2003). High horizontal permeability improves the lateral movement of CO₂ and, in turn, increases solubility and residual trapping (Sifuentes et al., 2012). Based on a study by Flett et al. (2007), increasing shale content within a rock is correlated to a decrease in rock permeability which promotes less upward CO₂ movement and enhanced lateral movement. Although the rate of residual trapping is diminished in formations with higher shale content, there is more time to reach equilibrium resulting in less mobile CO₂ accumulating under the caprock constructed of layered shales. This may be beneficial in reducing the reliance on higher-risk structural trapping mechanisms. Goater et al. (2013) compared typical results for homogeneous and heterogeneous cases in a relatively low average permeability model (i.e., 11 md). They concluded that localized pressure buildup due to low permeability regions in the heterogeneous case led to poor and uneconomical injectivity. However, in relatively moderate to high average permeability systems (i.e., approximately 100 to 1000 mD), the heterogeneous case provides larger storage capacity compared to the homogeneous case. Layered rock characteristics due to the presence of shale (i.e., low permeability regions) improve the lateral movement leading to an increase in residual and

dissolution trapping. Aside from considering formation heterogeneity, injection strategies such as water alternating gas (WAG) (Juanes et al., 2006) and mixed CO₂-brine injection (Qi et al., 2009) can help to increase the portion of CO₂ trapped in a residual phase. Chased water is expected to boost the imbibition compared to natural imbibition induced by buoyant effect; thus, it also increases the amount of CO₂ under residual trapping. Injecting the CO₂ into deeper interval, even at the base of a formation, is suggested to provide larger CO₂-brine interactions which can enhance storage capacity (Kumar et al., 2005; Sifuentes et al., 2012).

However, the influence of rock wettability on CO₂ plume evolution and as a result the amount of trapped CO₂ is less understood. A detailed sensitivity analysis was done by Al-Khdheawi et al., (2017a; 2017b) to evaluate the impact of varied wettability on CO₂ plume and storage capacities. The authors examined five different wettability characteristics (i.e., strongly water-wet, weakly water-wet, intermediate-wet, weakly CO₂-wet, and strongly CO₂-wet) by using a hypothetical model for each. Comparatively, strongly water-wet rock exhibited the lowest CO₂ plume propagation with less mobile CO₂ trapped under the caprock, the lowest amount of CO₂ dissolution trapping, and the greatest amount of CO₂ residual trapping. For storage integrity purposes, a strongly water-wet formation is preferable due to a greater reliance on residual trapping thus preventing unwanted CO₂ migration beyond the targeted formation. However, the simple capillary residual trapping model that uses two sets of relative permeability (k_r) representing drainage and imbibition, respectively, could lead to inaccurate predictions of immobile CO₂ due to hysteresis effects. It is well known that this mechanism is strongly affected by the initial CO₂ saturation immediately prior to imbibition commencing (Krevor et al., 2015). Land's (1968) empirical model is widely used to correlate initial-residual (IR) saturations of CO₂ to represent the hysteresis process and is mathematically given by,

$$S_{CO2r} - S_{CO2c} = \frac{S_{CO2i} - S_{CO2c}}{1 + C(S_{CO2i} - S_{CO2c})} \quad (22)$$

where S_{CO2c} , S_{CO2i} , and S_{CO2r} are critical (representing the fraction not contributing to flow), initial (at imbibition) and residual CO₂ saturation. C is Land's constant which characterizes the IR relationship after a cycle of drainage-imbibition. The constant can be calculated from a set of drainage-imbibition experiments using the following expression,

$$C = \frac{1}{S_{CO2r} - S_{CO2c}} - \frac{1}{S_{CO2i} - S_{CO2c}} \quad (23)$$

The typical IR relationship is shown in Figure 34 that includes several C -values for comparison.

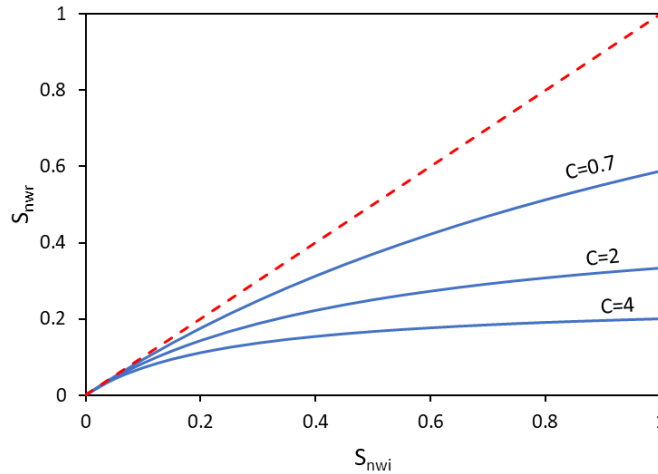


Figure 34. Typical initial-residual (IR) saturation relationship of non-wetting phase (S_{nwi} vs S_{nwr}) plot showing different C-constants from Land's (1968) empirical model

A recent study by Zhang et al. (2023) simulated underground CO_2 storage in two reservoirs where the only difference was the wettability condition (i.e., water-wet and CO_2 -wet). The numerical model was validated in part by adopting experimental results of multiphase flow under different wettability characteristics (from Arjomand et al. (2020b)). In this experimental study, the CO_2 -wet characteristic was obtained by treating the core using a silane chemical with the intent to only modify the wettability and not affect the porosity or pore connectivity. Upon silane chemical treatment of sandstone samples, the measured contact angles at elevated pressure and temperature (i.e., 21 MPa and 333 K) increased from 14° to 151° corresponding to a change from water-wet to CO_2 -wet conditions. In Zhang et al. (2023), the difference in the curvature of the relative permeability curves representing these two contrasting scenarios is significantly smaller than that used by Al-Khdheawi et al (2017a; 2017b). The same trend is applicable to the saturation endpoints. This insignificant change in relative permeability over two contrasted wettability characteristics is consistent with other studies such as Li et al. (2011) and Lopez et al. (2021; 2023). Zhang et al. (2023) applied a value of $C = 1$ in Land's model for the water-wet case and assumed that capillary residual trapping was absent in the CO_2 -wet case. The latter assumption may be unrealistic in actual subsurface formations with complex pore geometry. Furthermore, even though simulation studies in Al-Khdheawi et al. (2017b) and Zhang et al. (2023) have considered heterogeneity effects by using 10th SPE (Society of Petroleum Engineers) comparative solution project, the application of a single relative permeability curve over a wide range of rock properties seems may not be representative of realistic conditions. There is also a possibility of differences in capillary trapping behaviour (i.e., a strong IR correlation) with different hydraulic rock types.

With some gaps identified in previous studies, further understanding of how wettability impacts multiphase flow and capillary residual trapping in underground CO₂ storage scenarios is necessitated. In this study, a critical review of wettability impacts on capillary trapping is provided. To further understand these phenomena, several sets of numerical simulations encompassing different rock wettability characteristics were conducted based on the results of multiphase flooding experiments corresponding to these different rock conditions. Experimental results obtained by Arjomand et al. (2020b) which characterized multiphase flow of two contrast wettability samples were used. An intermediate case was also included based on a similar approach from Lopez et al. (2021). Storage capacity and CO₂ plume propagation were then evaluated at a field scale using a numerical simulation model. A homogeneous box model was used to address the lack of capillary trapping models for different wettability states at the time of this study.

4.2. Multiphase Flow of Gas/Supercritical CO₂-Brine System under Different Wettabilities

To elucidate the impact of only wettability on the multiphase flow, this variation must be isolated without changing other rock properties that affect fluids flow (i.e., porosity and permeability). This can be accomplished by using a chemical treatment to form a very thin layer (or even a monolayer) on the surface to alter the wettability toward less water-wet. This approach has application in addressing water blockage and liquid holding in gas condensate reservoirs while having a minimal impact on porosity/permeability (i.e., pore size and connectivity characteristics). These treatments generally functionalize the rock surface, mostly quartz, to become more hydrophobic. Several approaches include application of fluorinated polymeric chemicals (Tang & Firoozabadi, 2003; Fahes & Firoozabadi, 2007; Wu & Firoozabadi, 2010), silane-based chemicals (Arjomand et al., 2020a; 2020b), and benzoxazine resin precursors (Lopez et al., 2021; 2023). However, none of those studies completed a cycle of drainage-imbibition flooding to mimic the capillary residual trapping processes seen in a geological CO₂ storage scheme.

El-Maghraby & Blunt (2013) used a combined drainage-imbibition flooding experiment to obtain IR relationships; they also considered the effects that CO₂ has on rock wettability to a more water-wet state due to chemical interactions with Ca²⁺ ions. Flooding with CO₂-saturated brine into a core sample at elevated pressure and temperature was used to represent actual aquifer conditions and to mitigate mineral dissolution. Supercritical CO₂ (scCO₂) flooding is then performed until irreducible water saturation (S_{wirr}) is reached; the ScCO₂ is water-saturated to mitigate water evaporation during this step. Saturated brine is then reinjected until S_{CO2r} is reached. From this, an IR relationship is generated using $S_{CO2i} = 1 - S_{wirr}$ and S_{CO2r} in a cartesian plot with the data being fitted to Land's model (Eq. 23) to obtain

a C value. A complete schematic of this process is given in the graphical abstract of El-Maghraby & Blunt (2013) and in Figure 7 of Krevor et al. (2015).

Comparing the multiphase flow results from samples with differing wettability by Arjomand et al. (2020b), the water-wet sample (i.e., an untreated Gray Berea (GB) sandstone sample) gave a higher S_{wirr} value of 0.615 compared to 0.455 for a nearly identical sample that had been silane treated to achieve a CO_2 -wet state. These results are expected showing that water wetness suppresses the effectiveness of scCO_2 displacement. A similar effect is shown by Lopez et al. (2021) using Berea Upper Gray (BUG) sandstone and Lopez et al. (2023) using lower porosity-permeability Carbon Tan sandstone cores. Table 6 shows the rock core parameters and drainage results for both untreated and treated samples from Arjomand et al. (2020b) and Lopez et al. (2021). Table 7 shows the rock typing for both cores using the hydraulic flow unit method (Amaefule et al., 1993). In a practical sense, both cores can be classified into the same rock type which is supported by the S_{wirr} values for both original cores being similar. As such, the results from both works are comparable despite different flooding pore pressures (21 MPa for Arjomand and 10.35 MPa for Lopez) applied in these studies. Several studies have validated that S_{wirr} is a rock characteristic being used in rock typing (Xu et al., 2013) and relatively insensitive to experimental conditions (Tokunaga et al., 2013).

Table 6. Core samples properties being compared and endpoints of drainage coreflooding results

Source	Sample code	k (md)	ϕ (fraction)	Coreflood	
				S_{wirr}	S_{gmax}
Arjomand et al. (2020)	GB.2 - untreated	223.85	0.19	0.62	0.38
Arjomand et al. (2020)	GB.2 - treated	223.85	0.19	0.46	0.54
Lopez et al. (2021)	BUG2 - untreated	130	0.191	0.6	0.4
Lopez et al. (2021)	BUG1 - treated	121	0.182	0.56	0.44

Table 7. Rock typing of original cores from compared studies by using hydraulic flow unit method (Amaefule et al., 1993)

Source	Sample code	k (md)	ϕ (fraction)	RQI	ϕ_z	FZI	HU
Arjomand et al. (2020)	GB.2 – untreated	223.85	0.19	1.08	0.23	4.59	14
Lopez et al. (2021)	BUG2 – untreated	130	0.191	0.82	0.24	3.47	13

To compare the wettability of the treated core in Lopez et al. (2021) with that in Arjomand et al. (2020), the measured contact angle needs to be adjusted to account for expected changes in contact angle with variation in pressure and temperature conditions. Lopez et al. (2021) reported that a benzoxazine treated BUG had a contact angle of 89° at atmospheric condition (0.1 MPa; 298 K) while Arjomand et al. (2020) reports results at 10 MPa and 60°C . Al-Yaseri et al. (2017) observed at 15 MPa with a hydrophobic dolomite a decrease in the CO_2 -brine advancing contact angle from 110° at 308 K to 98° at 343 K. Furthermore, at a constant temperature of 308 K, the contact angle increased from 92° at 0.1 MPa to 110° at 15 MPa. Generally, on hydrophobic surfaces, they observed that the contact angle increases with pressure and decreases with temperature. For a CO_2 -brine system on a hydrophobic surface, Liang et al. (2017) reports at ambient temperature an increase in contact angle from approximately 100° at ambient pressure to 150° at 20 MPa. A significant increase in the contact angle occurs when the pressure traverses the CO_2 vapor-liquid phase boundary (i.e., from a gas at ambient pressure to a liquid at approximately 7 MPa) while the contact angle remained comparatively constant in the CO_2 liquid region (i.e., from 7 to 20 MPa). Others have shown on a hydrophobic surface that the scCO_2 -brine contact angle is less than that of liquid CO_2 -brine (Li & Fan, 2015) which corresponds to a temperature increase and confirms the study by Al-Yaseri et al. (2017). Liang et al. (2017) shows that the CO_2 -water interfacial tension (IFT) slightly decreases around 17% when the temperature is increased from 296 to 383 K; this is consistent with decrease in contact angle with increasing temperature. The impact of salinity on contact angle is comparatively insignificant (Chiquet et al., 2007; Li & Fan, 2015; Alnili et al., 2018).

Thus, we believe that contact angle of treated BUG sample lays between 89° and 151° (reported contact angle of treated GB.2 in Arjomand et al. (2020)) at elevated pressure-temperature applied in Arjomand et al. (2020), i.e., 21 MPa and 333 K. For this estimation, the nearest analogy is taken from study by Al Yaseri et al. (2017) as explained above. Assigned treated BUG sample as intermediate case, a good trend of S_{wirr} over the wettability characteristics based on contact angle can be made (Figure 35). This relationship is used for numerical simulation in Chapter 4.

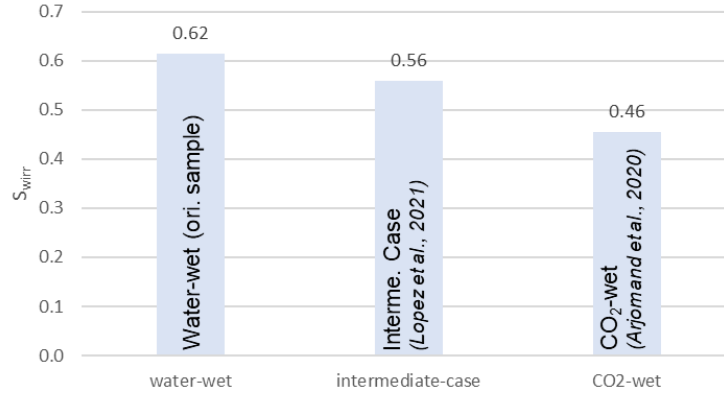


Figure 35. Irreducible water saturation (S_{wirr}) summary for generated case study on wettability states

4.3. Capillary Residual Trapping under Different Wettabilities

CO₂ can be trapped as a residual phase due to capillary pinning during injection into heterogeneous reservoirs and is caused by post-injection snapping-off and flow bypass (Gershenson et al., 2017; Krevor et al., 2015; Hu et al., 2017). Capillary pinning is also known as local capillary trapping where CO₂ vertical movement due to buoyancy is suppressed due to an overlying low porosity/permeability layer (typically a shale barrier) (Gershenson et al., 2017; Ren & Trevisan, 2020). This layer has a high capillary entry pressure due to the tiny pore sizes typical of low porosity/permeability layers. Generally, this local capillary trapping is like structural trapping in that there is a low permeability overlying layer (typically, shale) comprising the storage formation (this is illustrated in Figure 11 of Gershenson et al. (2017)). Under this condition, the following expression is applied (Gershenson et al., 2017),

$$\Delta\rho gh < p_{C,sh}(S_{CO_2,sh}) - p_{C,ss}(S_{CO_2,ss}) \quad (24)$$

where $\Delta\rho gh$ is the buoyant force affecting vertical flow with $\Delta\rho$ being the density difference between brine and CO₂, $p_{C,sh}(S_{CO_2,sh})$ is the capillary pressure at the shale barrier as a function of CO₂ saturation and $p_{C,ss}(S_{CO_2,ss})$ is the capillary pressure at the aquifer zone rock underlying the shale barrier as a function of CO₂ saturation (an illustration of this is shown in Figure 12 in Gershenson et al. (2017)). Trevisan et al. (2015) the spatial distribution of CO₂ plume in the capillary barrier experimentally with the results confirming the prediction of residual trapping in the homogeneous model while heterogeneity results in greater trapping of CO₂ as an immobile phase due to a wider range of capillarity behaviour.

The snapping-off mechanism takes place when displaced brine re-imbibes the swept zone occupied by CO₂ at the post-injection stage which restrains a certain amount of CO₂ trapped within the pores (Hunt et al., 1988; Iglauer et al., 2011; Krevor et al., 2015). The

capillarity of the rock dominates throughout these processes (Ali et al., 2022) and is similar to the drainage-imbibition processes in petroleum systems, known as hysteresis. During imbibition, brine fills the pores with the smallest sized pores first. Supported by gravity, the portion of brine in pores will increase until the brine saturation reaches a forced percolation-like characteristic (Blunt & Scher, 1995). Until sufficient brine (i.e., wetting phase) pressure is reached, a certain amount of CO₂ ganglia will be disconnected from the main flow resulting in immobile CO₂. The degree of water wetness determines the rate of the filling process. As the water film thickness in less water wet scenarios is thinner, brine flow is slowed and may suppress its ability to snap-off counter-flow from the CO₂ plume (Blunt, 1998; Zhao et al., 2010). This results in more CO₂ trapped behind the main plume in a water-wet scenario compared to a weakly water-wet scenario. This comparison has been investigated at the laboratory scale in several studies (Al-Menhali & Krevor, 2016; Chaudhary et al., 2013; and Rahman et al., 2016). With greater quantities of CO₂ residually trapped in a water-wet scenario, the rate of plume growth decreases as water-wetness increases. This process causes the plume to reach the top of formation earlier in a weakly water-wet rock if there are no external forces interrupting.

An IR relationship is normally used to categorize the trapping behaviour of a rock sample. Several correlations have been proposed such as the Land (1968) (seen in Eq. 22), Jerauld (1997) and Spiteri et al. (2008) models. Another approach is to correlate residual gas saturation with core porosity (Kralik et al., 2000; Lamy et al., 2010). However, a wide range of residual gas saturations have been observed from a single porosity value resulting in large prediction uncertainty. This can be attributed to a varied pore geometry structure and initial CO₂ saturation (S_{CO_2i}) immediately before imbibition begins. Land's model is commonly used in recent studies examining trapped CO₂ saturation following a series of drainage-imbibition cycles. While this model accommodates changes in S_{CO_2i} for predicting capillary residual trapping efficiency, there is a lack of understanding of how rock wettability in the scCO₂-brine system affects the C -constant in Land's model (see Eq. 22 and 23). In an effort to understand the parameters that influence residual saturation, Burnside & Naylor (2014) concluded that the ratio of trapped CO₂ to initial saturation in sandstones is inversely correlated to S_{CO_2i} . They found no correlation between this ratio and the relative permeability endpoints. The most recent conclusion for this phenomenon is that IR relationship is a specific characteristic for the targeted formation (Krevor et al., 2015).

Considering this gap in knowledge, an effort was made to characterize the effect of rock wettability on the capillary residual trapping through the C -constant in Land's model. Most of the work investigating the IR relationship performed the experiments using Berea sandstone. We found that Berea sandstone and other samples (including carbonate, Bentheimer,

Fontainebleau, and some actual sandstones) representing strong water wet has C -constant ranging from 0.7 – 2 (Bennion & Bachu, 2008; Lamy et al., 2010; Pentland et al., 2011; Shi et al., 2011a; Bull et al., 2011; Krevor et al., 2012; Akbarabadi & Piri, 2013; Niu et al., 2015; Al-Menhali & Krevor, 2016; Reynolds, et al., 2018; Ni et al., 2019). According to datasets of Berea sandstones as reported in Krevor et al. (2015), Berea sandstones also gives C -constant range of 0.7 – 2. Berea sandstones is normally known as strong water wet rock in scCO_2 -brine system. We also collected some experimental results executed on actual sandstones, carbonates, and treated cores which were characterized as either mixed or less water wet in scCO_2 -brine system. In this characteristic, C -constant ranges from 2.8 – 4.7 (Shi et al., 2011b; El-Maghraby & Blunt, 2013; Al-Menhali & Krevor, 2016; Pairoys & Caubit, 2023). Figure 36 shows the distribution of datasets collected in this study. All the data were shown in 45% transparent coloured shapes. Darker colour due to shapes overlapping will give an indication of where the data is concentrated. The references which have large dataset are simply depicted by irregular shape to cover all results ranges. Some references show the uncertainty in their results which are depicted by a rectangle shape in this work. Some others shown by dots were digitized from references by using WebPlotDigitizer version 4.6 (2022). Some outliers beyond these characteristics were also found (not shown in Figure 36) such those reported in Rahman et al. (2016) (water wet = 4.7; oil wet = 9.5) and Abdoulghafour et al. (2020) (water wet Bentheimer ranges from 1.5 – 4).

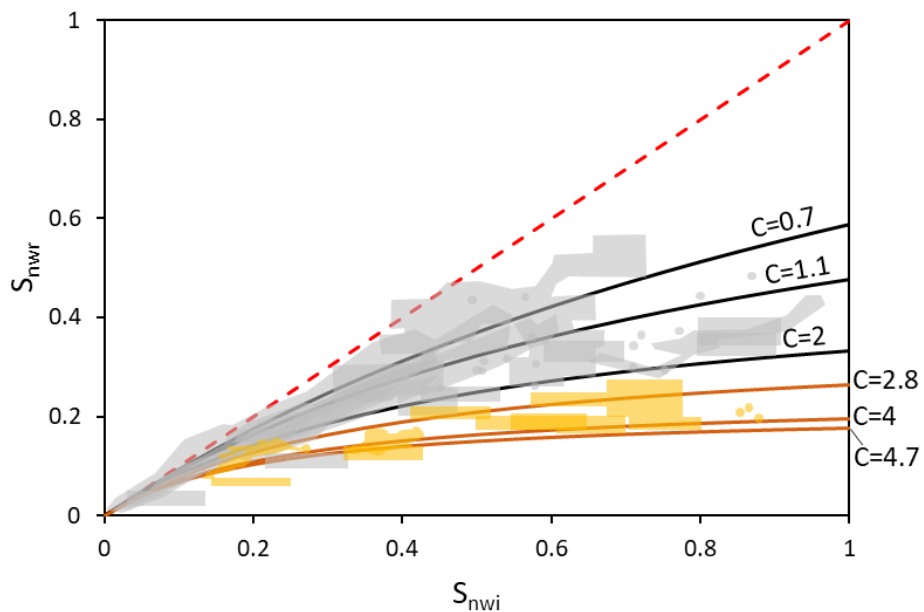


Figure 36. Initial-residual (IR) saturation relationship of non-wetting phase (S_{nwi} vs S_{nwr}) after classification based on wettability states, i.e., strong water-wet (— and ■) and less water-wet (— and ■). Variable “C” refers to trapping coefficient in Land’s (1968) empirical model.

Investigating the wettability impact on residual trapping without changing other properties (e.g., permeability, porosity, pore connectivity) is preferred; application of chemical treatments on rock that functionalize the rock surface with a thin layer (or even just a monolayer) is ideal for this type of study. Al-Menhali & Krevor (2016) considered asphaltene precipitation resulting in mixed wet conditions on carbonate rock surface. However, with asphaltene precipitations, besides changes in wettability, pore geometry and connectivity can also be altered making the various petrophysical properties of the modified sample to differ from its original state (i.e., untreated). In other words, the impact of wettability alteration may be interrupted by the change of pore structure due to solid asphaltene. In another publication, Al-Menhali et al. (2016) examines this further by measuring the contact angles formed within the pores. In the original carbonate sample, the contact angles are in a range of 20° to 50° (with 34° of mean average) giving C -constant of 1.7. A wider range of contact angles are formed in mixed wet cores, i.e., 25° to 128° (with 94° of mean average) giving C -constant of 4.1. Rahman et al. (2016) used silane to treat Bentheimer core to obtain less water wet condition. They reported 130° of contact angle formed at ambient conditions in air. The observation was made using an X-ray micro-computed tomograph (μ CT) on a very small core (5 mm of diameter and 10 mm of length). The C -constant obtained for water wet and less water wet (the author used “oil wet” term) are 4.7 and 9.5, respectively. The results are beyond our classification as shown in Figure 36. Surface-area-to-volume ratio can be the reason for the different results obtained in coreflooding using different dimensions.

On the other hand, some other works found opposite impact of wettability on residual gas saturation (Fahes & Firoozabadi, 2007; Wang et al., 2016; Hu et al., 2017; Wang et al., 2023). Less water wet was found to trap more CO₂ in the residual form. The basic reasons for this different trend are various approaches and methods used to observe the process. Hu et al. (2017) utilized a uniform micromodel to track the flow path of CO₂ and brine during drainage-imbibition cycle. Brine fingers during imbibition in water wet model has a wider size compared to that in intermediate wet. This implies a quicker front movement in intermediate case leaving a large amount of CO₂ trapped behind. Fahes & Firoozabadi (2007) performed a chemical treatment to Berea sandstone to get less water wet sample (150° of contact angle at ambient condition). An imbibition coreflood by brine was conducted to an air-saturated core for untreated and treated cores (noting that this is not a cycle of drainage-imbibition). They observed a consistent lower liquid saturation for the treated core at breakthrough and steady state flow. This incurs a larger amount of air trapped within the treated cores (less water wet). Wang et al. (2016) studied the capillary pressure-saturation relations using a custom-built porous plate. The capillary pressure curves were generated from a cycle of drainage-imbibition for sandstones and carbonates. A larger amount of residual scCO₂ representing less water wet

system was observed compared to residual air representing water wet. However, whether the impact is caused by wettability or density contrast requires further investigation. Wang et al. (2023) simulated an algorithm for multiphase flow in a porous media model consisting of circular spots arranged on a triangular lattice. A cycle of drainage-imbibition flooding was run to a varied fluids-rock contact angle. Increasing contact angles from 45° to 75° , signalling a change from water wet to intermediate wet, gives slightly less CO_2 trapped. However, the further increase of contact angles up to 135° shows the increasing C -constant (more trapped CO_2).

4.4. Numerical Simulation

4.4.1. Aquifer Grid and Multiphase Flow Model

Numerical simulations were performed using Computer Modelling Group (CMGTM) software coupled with a compositional multiphase flow module which includes a greenhouse gas option model, i.e., GEMTM. An aquifer was built based on a homogeneous box model from Nghiem et al. (2009). The geometry size of this symmetry model is 1065 m (length) x 1065 m (width) x 300 m (thickness) in a uniform 71 (15 m) x 71 (15 m) x 100 (3 m) grid configuration. Porosity and permeability were set similar to the rock samples used in Arjomand et al. (2020b), i.e., 0.19 of porosity and 224 mD ($2.2 \times 10^{-13} \text{ m}^2$) of permeability. The vertical to horizontal permeability ratio was assumed 0.1. The same assumption was also used by Giorgis et al. (2007), Nghiem et al. (2009), Al-Khdheawi et al. (2017a), and Zhang et al. (2023). Aquifer initial conditions were as follows: pressure = 21 MPa, temperature = 333 K, brine salinity = 60,000 ppm. Large volume modifiers (10^4) were implemented at the outer boundaries to represent an infinite acting aquifer. This approach was also used in Nghiem et al. (2009). A 3D view of the reservoir and injection well are shown in Figure 37. The well was perforated near the bottom of aquifer at a depth of 2276 m. CO_2 was injected at constant rate constraint, i.e., 9000 m^3/day (6143 ton/year), for 25 years. Observations were done for 80 years after injection was halted. Mineralization was not studied in this work as the observation period is relatively short.

To improve recent field-scale simulation studies examining the impacts of wettability on aquifer storage capacity and CO_2 plume migration, we ran a set of case studies incorporating the wettability characteristics into multiphase flow and capillary residual modelling. Two contrasting wettabilities impacting the multiphase flow of scCO_2 -brine were adopted from set of experiments conducted by Arjomand et al. (2020b). An intermediate case was also included as adopted from Lopez et al. (2021). The saturation endpoints characterizing the wettability of the model shown in Figure 35 were used. The relative permeability curves of drainage process were generated based on Sigmund & McCaffery (1979) model as follows,

$$S_w^* = \frac{S_w - S_{wirr}}{1 - S_{wirr}} \quad (25)$$

$$k_{rw} = k_{rw}' \frac{(S_w^*)^{N_w} + AS_w^*}{1 + A} \quad (26)$$

$$k_{rg} = k_{rg}' \frac{(1 - S_w^*)^{N_g} + B(1 - S_w^*)}{1 + B} \quad (27)$$

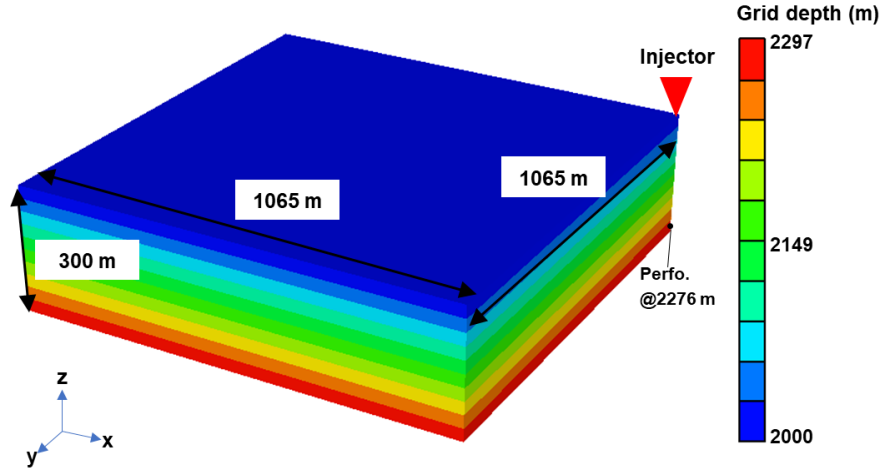


Figure 37. Aquifer model geometry and injection well location

The model properties are listed in Table 8 as reported in Arjomand et al. (2020b) and Lopez et al. (2021). The relative permeability model for the intermediate case was similar to the CO₂-wet case with the k_{rg}' endpoint being interpolated based on S_{wirr} .

Table 8. Sigmund & McCaffery's relative permeability model for each case study

Case	N_w	N_g	A	B	k_{rw}'	k_{rg}'	Source
Water wet	3.6	3.33	0.12	0.01	1	0.16	Arjomand et al. (2020b)
Intermediate	4.19	3.39	0.11	0.03	1	0.17	Adjusted
CO ₂ wet	4.19	3.39	0.11	0.03	1	0.19	Arjomand et al. (2020b)

4.4.2. CO₂ Trapping Model

Solubility Trapping Model

CO₂ solubility in brine was modelled based on a phase equilibrium process which applies the equality of component fugacity in gas (supercritical phase was denoted as gas in this work) and aqueous phases (Nghiem et al., 2009) as follows,

$$f_{CO_2,g} = f_{CO_2,aq} \quad (28)$$

The gas fugacity of CO₂ ($f_{CO_2,g}$) was calculated using Peng-Robinson equation of state (1976). Henry's law was used to calculate the aqueous fugacity of CO₂ (Li & Nghiem, 1986) as formulated by,

$$f_{CO_2,aq} = H_{CO_2} w_{CO_2} \quad (29)$$

where H_{CO_2} and w_{CO_2} are Henry's law constant for CO₂ and CO₂ mole fraction in aqueous phase, respectively. Henry's constants are functions of pressure, temperature, and brine salinity (Nghiem et al., 2009) which can be calculated as follows:

$$\ln(H_{CO_2}) = \ln(H_{CO_2}^*) + \frac{1}{RT} \int_{p^*}^p \bar{v}_{CO_2} dp \quad (30)$$

where H_{CO_2} and $H_{CO_2}^*$ are the constants at p-T and p*-T, respectively. \bar{v}_{CO_2} is a partial molar volume of CO₂ in solution. Pure brine density was calculated based on a correlation proposed by (Rowe & Chou, 1970). The density of brine saturated by CO₂ is estimated based on an approach by Garcia (2001) which uses partial molar volume of CO₂ in the mixture. Convective flow will take place due to a buoyant effect between a denser saturated brine and original brine.

Residual Trapping Model

Land's model as expressed by Equation 21 was implemented in this numerical simulation. S_{CO_2c} is assumed 0 in this work, then residual gas saturation of each grid at turning point of imbibition can be formulated as,

$$S_{CO_2r}^* = \frac{S_{CO_2i}^*}{1 + CS_{CO_2i}^*} \quad (31)$$

Symbol (*) denotes the varied condition of saturations at turning point of imbibition for each grid. A simple illustration of different residual gas saturation is shown in Figure 38 for two different saturations right before imbibition takes place.

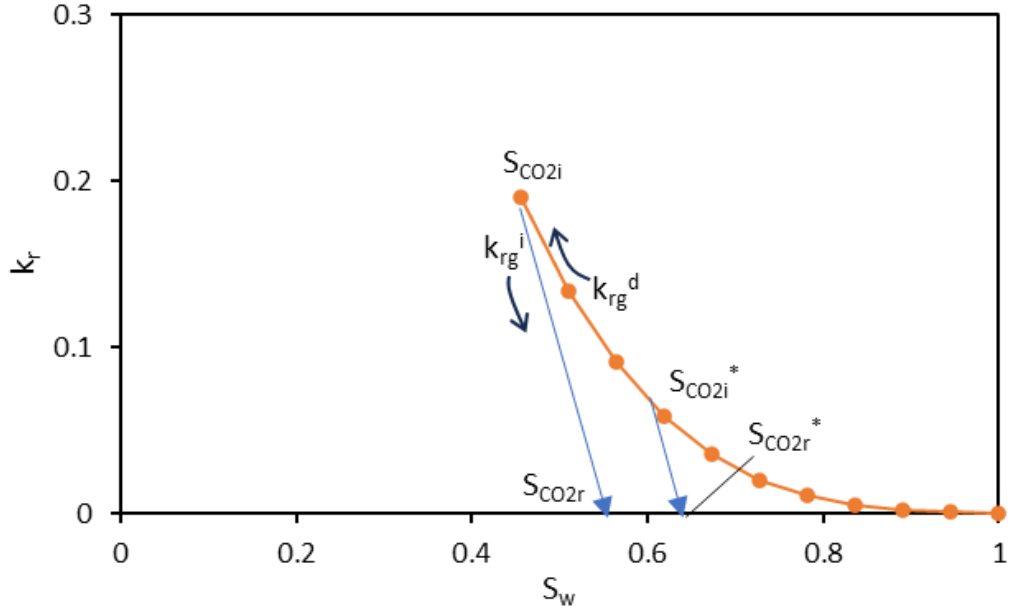


Figure 38. Illustration of residual trapping occurring in a relative permeability vs. brine saturation (k_r vs. S_w) curve in both drainage (—●—) and imbibition (—) processes.

Relative permeability for imbibition process was modelled based on Land's (1968) derivation, i.e.,

$$k_{rg}^i(S_{CO2}) = k_{rg}^d(S_{CO2,shifted}) \quad (32)$$

$$S_{CO2,shifted} = 0.5 \left\{ (S_{CO2} - S_{CO2r}^*) + \sqrt{(S_{CO2} - S_{CO2r}^*)^2 + \frac{4}{C}(S_{CO2} - S_{CO2r}^*)} \right\} \quad (33)$$

where k_{rg}^i and k_{rg}^d are relative permeability of CO_2 under imbibition and drainage processes, respectively.

We used $C = 1.1$ for water wet case in the simulation as majority results observed for Berea sandstone (Krevor et al., 2012; Akbarabadi & Piri, 2013; Niu et al., 2015). The selected constant also qualitatively passes through the darker zone in Figure 36 (shown in grey colour). Intermediate case in the simulation work used $C = 4$ which lays in range of mix wet zone in Figure 36 (shown in orange colour). The selected constant is based on actual Tako sandstone (Shi et al., 2011b) and treated limestone in Al-Menhali & Krevor (2016) and Al-Menhali et al.

(2016). For CO₂ wet, we selected the maximum Land constant observed in Krevor et al. (2015) as the most pessimistic number for capillary residual trapping, i.e., $C = 5$.

4.4.3. Simulation Results & Discussion

The plume migration for all cases was evaluated after 10 years of injection, the end of injection (year 25), and 80 years of storage (Figure 39). The cross sections included in Figure 39 show the profile of gas saturation from injector toward positive y-axis in a single x-axis plane. For easier comparison of CO₂ plume in 10 years of injection, red arrows in vertical and horizontal directions were drawn on the corresponding cross sections. A wider plume movement in CO₂ wet and intermediate case, i.e., 1-grid (equivalent to 15 m) wider than water wet plume, indicates more space for CO₂ to displace brine as implied by the saturation endpoints differences (Figure 2). According to Figure 2, S_{wirr} reduces as decreasing of degree of water wetness. CO₂ occupies more space in pores as S_{wirr} reduces. Consequently, the vertical movement of water wet case is more advanced compared to that of other cases due to the limited space in pores. This causes a quicker time for the plume in water wet to reach the top of formation if lack of shale barrier exists. For the same reasons, the spread of plume in water wet is the widest but the least saturation at the end of injection compared to those of other cases (see Figure 39 in the middle column). Different from the results in this work, Al Khdheawi et al. (2017a) shows higher CO₂ vertical migration in CO₂ wet case. This can be attributed to a significant difference in k_r curvature they simulated between water wet and CO₂ wet. In this work, the same relative permeability curves used in Zhang et al. (2023) were applied based on experimental work by Arjomand et al. (2020b).

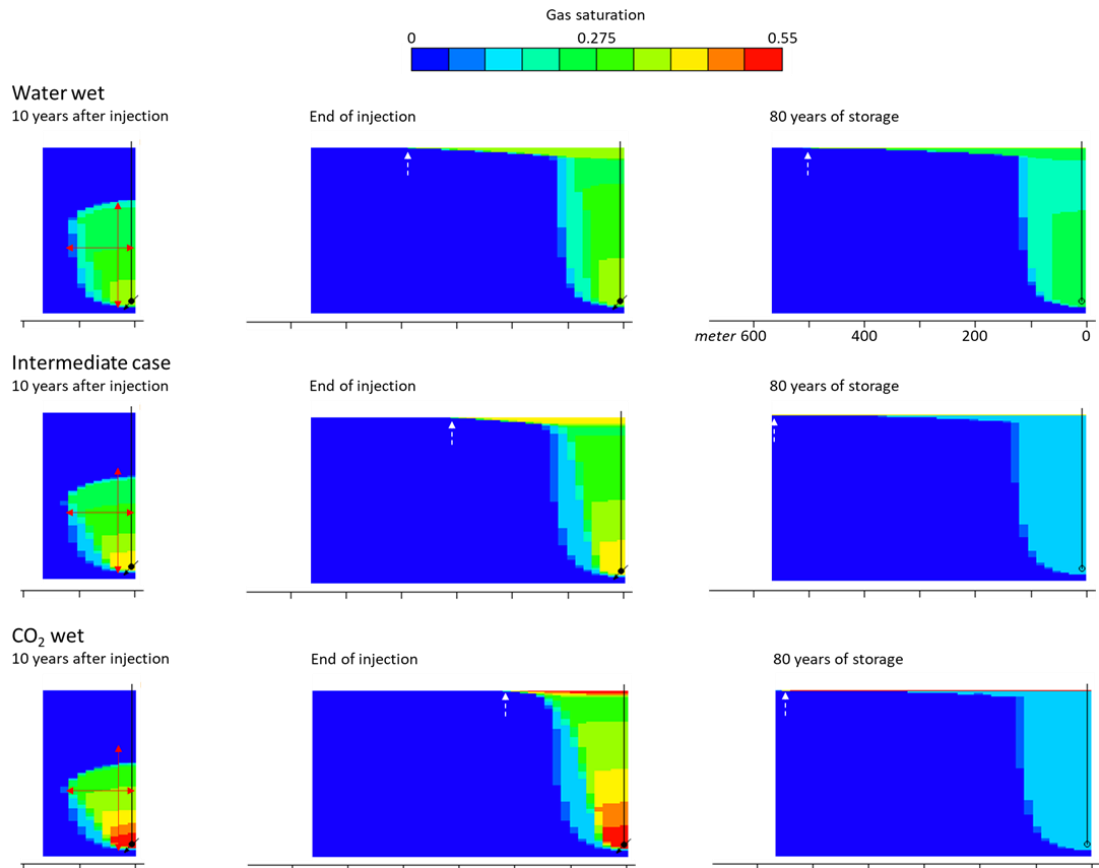


Figure 39. Plume migration for all case studies in 10 years of injection, end of injection (year 25), and 80 years of storage. Red arrows assist the comparison of lateral and vertical plume movement. White arrows with dashed line indicate the furthest plume position.

At the 80 years of storage (right column in Figure 39), the moveable CO₂ keeps flowing horizontally beneath the caprock as more CO₂ rises due to buoyant effect. In water wet, the movement seems slower as indicated by ~120 m spread from the last position at the end of injection. The movement in intermediate case and CO₂ wet are ~270 m and ~345 m, respectively. The massive imbibition brine in water wet case suppresses this movement by snapping-off the flowing upward CO₂. Qualitatively, a larger amount of CO₂ trapped behind the plume in water wet compared to that in other cases can be seen in Figure 39 (the right-side column). As also expected, a larger percentage of residual trapped CO₂ in water wet is obtained after an 80-year storage (depicted in Figure 40). Both intermediate case and CO₂ wet provide likely length of extended moveable plume beneath the caprock. This promotes a large contact area for a dissolution process of CO₂ into the aqueous brine. Therefore, the amount of CO₂ under solubility trapping seems similar for both cases (see Figure 40). The dissolution process keeps continuing at the end of simulation time. A convective flow due to a denser CO₂-rich brine seems still at the early stage (Figure 41). Most of dissolution occurs in CO₂ swept zone

while slower reaction proceeds in the front (indicated by gradual colours in the convective flow).

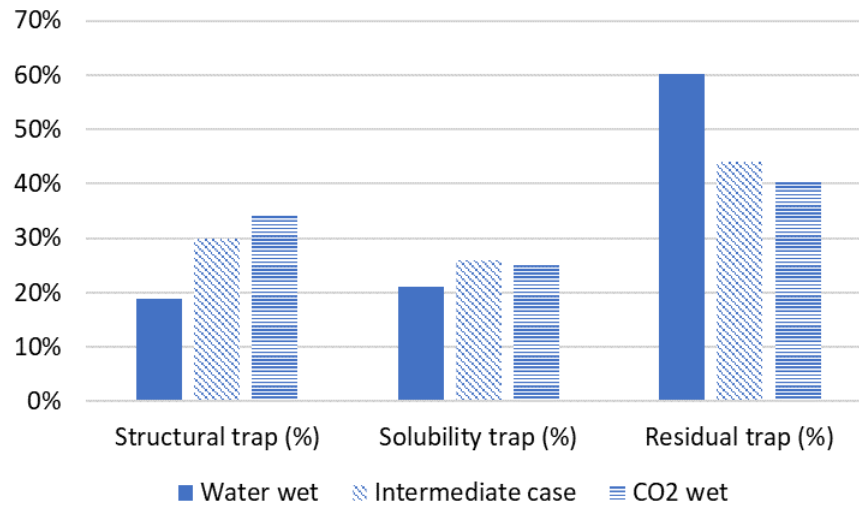


Figure 40. CO₂ storage capacities in percentage presenting each trapping mechanisms for all wettability case study

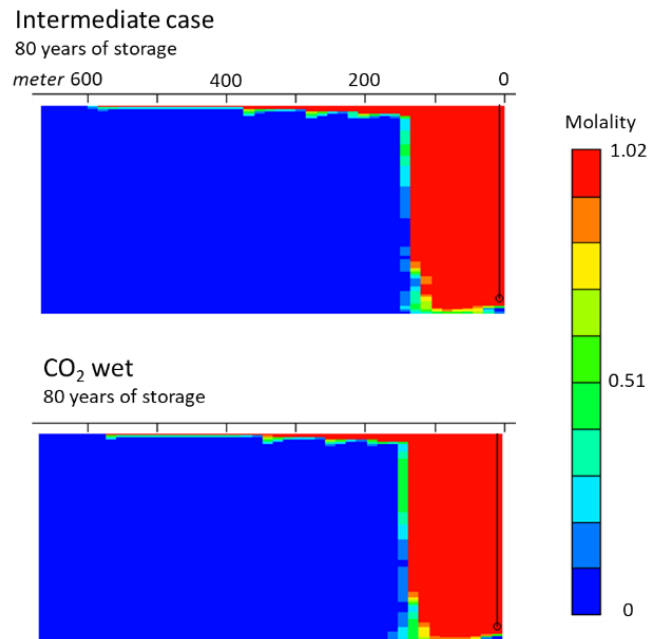


Figure 41. CO₂ molality in the aqueous phase after 80 years of storage.

4.5. Conclusions

Multiphase flow properties and capillary residual trapping during subsurface CO₂ storage have been investigated in the literature under different wettabilities. In more recent studies, it has been found that, for the case of scCO₂-brine fluid system, the relative

permeability curves are less sensitive to wettability shift (compared to that previously assumed). In this study, a classification is established regarding the impact of wettability on residual capillary trapping. Completing the previous collection of work by Krevor et al. (2015), this study can classify a water wet outcrop sample (mostly from Berea and Bentheimer sandstones) as having L_{and} constant falling in the range of 0.7-2. Interestingly, for some limestones also the constant falls in the same range. The constant for some sandstones taken from real reservoir cores and treated samples representing mix wet lay in a range of 2.8-4.1. Some outliers in collected data were also found. In the reviewed literature, some studies have found contradicting findings regarding the amount of CO₂ residually trapped under water wet and CO₂ wet conditions. The review has found that the lack of standardized method to investigate the wettability impact on multiphase flow and capillary residual trapping results in such a wide ranges of L_{and} constant being reported. Some researchers have used asphaltene precipitation to get a mix wet sample while others functionalized the rock with a chemical to create a hydrophobic surface. The latter method is considered more reliable for giving a contrast wettability without appreciable changes in porosity, permeability, pore structure, etc.

Subsequent to the above detailed literature review, to provide a more comprehensive insight into how multiphase flow and capillary residual trapping may be impacted by different wettabilities, a set of numerical simulations have been run in this study. A wider plume is obtained with decreasing the degree of water wetness. This observation is caused by lower irreducible water saturation which provides more space for CO₂ to flow in lateral direction. Consequently, a more advanced vertical plume migration is seen in water wet case resulting in shorter time to reach the caprock. Due to less CO₂ being residually trapped, both intermediate and CO₂ wet cases result in a large volume of mobile CO₂ reaching the top of the storage medium and spreading underneath the caprock.

Chapter 5 Conclusions, Recommendations, and Future Work

5.1. Conclusions

This study has evaluated the use of wettability alteration to remediate salt precipitation and entailing injectivity issues. It has also explored the impact of wettability on the plume propagation and residual trapping mechanism. A set of experimental results from published literatures were adopted in modelling the effect of wettability on various input data required for the planned numerical simulation cases. The required input data were collected during a comprehensive review of the relevant literature.

The following are the major conclusions drawn from the simulation study work:

- Simulation study of injectivity issue remediation:
 - a. Kinetics approach model for water evaporation was generated based on the recent finding that was considered more reasonable for salt precipitation modelling. A validation process was conducted using coreflooding results from a published work showing a good agreement with the simulation results obtained in this study.
 - b. According to the simulation results, with hydrophobic silylation, the combined impact of salt precipitation and water blockage on relative injectivity change (RIC) decrease on an absolute basis by up to 7% (i.e., injectivity is improved). The scCO₂ based silylation can decrease the amount of water trapped near the wellbore and, thus, alleviate the amount of salt potentially being deposited.
- Simulation study of wettability impacts on multiphase flow, residual trapping, and storage performance:
 - a. The impact of different wettability states on multiphase flow in CO₂-brine system was found to be insignificant as revealed by the critical review conducted in this work. Even though an extreme wettability contrast was evident from contact angle measurements reported in experimental work reviewed, the relative permeabilities were not impacted as significant as the hypothetical datasets used in previous numerical simulation studies.
 - b. An attempt to classify Land trapping coefficient based on wettability states gives a range of 0.7-2 and 2.8-4.1 for water wet and mix wet conditions, respectively. A lack of standardized experimental procedures, not to mention the heterogeneities of the

samples used by the investigators, is believed to be responsible for the high uncertainty in the coefficient ranges reported for different wettability states.

- c. The simulation results obtained in this work using a homogeneous box model show a faster advancing of vertical plume movement in water-wet case compared to that in other wettability states. This is caused by the relatively higher irreducible water saturation in the water-wet case that leaves limited pore space for CO₂ to occupy. The lateral extension of plume from all cases seems comparable. This could be due to a minor deviation in relative permeability curves across different wettability states. This outcome differs from those reported by prior simulation studies that use hypothetical/assumed datasets to characterize the multiphase flow under different wettability states.

As elaborated by the outcomes of this study, wettability is impactful towards technical evaluation of various aspects of CO₂ geo-sequestration in aquifers, i.e., injectivity, trapping mechanisms, and plume migration. A water-wet state near the wellbore can be problematic for well injectivity. The application of wettability alteration using chemical treatment (scCO₂ based silylation) may be used to alleviate the issue. However, water-wet condition for bulk of the aquifer formation is expected to give much CO₂ trapped under residual trapping. Thus, the risks posed by a large of volume of CO₂ accumulating under the caprock is reduced.

5.2. Recommendations and Future Works

The following recommendations can be considered in any future study centered around the application of wettability alteration using chemical treatment:

- ScCO₂ based silylation must be applied as early as possible to reduce the severity of salt precipitation. The formation of solid salts covering the pore surface may halt the silylation process in altering wettability. Silane may fail to access quartz which is already covered by salt. This phenomenon was recognized by Arjomand et al. (Arjomand et al. 2020b).
- Specific experiments are required to investigate the effects of evaporation and silylation when they take place simultaneously. The evaporation rate of water component in the presence of silane in CO₂ phase may not be the same as that for the pure CO₂ injection. The current work does not consider the existence of silane in evaporation model.
- There could be another wettability alteration mechanism taking place due to salt precipitation which has been investigated by others as a hydrophilic microporous crystal (Kim et al., 2013; Miri et al., 2015; Miri & Hallevang, 2016). In this case, the suction of brine toward evaporation front under capillary force may be stronger.

- Further study needs to be done considering the pore geometry to complete the wettability-based classification of the Land trapping coefficient. This could assist the modelling process for CO₂ geo-sequestration.
- All simulation work in this study was performed using a homogeneous box model. The use of a heterogeneous model is recommended for any future work.

References

- Abdoulghafour, H., Sarmadivaleh, M., Hauge, L. P., Fernø, M., & Iglauer, S. (2020). Capillary Pressure Characteristics of CO₂-Brine-Sandstone Systems. *International Journal of Greenhouse Gas Control*, *94*, 102876.
- Abidoeye, L. K., Khudaida, K. J., & Das, D. B. (2015). Geological Carbon Sequestration in the Context of Two-Phase Flow in Porous Media: A Review. *Critical Reviews in Environmental Science and Technology*, *45*, 1105–1147.
- Ahmed, T. (2001). *Reservoir Engineering Handbook* (2nd ed.). Houston: Butterworth-Heinemann.
- Ajayi, T., Gomes, J. S., & Bera, A. (2019). A Review of CO₂ Storage in Geological Formations Emphasizing Modeling, Monitoring and Capacity Estimation Approaches. *Petroleum Science*, *16*, 1028–1063.
- Akbarabadi, M., & Piri, M. (2013). Relative Permeability Hysteresis and Permanent Capillary Trapping Characteristics of Supercritical CO₂/brine Systems: An Experimental Study at Reservoir Conditions. *Advances in Water Resources*, *52*, 190–206.
- Al Hameli, F., Belhaj, H., & Al Dhohoori, M. (2022). CO₂ Sequestration Overview in Geological Formations: Trapping Mechanisms Matrix Assessment. *Energies*, *15*, 7805.
- Al-Anazi, H. A., Walker, J. G., Pope, G. A., Sharma, M. M., & Hackney, D. F. (2003). A successful Methanol Treatment in a Gas-Condensate Reservoir: Field Application. *SPE Production and Operation Symposium*. 22-25 March. Oklahoma City, OK, USA.
- Ali, M., Aftab, A., Awan, F. U., Akhondzadeh, H., Keshavarz, A., Saeedi, A., . . . Sarmadivaleh, M. (2021). CO₂-Wettability Reversal of Cap-rock by Alumina Nanofluid: Implications for CO₂ Geo-storage. *Fuel Processing Technology*, *214*, 106722.
- Ali, M., Jha, N. K., Pal, N., Keshavarz, A., Hoteit, H., & Sarmadivaleh, M. (2022). Recent Advances in Carbon Dioxide Geological Storage, Experimental Procedures, Influencing Parameters, and Future Outlook. *Earth-Science Reviews*, *225*, 103895.
- Al-Khdheawi, E. A., Vialle, S., Barifcani, A., Sarmadivaleh, M., & Iglauer, S. (2017a). Influence of Rock Wettability on CO₂ Migration and Storage. *Energy Procedia*, *114*, 4357 – 4365.

- Al-Khdheawi, E. A., Vialle, S., Barifcani, A., Sarmadivaleh, M., & Iglauer, S. (2017b). Impact of Reservoir Wettability and Heterogeneity on CO₂-plume Migration and Trapping Capacity. *International Journal of Greenhouse Gas Control*, 58, 142–158.
- Al-Khdheawi, E. A., Vialle, S., Barifcani, A., Sarmadivaleh, M., & Iglauer, S. (2018). Enhancement of CO₂ Trapping Efficiency in Heterogeneous Reservoirs by Water Alternating Gas Injection. *Greenhouse Gases: Science and Technology*, 8, 920-931.
- Al-Maamari, R. S., & Buckley, J. S. (2003). Asphaltene Precipitation and Alteration of Wetting: The Potential for Wettability Changes During Oil Production. *SPE Reservoir Evaluation & Engineering*, 6, 210–214.
- Al-Menhali, A. S., & Krevor, S. (2016). Capillary Trapping of CO₂ in Oil Reservoirs: Observations in a Mixed Wet Carbonate Rock. *Environmental Science & Technology*, 50, 2727-2734.
- Al-Menhali, A. S., Menke, H. P., Blunt, M. J., & Krevor, S. C. (2016). Pore Scale Observations of Trapped CO₂ in Mixed-Wet Carbonate Rock: Applications to Storage in Oil Fields. *Environmental Science & Technology*, 50, 10282-10290.
- Alnili, F., Al-Yaseri, A., Roshan, H., Rahman, T., Verall, M., Lebedev, M., . . . Barifcani, A. (2018). Carbon Dioxide/Brine Wettability of Porous Sandstone Versus Solid Quartz: An Experimental and Theoretical Investigation. *Journal of Colloid and Interface Science*, 524, 188-194.
- Amaefule, J. O., Altunbay, M., Tiab, D., Kersey, D. G., & Keelan, D. K. (1993). Enhanced Reservoir Description: Using Core and Log Data to Identify Hydraulic (Flow) Units and Predict Permeability in Uncored Intervals/Wells. *the SPE Annual Technical Conference and Exhibition*. Houston, TX, USA, 3–6 October .
- Amin, J. S., Nikoee, E., Ayotollahi, S., & Alamdari, A. (2010). Investigating Wettability Alteration due to Asphaltene Precipitation: Imprints in Surface Multifractal Characteristics. *Applied Surface Science*, 256, 6466–6472.
- Aminu, M. D., Nabavi, S. A., Rochelle, C. A., & Manovic, V. (2017). A Review of Developments in Carbon Dioxide Storage. *Applied Energy*, 208, 1389-1419.
- André, L., Peysson, Y., & Azaroual, M. (2014). Well Injectivity during CO₂ Storage Operations in Deep Saline Aquifers – Part 2: Numerical Simulations of Drying, Salt Deposit Mechanisms and Role of Capillary Forces. *International Journal of Greenhouse Gas Control*, 22, 301-312.

- Arif, M., Barifcani, A., Lebedev, M., & S., I. (2016). Structural Trapping Capacity of Oil-wet Caprock as a Function of Pressure, Temperature and Salinity. *International Journal of Greenhouse Gas Control*, 50, 112-120.
- Arjomand, E., Easton, C. D., Myers, M., Tian, W., Saeedi, A., & Wood, C. D. (2020a). Changing Sandstone Rock Wettability with Supercritical CO₂-Based Silylation. *Energy & Fuels*, 34, 2015–2027.
- Arjomand, E., Myers, M., Al Hinai, N., Wood, C. D., & Saeedi, A. (2020b). Modifying the Wettability of Sandstones Using Nonfluorinated Silylation: To Minimize the Water Blockage Effect. *Energy Fuels*, 34, 709–719.
- Armitage, P. J., Faulkner, D. R., & H, W. R. (2013). Caprock Corrosion. *Nature Geoscience*, 6, 79-80.
- Armitage, P. J., Worden, R. H., Faulkner, D. R., Aplin, A. C., Butcher, A. R., & Iliffe, J. (2010). Diagenetic and Sedimentary Controls on Porosity in Lower Carboniferous Fine-grained Lithologies, Krechba Field, Algeria: A Petrological Study of a Caprock to a Carbon Capture Site. *Marine and Petroleum Geology*, 27, 1395-1410.
- Aycaguer, A., Lev-On, M., & Winer, A. M. (2001). Reducing Carbon Dioxide Emissions with Enhanced Oil Recovery Projects: A Life Cycle Assessment Approach. *Energy & Fuels*, 15, 303-308.
- Bachu, S. (2000). Sequestration of CO₂ in Geological Media: Criteria and Approach for Site Selection in Response to Climate Change. *Energy Conversion & Management*, 41, 953–970.
- Bachu, S., Gunter, W. D., & Perkins, E. H. (1994). Aquifer Disposal of CO₂: Hydrodynamic, and Mineral Trapping. *Energy Conversion and Management*, 35, 269-279.
- Batistelli, A., Calore, C., & Pruess, K. (1997). The Simulator TOUGH2/EWASG for Modelling Geothermal Reservoirs with Brine and Non-condensable Gas. *Geothermics*, 26, 437-464.
- Beaubien, S. E., Jones, D. G., Gal, F., Barkwith, A. K., Braibant, G., Baubron, J. C., . . . Strutt, M. H. (2013). Monitoring of Near-surface Gas Geochemistry at the Weyburn, Canada, CO₂-EOR site, 2001–2011. *International Journal of Greenhouse Gas Control*, 16, S236-S262.
- Bennion, D. B. (2002). An Overview of Formation Damage Mechanisms Causing a Reduction in the Productivity and Injectivity of Oil and Gas Producing Formations. *Journal of Canadian Petroleum Technology*, 41(11).

- Bennion, D. B., & Bachu, S. (2008). Drainage and Imbibition Relative Permeability Relationships for Supercritical CO₂/Brine and H₂S/Brine Systems in Intergranular Sandstone, Carbonate, Shale, and Anhydrite Rocks. *SPE Reservoir Evaluation & Engineering*, *11*, 487-496.
- Bennion, D. B., Thomas, F. B., & Bietz, R. F. (1996). Low Permeability Gas Reservoirs: Problems, Opportunities and Solutions for Drilling, Completion, Stimulation and Production. *Gas Technology Conference*. 28 April - 1 May. Calgary, Alberta, Canada.
- Benson, S. M., Li, B., Krause, M., Krevor, S., Kuo, C., Pini, R., & Zuo, L. (2013). *Investigations in Geologic Carbon Sequestration: Multiphase Flow of CO₂ and Water in Reservoir Rocks*. Annual Report. Stanford University.
- Bergstad, M., & Shokri, N. (2016). Evaporation of NaCl Solution from Porous Media with Mixed Wettability. *Geophysical Research Letters*, *43*, 4426–4432.
- Blunt, M. J. (1998). Physically-based Network Modeling of Multiphase Flow in Intermediate-wet Porous Media. *Journal of Petroleum Science and Engineering*, *20*, 117-125.
- Blunt, M. J., & Scher, H. (1995). Pore-level Modeling of Wetting. *Physical Review E*, *52*, 6.
- Bryant, S. L., Lakshminarasimhan, S., & Pope, G. A. (2008). Buoyancy-Dominated Multiphase Flow and Its Effect on Geological Sequestration of CO₂. *SPE Journal*, *13*, 447–454.
- Bull, Ø., Bratteli, F., Ringen, J. K., Melhuus, K., Bye, A. L., & Iversen, J. E. (2011). The Quest for the True Residual Gas Saturation – An Experimental Approach. *the International Symposium of the Society of Core Analysts*. Austin, Texas, USA, 18-21 September.
- Burnside, N. M., & Naylor, M. (2014). Review and Implications of Relative Permeability of CO₂/Brine Systems and Residual Trapping of CO₂. *International Journal of Greenhouse Gas Control*, *23*, 1-11.
- Cai, M., Su, Y., Li, L., Hao, Y., & Gao, X. (2021). CO₂-Fluid-Rock Interactions and the Coupled Geomechanical Response during CCUS Processes in Unconventional Reservoirs. *Geofluids*, *2021*, 6671871.
- Canal, J., Delgado, J., Falcón, I., Yang, Q., Juncosa, R., & Barrientos, V. (2013). Injection of CO₂-Saturated Water through a Siliceous Sandstone Plug from the Hontomin Test Site (Spain): Experiment and Modeling. *Environmental Science & Technology*, *47*, 159–167.
- Cao, C., Fadeev, A. Y., & McCarthy, T. J. (2001). Reactions of Organosilanes with Silica Surfaces in Carbon Dioxide. *Langmuir*, *17*, 757-761.

- Carman, P. C. (1937 (online in 1997)). Fluid Flow through Granular Beds. *Chemical Engineering Research and Design*, 75, S32-S48.
- Cavanagh, A. J., & Haszeldine, R. S. (2014). The Sleipner Storage Site: Capillary Flow Modeling of a Layered CO₂ Plume Requires Fractured Shale Barriers within the Utsira Formation. *International Journal of Greenhouse Gas Control*, 21, 101-112.
- Cavanagh, A., & Ringrose, P. (2011). In Salah High-resolution Heterogeneous Simulations of CO₂ Storage. *Energy Procedia*, 4, 3730-3737.
- Chadwick, A., Arts, R., Bernstone, C., May, F., Thibeau, S., & Zweigel, P. (2008). *Best Practice for the Storage of CO₂ in Saline Aquifers*. Amersham: Halstan & Co. Ltd.
- Chang, Y., Coats, B. K., & Nolen, J. S. (1996). A Compositional Model for CO₂ Floods Including CO₂ Solubility in Water. *the Permian Basin Oil and Gas Recovery*. Midland, TX, USA, 27-29 March.
- Chaudhary, K., Cardenas, M. B., Wolfe, W. W., Maisano, J. A., Ketcham, R. A., & Bennet, P. C. (2013). Pore-scale Trapping of Supercritical CO₂ and the Role of Grain Wettability and Shape. *Geophysical Research Letters*, 40, 3878-3882.
- Chilingar, G. V., & Yen, T. F. (1983). Some Notes on Wettability and Relative Permeabilities of Carbonate Reservoir Rocks, II. *Energy Sources*, 7, 67-75.
- Chiquet, P., Broseta, D., & Thibeau, S. (2007). Wettability Alteration of Caprock Minerals by Carbon Dioxide. *Geofluids*, 7, 112-122.
- Cho, J., Kim, T. H., & Lee, K. S. (2016). Compositional Modeling of Hybrid CO₂ EOR with Intermediate Hydrocarbon Solvents to Analyze the Effect of Toluene on Asphaltene Deposition. *Journal of Petroleum Science and Engineering*, 146, 940-948.
- Choi, B., Choi, J., & Lee, K. S. (2015). Integrated Analysis of Permeability Reduction Caused by Polymer Retention for Better Understanding Polymer Transport. *Journal of Chemistry*, 2015, 291905.
- CMG. (2020). *STARS User Guide: Thermal & Advanced Processes Simulator*. Calgary: Computer Modeling Group Ltd.
- Combes, J. R., White, L. D., & Tripp, C. P. (1999). Chemical Modification of Metal Oxide Surfaces in Supercritical CO₂: In Situ Infrared Studies of the Adsorption and Reaction of Organosilanes on Silica. *Langmuir*, 15, 7870-7875.
- Connel, L., Down, D., Lu, M., Hay, D., & Heryanto, D. (2015). An Investigation into the Integrity of Wellbore Cement in CO₂ Storage Wells: Core Flooding Experiments and Simulations. *International Journal of Greenhouse Gas Control*, 37, 424-440.

- Craft, B. C., & Hawkins, M. F. (1991). *Applied Petroleum Reservoir Engineering* (2nd ed.). Englewood Cliffs: Prentice Hall PTR.
- Cui, G., Wang, Y., Rui, Z., Chen, B., Ren, S., & Zhang, L. (2018). Assessing the Combined Influence of Fluid-Rock Interactions on Reservoir Properties and Injectivity during CO₂ Storage in Saline Aquifers. *Energy*, *155*, 281-296.
- Darabi, H., Shirdel, M., Kalaei, M. H., & Sapehnoori, K. (2014). Aspects of Modeling Asphaltene Deposition in a Compositional Coupled Wellbore/Reservoir Simulator. *SPE Improved Oil Recovery Symposium*. 12-16 April. Tulsa, OK. USA.
- de Gennes, P., Brochard-Wyart, F., & Quéré, D. (2004). *Capillarity and Wetting Phenomena: Drops, Bubbles, Pearls, Waves*. New York, USA: Springer-Verlag.
- Department of Energy & Climate Change (DECC). (2012). *CCS Roadmap: Supporting Deployment of Carbon Capture and Storage in the UK*. UK.
- Doughty, C. (2007). Modeling Geologic Storage of Carbon Dioxide: Comparison of Non-hysteretic and Hysteretic Characteristic Curves. *Energy Conversion and Management*, *48*, 1768–1781.
- Downey, M. W. (1984). Evaluating Seals for Hydrocarbon Accumulations. *AAPG Bulletin*, *68*, 1752-1763.
- Druetta, P., & Picchioni, F. (2019). Influence of the Polymer Degradation on Enhanced Oil Recovery Processes. *Applied Mathematical Modelling*, *69*, 142-163.
- Ebigbo, A., Bielinski, A., Kopp, A., Class, H., & Helmig, R. (2006). Numerical Modeling of CO₂ Sequestration with MUFTE-UG. *XVI International Conference on Computational Methods in Water Resources*. Copenhagen, Denmark, 18-22 June.
- El-Maghraby, R. M., & Blunt, M. J. (2013). Residual CO₂ Trapping in Indiana Limestone. *Environmental Science & Technology*, *47*, 227-233.
- Emmanuel, S., Ague, J. J., & Walderhaug, O. (2010). Interfacial Energy Effects and the Evolution of Pore Size Distributions during Quartz Precipitation in Sandstone. *Geochimica et Cosmochimica Acta*, *74*, 3539–3552.
- Ennis-King, J., & Paterson, L. (2002). Engineering Aspects of Geological Sequestration of Carbon Dioxide. *at the SPE Asia Pacific Oil and Gas Conference and Exhibition*. Melbourne, Australia, 8-10 October.
- Ennis-King, J., & Paterson, L. (2005). Role of Convective Mixing in the Long-Term Storage of Carbon Dioxide in Deep Saline Formations. *SPE Journal*, *10*, 349–356.

- Fahes, M., & Firoozabadi, A. (2007). Wettability Alteration to Intermediate Gas-Wetting in Gas-Condensate Reservoirs at High Temperatures. *SPE Journal*, 12, 397-407.
- Fan, Y. (2006). *Development of CO₂ Sequestration Modeling Capabilities in Stanford General Purpose Research Simulator*. MSc Thesis. Stanford University.
- Farcas, A., & Woods, A. W. (2008). The Effect of Drainage on the Capillary Retention of CO₂ in a Layered Permeable Rock. *Journal of Fluid Mechanics*, 618, 349-359.
- Flett, M., Gurton, R., & Weir, G. (2007). Heterogeneous Saline Formations for Carbon Dioxide Disposal: Impact of Varying Heterogeneity on Containment and Trapping. *Journal of Petroleum Science and Engineering*, 57, 106–118.
- Ford, W. G., Penny, G. S., & Briscoe, J. E. (1988). Enhanced Water Recovery Improves Stimulation Results. *SPE Production Engineering*, 3, 515-521.
- Garcia, J. E. (2001). *Density of Aqueous Solutions of CO₂*. Berkeley (CA, USA): Lawrence Berkeley National Lab. (LBNL).
- Gaus, I. (2010). Role and Impact of CO₂–Rock Interactions during CO₂ Storage in Sedimentary Rocks. *International Journal of Greenhouse Gas Control*, 4, 73–89.
- Gershenson, N. I., Ritzi Jr., R. W., Dominic, D. F., Mehnert, E., & Okwen, R. T. (2017). Capillary Trapping of CO₂ in Heterogeneous Reservoirs during the Injection Period. *International Journal of Greenhouse Gas Control*, 59, 13-23.
- Ghiat, I., & Al-Ansari, T. (2021). A Review of Carbon Capture and Utilisation as a CO₂ Abatement Opportunity within the EWF Nexus. *Journal of CO₂ Utilization*, 45, 101432.
- Giorgis, T., Carpita, M., & Battistelli, A. (2007). 2D Modeling of Salt Precipitation during the Injection of Dry CO₂ in a Depleted Gas Reservoir. *Energy Conversion and Management*, 48, 1816-1826.
- Global CCS Institute. (2022). *Global Status of CCS 2022*.
- Goater, A. L., Bijeljic, B., & Blunt, M. J. (2013). Dipping Open Aquifers—the Effect of Top-surface Topography and Heterogeneity on CO₂ Storage Efficiency. *International Journal of Greenhouse Gas Control*, 17, 318–331.
- Guyant, E., Han, W. S., Kim, K., Park, M., & B., K. (2015). Salt Precipitation and CO₂/Brine Flow Distribution under Different Injection Well Completions. *International Journal of Greenhouse Gas Control*, 37, 299–310.
- Herzog, H., & Golomb, D. (2004). Carbon Capture and Storage from Fossil Fuel Use. In C. J. Cleveland, *Encyclopedia of Energy* (pp. 277-287). Elsevier.

- Hildenbrand, A., Schlömer, S., & Kroos, B. M. (2002). Gas Breakthrough Experiments on Fine-grained Sedimentary Rocks. *Geofluids*, 2, 3-23.
- Hildenbrand, A., Schlömer, S., Kroos, B. M., & Littke, R. (2004). Gas Breakthrough Experiments on Pelitic Rocks: Comparative Study with N₂, CO₂ and CH₄. *Geofluids*, 4, 61-80.
- Ho, T. M., & Tsai, P. A. (2020). Microfluidic Salt Precipitation: Implications for Geological CO₂ Storage. *Lab on a Chip*, 20, 3806.
- Holditch, S. A. (1979). Factors Affecting Water Blocking and Gas Flow from Hydarulically Fractured Gas Wells. *Journal of Petroleum Technology*, 31(12), 1515-1524.
- Hu, R., Wan, J., Kim, Y., & Tokunaga, T. K. (2017). Wettability Impact on Supercritical CO₂ Capillary Trapping: Pore-scale Visualization and Quantification. *Water Resources Research*, 53, 6377-6394.
- Hu, Y., Ray, J. R., & Jun, Y. (2011). Biotite–Brine Interactions under Acidic Hydrothermal Conditions: Fibrous Illite, Goethite, and Kaolinite Formation and Biotite Surface Cracking. *Environmental Science & Technology*, 45, 6175–6180.
- Hunt, J. R., Sitar, N., & Udell, K. S. (1988). Nonaqueous Phase Liquid Transport and Cleanup: 1. Analysis of Mechanisms. *Water Resources Research*, 24, 1247-1258.
- Hurter, S., Labregere, D., & Berge, J. (2007). Simulations for CO₂ Injection Projects with Compositional Simulator. *Offshore Europe 2007*. Aberdeen, UK, 4-7 September.
- Iglauer, S., Al-Yaseri, A. Z., Rezaee, R., & Lebedev, M. (2015b). CO₂ Wettability of Caprocks: Implications for Structural Storage Capacity and Containment Security. *Geophysical Research Letters*, 42, 9279–9284.
- Iglauer, S., Paluszny, A., Pentland, C. H., & Blunt, M. J. (2011). Residual CO₂ Imaged with X-ray Micro-tomography. *Geophysical Research Letters*, 38, L21403.
- Iglauer, S., Pentland, C. H., & Busch, A. (2015a). CO₂ Wettability of Seal and Reservoir Rocks and the Implications for Carbon Geo-sequestration. *Water Resources Research*, 51, 729–774.
- Iglauer, S., Sarmadivaleh, M., Al-Yaseri, A., & Lebedev, M. (2014). Permeability Evolution in Sandstone due to Injection of CO₂-saturated Brine or Supercritical CO₂ at Reservoir Conditions. *Energy Procedia*, 63, 3051 – 3059.
- Issa, A. A., & Luyt, A. S. (2019). Kinetics of Alkoxysilanes and Organoalkoxysilanes Polymerization: A Review. *Polymers*, 11, 537.

- Jeddizahed, J., & Rostami, B. (2016). Experimental Investigation of Injectivity Alteration due to Salt Precipitation during CO₂ Sequestration in Saline Aquifers. *Advances in Water Resources*, 96, 23–33.
- Jerauld, G. R. (1997). General Three-Phase Relative Permeability Model for Prudhoe Bay. *SPE Reservoir Engineering*, 12, 255-263.
- Ji, X., Tan, S. P., Adidharma, H., & Radosz, M. (2005). SAFT1-RPM Approximation Extended to Phase Equilibria and Densities of CO₂-H₂O and CO₂-H₂O-NaCl Systems. *Industrial & Engineering Chemistry Research*, 44, 8419-8427.
- Jiang, X. (2011). A Review of Physical Modelling and Numerical Simulation of Long-term Geological Storage of CO₂. *Applied Energy*, 88, 3557–3566.
- Juanes, R., MacMinn, C. W., & Szulczewski, M. L. (2010). The Footprint of the CO₂ Plume during Carbon Dioxide Storage in Saline Aquifers: Storage Efficiency for Capillary Trapping at the Basin Scale. *Transport in Porous Media*, 82, 19–30.
- Juanes, R., Spiteri, E. J., Orr Jr., F. M., & Blunt, M. J. (2006). Impact of Relative Permeability Hysteresis on Geological CO₂ Storage. *Water Resources Research*, 42, W12418.
- Kim, K., Han, W. S., Oh, J., Kim, T., & Kim, J. (2012). Characteristics of Salt-Precipitation and the Associated Pressure Build-Up during CO₂ Storage in Saline Aquifers. *Transport in Porous Media*, 92, 397–418.
- Kim, M., Sell, A., & Sinton, D. (2013). Aquifer-on-a-chip: Understanding Pore-scale Salt Precipitation Dynamics during CO₂ Sequestration. *Lab Chip*, 13, 2508-2518.
- Kleinitz, W., Koehler, M., & Dietzsch, G. (2001). The Precipitation of Salt in Gas Producing Wells. *the SPE European Formation Damage Conference*. The Hague, The Netherlands, 21-22 May.
- Kohse, B. F., & Nghiem, L. X. (2004). Modelling Asphaltene Precipitation and Deposition in a Compositional Reservoir. *SPE/DOE Symposium on Improved Oil Recovery*. 17-21 April. Tulsa, OK, USA.
- Kralik, J. G., Manak, L. J., Jerauld, G. R., & Spence, A. P. (2000). Effect of Trapped Gas on Relative Permeability and Residual Oil Saturation in an Oil-Wet Sandstone. *the SPE Annual Technical Conference and Exhibition*. Dallas, Texas, USA, 1-4 October.
- Krause, M., Perrin, J. C., & Benson, S. M. (2011). Modeling Permeability Distributions in a Sandstone Core for History Matching Coreflood Experiments. *SPE Journal*, 16, 768-777.

- Krevor, S., Blunt, M. J., Benson, S. M., Pentland, C. H., Reynolds, C., Al-Menhali, A., & Niu, B. (2015). Capillary Trapping for Geologic Carbon Dioxide Storage – From Pore Scale Physics to Field Scale Implications. *International Journal of Greenhouse Gas Control*, 40, 221–237.
- Krevor, S., Pini, R., Zuo, L., & Benson, S. M. (2012). Relative Permeability and Trapping of CO₂ and Water in Sandstone Rocks at Reservoir Conditions. *Water Resources Letter*, 48, W02532.
- Kumar, A., Ozah, R., Noh, M., Pope, G. A., Bryant, S., Sepehrnoori, K., & Lake, L. W. (2005). Reservoir Simulation of CO₂ Storage in Deep Saline Aquifer. *SPE Journal*, 10, 336–348.
- Lamy, C., Iglauer, S., Pentland, C. H., Blunt, M. J., & Maitland, G. (2010). Capillary Trapping in Carbonate Rocks. *the SPE EUROPEC/EAGE Annual Conference and Exhibition*. Barcelona, Spain, 14–17 June.
- Land, C. S. (1968). Calculation of Imbibition Relative Permeability for Two- and Three-Phase Flow from Rock Properties. *SPE Journal*, 8, 149 - 156.
- Li, K., Liu, Y., Zheng, H., Huang, G., & Li, G. (2011). Enhanced Gas-condensate Production by Wettability Alteration to Gas Wetness. *Journal of Petroleum Science and Engineering*, 78, 505-509.
- Li, X., & Fan, X. (2015). Effect of CO₂ Phase on Contact Angle in Oil-wet and Water-wet Pores. *International Journal of Greenhouse Gas Control*, 36, 106-113.
- Li, Y., & Nghiem, L. (1986). Phase Equilibria of Oil, Gas and Water/Brine Mixtures from a Cubic Equation of State and Henry's Law. *The Canadian Journal of Chemical Engineering*, 64, 486-496.
- Li, Z., Dong, M., Li, S., & Huang, S. (2006). CO₂ Sequestration in Depleted Oil and Gas Reservoirs—Caprock Characterization and Storage Capacity. *Energy Conversion and Management*, 47, 1372–1382.
- Liang, Y., Tsuji, S., Jia, J., Tsuji, T., & Matsuoka, T. (2017). Modeling CO₂-Water-Mineral Wettability and Mineralization for Carbon Geosequestration. *Accounts of Chemical Research*, 50, 1530-1540.
- Lindeberg, E., & Wessel-Berg, D. (1997). Vertical Convection in an Aquifer Column under a Gas Cap of CO₂. *Energy Conversion and Management*, 38, S229-S234.

- Liu, F., Lu, P., Griffith, C., Hedges, S. W., Soong, Y., Hallevang, H., & Zhu, C. (2012). CO₂–Brine–Caprock Interaction: Reactivity Experiments on Eau Claire Shale and a Review of Relevant Literature. *International Journal of Greenhouse Gas Control*, 7, 153–167.
- Lopez, G. M., Myers, M. B., Xie, Q., Wood, C. D., & Saeedi, A. (2021). Wettability Alteration Using Benzoxazine Resin: A Remedy for Water Blockage in Sandstone Gas Reservoirs. *Fuel*, 291, 120189.
- Lopez, G. M., Myers, M. B., Xie, Q., Wood, C. D., Al-Bayati, D., & Saeedi, A. (2023). Wettability Alteration to Reduce Water Blockage in Low-Permeability Sandstone Reservoirs. *Transport in Porous Media*, 147, 401-428.
- López-Aranguren, P., Saurina, J., Vega, L. F., & Domingo, C. (2012). Sorption of Tryalkoxysilane in Low-cost Porous Silicates Using a Supercritical CO₂ Method. *Microporous and Mesoporous Materials*, 148, 15–24.
- Lorenz, S., & Müller, W. (2003). Modelling of Halite Formation in Natural Gas Storage Aquifers . *TOUGH Symposium*. Berkeley, CA, USA, 12-14 May.
- Loste, E., Fraile, J., Fanovich, M. A., Werlee, G. G., & Domingo, C. (2004). Compositional Modeling of Hybrid CO₂ EOR with Intermediate Hydrocarbon Solvents to Analyze the Effect of Toluene on Asphaltene Deposition. *Advanced Materials*, 16, 739-744.
- MacDowell, N., Florin, N., Buchard, A., Hallett, J., Galindo, A., Jackson, G., . . . Fennell, P. (2010). An Overview of CO₂ Capture Technologies. *Energy & Environmental Sciences*, 3, 1645-1669.
- Mahadevan, J., & Sharma, M. M. (2003). Clean-up of Water Blocks in Low Permeability Formations. *SPE Annual Technical Conference and Exhibition*. 5-8 October. Denver, CO, USA.
- Meng, Q., & Jiang, X. (2014). Numerical Analyses of the Solubility Trapping of CO₂ Storage in Geological Formations. *Applied Energy*, 130, 581–591.
- Meng, Q., Jiang, X., Li, D., & Xie, Q. (2015). Numerical Simulations of Pressure Buildup and Salt Precipitation during Carbon Dioxide Storage in Saline Aquifers. *Computers and Fluids*, 121, 92-101.
- Miri, R., & Hellevang, H. (2016). Salt Precipitation during CO₂ Storage—A Review. *International Journal of Greenhouse Gas Control*, 51, 136-147.
- Miri, R., van Noort, R., Aagaard, P., & Hellevang, H. (2015). New Insights on the Physics of Salt Precipitation during Injection of CO₂ into Saline Aquifers. *International Journal of Greenhouse Gas Control*, 43, 10-21.

- Mohamed, I. M., He, J., & Nasr-El-Din, H. A. (2012). Carbon Dioxide Sequestration in Sandstone Aquifers: How Does It Affect Permeability. *Carbon Management Technology Conference*. 7-9 February. Orlando, FL, USA.
- Mostaghimi, P., Blunt, M. J., & Bijeljic, B. (2013). Computations of Absolute Permeability on Micro-CT Images. *Mathematical Geosciences*, 45, 103–125.
- Muslemani, H., Liang, X., Kaesehage, K., & Wilson, J. (2020). Business Models for Carbon Capture, Utilization and Storage Technologies in the Steel Sector: A Qualitative Multi-Method Study. *Processes*, 8, 576.
- National Aeronautics and Space Administration (NASA). (2023). *Vital Signs: Carbon Dioxide*. Retrieved February 21, 2023, from <https://climate.nasa.gov/vital-signs/carbon-dioxide/>
- Nghiem, L., Sammon, P., Grabenstetter, J., & Ohkuma, H. (2004). Modeling CO₂ Storage in Aquifers with a Fully-Coupled Geochemical EOS Compositional Simulator. *the SPE/DOE Symposium on Improved Oil Recovery*. Tulsa, OK, USA, 17-21 April.
- Nghiem, L., Yang, C., Shrivastava, V., Kohse, B., Hassam, M., & Card, C. (2009). Risk Mitigation Through the Optimization of Residual Gas and Solubility Trapping for CO₂ Storage in Saline Aquifers. *Energy Procedia*, 1, 3015–3022.
- Ni, H., Boon, M., Garing, C., & Benson, S. M. (2019). Predicting CO₂ Residual Trapping Ability based on Experimental Petrophysical Properties for Different Sandstone Types. *International Journal of Greenhouse Gas Control*, 86, 158–176.
- Niu, B., Al-Menhali, A., & Krevor, S. C. (2015). The Impact of Reservoir Conditions on the Residual Trapping of Carbon Dioxide in Berea Sandstone. *Water Resources Research*, 51, 2009-2029.
- Nordbotten, J. M., & Dahle, H. K. (2011). Impact of the Capillary Fringe in Vertically Integrated Models for CO₂ Storage. *Water Resources Research*, 47, W02537.
- Nordbotten, J. M., Celia, M. A., & Bachu, S. (2005). Injection and Storage of CO₂ in Deep Saline Aquifers: Analytical Solution for CO₂ Plume Evolution During Injection. *Transport in Porous Media*, 58, 339–360.
- Obi, E. I., & Blunt, M. J. (2006). Streamline-based Simulation of Carbon Dioxide Storage in a North Sea Aquifer. *Water Resources Research*, 42, W03414.
- Ott, H., Roels, S. M., & de Kloe, K. (2015). Salt Precipitation due to Supercritical Gas Injection: I. Capillary-driven Flow in Unimodal Sandstone. *International Journal of Greenhouse Gas Control*, 43, 247-255.

- Ott, H., Snippe, J., & de Kloe, K. (2021). Salt Precipitation due to Supercritical Gas Injection: II. Capillary Transport in Multi Porosity Rocks. *International Journal of Greenhouse Gas Control*, 105, 103233.
- Pairoys, F., & Caubit, C. (2023). Water-Gas Imbibition Relative Permeability: Literature Review, Direct versus Indirect Methods and Experimental Recommendations. *E3S Web of Conferences*, 367, 01007.
- Parvin, S., Masoudi, M., Sundal, A., & Miri, R. (2020). Continuum Scale Modelling of Salt Precipitation in the Context of CO₂ Storage in Saline Aquifers with MRST Compositional. *International Journal of Greenhouse Gas Control*, 99, 103075.
- Peng, D. Y., & Robinson, D. B. (1976). A New Two-Constant Equation of State. *Industrial & Engineering Chemistry Fundamentals*, 15, 59-64.
- Pentland, C. H., El-Maghraby, R., Iglauer, S., & Blunt, M. J. (2011). Measurements of the Capillary Trapping of Super-critical Carbon Dioxide in Berea Sandstone. *Geophysical Research Letters*, 38, L06401.
- Peysson, Y., Bazin, B., Magnier, C., Kohler, E., & Youssef, S. (2011). Permeability Alteration due to Salt Precipitation Driven by Drying in the Context of CO₂ Injection. *Energy Procedia*, 4, 4387–4394.
- Pickup, E. G., Jin, M., & Mackay, E. J. (2012). Simulation of Near-Well Pressure Build-up in Models of CO₂ Injection. *ECMOR XIII - 13th European Conference on the Mathematics of Oil Recovery*. Biarritz, France, 10-13 September.
- Pickup, G. E., Jin, M., Olden, P., Mackay, E. J., & Sohrabi, M. (2011). Modeling CO₂ Storage in Aquifers with a Fully-Coupled Geochemical EOS Compositional Simulator. *the SPE EUROPEC/EAGE Annual Conference and Exhibition*. Vienna, Austria, 23-26 May.
- Pinder, G. F., & Celia, M. A. (2006). *Subsurface Hydrology*. Hoboken, NJ: John Wiley & Sons, Inc.
- Pinho, S. P., & Macedo, E. A. (2005). Solubility of NaCl, NaBr, and KCl in Water, Methanol, Ethanol, and Their Mixed Solvents. *Journal of Chemical & Engineering Data*, 50, 29-32.
- Pruess, K. (2005). *ECO2N: A TOUGH2 Fluid Property Module for Mixtures of Water, NaCl, and CO₂*. Berkeley, CA: Lawrence Berkeley National Laboratory.

- Pruess, K., & Müller, N. (2009). Formation Dry-out from CO₂ Injection into Saline Aquifers: 1. Effects of Solids Precipitation and Their Mitigation. *Water Resources Research*, 45, W03402.
- Pruess, K., Garcia, J., Kovscek, T., Oldenburg, C., Rutqvist, J., Steefel, C., & Xu, T. (2002). *Intercomparison of Numerical Simulation Codes for Geologic Disposal of CO₂*. Berkeley, CA: Lawrence Berkeley National Laboratory (LBNL).
- Pruess, K., Xu, T., Apps, J., & Garcia, J. (2003). Numerical Modeling of Aquifer Disposal of CO₂. *SPE Journal*, 8, 49–60.
- Qi, R., LaForce, T. C., & Blunt, M. J. (2009). Design of Carbon Dioxide Storage in Aquifers. *International Journal of Greenhouse Gas Control*, 3, 195–205.
- Rackley, S. A. (2017). *Carbon Capture and Storage*. Oxford: Butterworth-Heinemann.
- Rahman, T., Lebedev, M., Barifcani, A., & Iglauer, S. (2016). Residual Trapping of Supercritical CO₂ in Oil-wet Sandstone. *Journal of Colloid and Interface Science*, 469, 63-68.
- Ren, B., & Trevisan, L. (2020). Characterization of Local Capillary Trap Clusters in Storage Aquifers. *Energy*, 193, 116795.
- Reynolds, C. A., Blunt, M. J., & Krevor, S. (2018). Multiphase Flow Characteristics of Heterogeneous Rocks From CO₂ Storage Reservoirs in the United Kingdom. *Water Resources Research*, 54, 729–745.
- Rezaee, R., Saeedi, A., Iglauer, S., & Evans, B. (2017). Shale Alteration after Exposure to Supercritical CO₂. *International Journal of Greenhouse Gas Control*, 62, 91–99.
- Riaz, A., & Cinar, Y. (2014). Carbon Dioxide Sequestration in Saline Formations: Part I—Review of the Modeling of Solubility Trapping. *Journal of Petroleum Science and Engineering*, 124, 367–380.
- Riaz, A., Hesse, M., Tchelepi, A., & Orr Jr., F. M. (2006). Onset of Convection in a Gravitationally Unstable Diffusive Boundary Layer in Porous Media. *Journal of Fluid Mechanics*, 548, 87–111.
- Rochelle, C. A., Czernichowski-Lauriol, I., & Milodowski, A. E. (2004). The Impact of Chemical Reactions on CO₂ Storage in Geological Formations: a Brief Review. *Geological Society, London, Special Publications*, 233, 87–106.
- Roels, S. M., El Chatib, N., Nicolaidis, C., & Zitha, P. L. (2016). Capillary-Driven Transport of Dissolved Salt to the Drying Zone During CO₂ Injection in Homogeneous and Layered Porous Media. *Transport in Porous Media*, 111, 411-424.

- Roels, S. M., Ott, H., & Zitha, P. L. (2014). μ -CT Analysis and Numerical Simulation of Drying Effects of CO₂ Injection into Brine-saturated Porous Media. *International Journal of Greenhouse Gas Control*, 27, 146-154.
- Rowe, A. M., & Chou, J. C. (1970). Pressure-Volume-Temperature-Concentration Relation of Aqueous Sodium Chloride Solutions. *Journal of Chemical and Engineering Data*, 15, 61-66.
- Rufai, A., & Crawshaw, j. (2018). Effect of Wettability Changes on Evaporation Rate and the Permeability Impairment due to Salt Deposition. *ACS Earth and Space Chemistry*, 2, 320–329.
- Rusanov, A. I., Esipove, N. E., & Sobolev, V. D. (2019). Strong Dependence of Contact Angle on Pressure. *Physical Chemistry*, 487, 87-90.
- Rutqvist, J. (2012). The Geomechanics of CO₂ Storage in Deep Sedimentary Formations. *Geotechnical and Geological Engineering*, 30, 525–551.
- Sánchez-Vicente, Y., Pando, C., Cortijo, M., & Cabañas, A. (2014). Chemical Surface Modification of Mesoporous Silica SBA-15 with a Tertiary Aminosilane Using Supercritical Carbon Dioxide. *Microporous and Mesoporous Materials*, 193, 145–153.
- Sawamura, S., Egoshi, N., Setoguchi, Y., & Matsuo, H. (2007). Solubility of Sodium Chloride in Water under High Pressure. *Fluid Phase Equilibria*, 254, 158-162.
- Sayegh, S. G., Krause, F. F., Girard, M., & DeBree, C. (1990). Rock/Fluid Interactions of Carbonated Brines in a Sandstone Reservoir: Pembina Cardium, Alberta, Canada. *SPE Formation Evaluation*, 5(4), 399-405.
- Schaefer, H. T., & McGrail, B. P. (2005). Direct Measurements of pH and Dissolved CO₂ in H₂O-CO₂ Brine Mixtures to Supercritical Conditions. *Proceedings of the 7th International Conference on Greenhouse Gas Control Technologies*, (pp. 2169-2173). Vancouver, Canada.
- Shao, H., Ray, J. R., & Jun, Y. (2010). Dissolution and Precipitation of Clay Minerals under Geologic CO₂ Sequestration Conditions: CO₂-Brine-Phlogopite Interactions. *Environmental Science & Technology*, 4, 5999–6005.
- Shi, J. Q., Xue, Z., & Durucan, S. (2011a). Supercritical CO₂ Core Flooding and Imbibition in Berea Sandstone – CT Imaging and Numerical Simulation. *Energy Procedia*, 4, 5001-5008.


- Shi, J. Q., Xue, Z., & Durucan, S. (2011b). Supercritical CO₂ Core Flooding and Imbibition in Tako Sandstone—Influence of Sub-core Scale Heterogeneity. *International Journal of Greenhouse Gas Control*, 5, 75-87.
- Sifuentes, W., Blunt, M. J., & Giddins, M. A. (2012). Modeling CO₂ Storage in Aquifers: Assessing the Key Contributors to Uncertainty. *the 2009 SPE Offshore Europe Oil & Gas Conference & Exhibition*. Aberdeen, UK, 8-11 September.
- Sigfusson, B., Gislason, S. G., Matter, J. M., Stute, M., Gunnlaugsson, E., Gunnarsson, I., . . . Oelkers, E. H. (2015). Solving the Carbon-dioxide Buoyancy Challenge: The Design and Field Testing of a Dissolved CO₂ Injection System. *International Journal of Greenhouse Gas Control*, 37, 213–219.
- Sigmund, P. M., & McCaffery, F. G. (1979). An Improved Unsteady-State Procedure for Determining the Relative-Permeability Characteristics of Heterogeneous Porous Media. *SPE Journal*, 19, 15-28.
- Sminchak, J., & Gupta, N. (2003). Aspects of Induced Seismic Activity and Deep-well Sequestration of Carbon Dioxide. *Environmental Geosciences*, 10, 81–89.
- Smith, N., Boone, P., Oguntimehin, A., van Essen, G., Guo, R., Reynolds, M. A., . . . O'Brien, S. (2022). Quest CCS Facility: Halite Damage and Injectivity Remediation in CO₂ Injection Wells . *International Journal of Greenhouse Gas Control*, 119, 103718.
- Sokama-Neuyam, Y. A., Ginting, P. U., Timilsina, B., & Ursin, J. R. (2017). The Impact of Fines Mobilization on CO₂ Injectivity: An Experimental Study. *International Journal of Greenhouse Gas Control*, 65, 195-202.
- Song, J. W., & Fan, L. W. (2022). Understanding the Effects of Pressure on the Contact Angle of Water on a Silicon Surface in Nitrogen Gas Environment: Contrasts between Low- and High-Temperature Regimes. *Journal of Colloid and Interface Science*, 607, 1571-1579.
- Spiteri, E. J., Juanes, R., Blunt, M. J., & Orr, F. M. (2008). A new Model of Trapping and Relative Permeability Hysteresis for All Wettability Characteristics. *SPE Journal*, 13, 277-288.
- Spycher, N., & Pruess, K. (2005). CO₂-H₂O Mixtures in the Geological Sequestration of CO₂. II. Partitioning in Chloride Brines at 12–100°C and up to 600 Bar. *Geochimica et Cosmochimica Acta*, 69, 3309–3320.
- Srivastava, R. K., Huang, S. S., & Dong, M. (1999). Asphaltene Deposition during CO₂ Flooding. *SPE Productions & Facilities*, 14(4), 235-246.

- Staroverov, S. M., & Fadeev, A. Y. (1991). Apparent Simplicity of Reversed Stationary Phases for High Performance Liquid Chromatography. *Journal of Chromatography*, 544, 77-98.
- Tang, G. Q., & Firoozabadi, A. (2003). Wettability Alteration to Intermediate Gas-Wetting in Porous Media at Elevated Temperatures. *Transport in Porous Media*, 52, 185-211.
- Tokunaga, T. K., Wan, J., Jung, J., Kim, T. W., Kim, Y., & Dong, W. (2013). Capillary Pressure and Saturation Relations for Supercritical CO₂ and Brine in Sand: High-pressure Pc(Sw) Controller/meter Measurements and Capillary Scaling Predictions. *Water Resources Research*, 49, 4566-4579.
- Trevisan, L., Pini, R., Cihan, A., Birkholzer, J. T., Zhou, Q., & Illangasekare, T. H. (2015). Experimental Analysis of Spatial Correlation Effects on Capillary Trapping of Supercritical CO₂ at the Intermediate Laboratory Scale in Heterogeneous Porous Media. *Water Resources Research*, 51, 8791-8805.
- Valluri, M., Mishra, S., & Ganesh, P. R. (2021). Injectivity Index: A Powerful Tool for Characterizing CO₂ Storage Reservoirs—A Technical Note. *Greenhouse Gases Science and Technology*, 11, 251-265.
- Verma, A., & Pruess, K. (1988). Thermohydrologic Conditions and Silica Redistribution near High-Level Nuclear Wastes Emplaced in Saturated Geological Formations. *Journal of Geophysical Research*, 93, 1159-1173.
- Voormeij, D. A., & Simandl, G. J. (2002). *Geological and Mineral CO₂ Sequestration Options: A Technical Review*. British Columbia Geological Survey: Geological Fieldwork.
- Wang, J., & Liu, H. (2014). A Novel Model and Sensitivity Analysis for Viscoelastic Polymer Flooding in Offshore Oilfield. *Journal of Industrial and Engineering Chemistry*, 20, 656-667.
- Wang, S., Tokunaga, T. K., Wan, J., Dong, W., & Kim, Y. (2016). Capillary Pressure-Saturation Relations in Quartz and Carbonate Sands: Limitations for Correlating Capillary and Wettability Influences on Air, Oil, and Supercritical CO₂ Trapping. *Water Resources Research*, 52, 6671-6690.
- Wang, Z., Pereira, J. M., Sauret, E., & Gan, Y. (2023). Wettability Impacts Residual Trapping of Immiscible Fluids during Cyclic Injection. *Journal of Fluid Mechanics*, 961, A19.
- White, S. P., Allis, R. G., Moore, J., Chidsey, T., Morgan, C., Gwynn, W., & Adams, M. (2005). Simulation of Reactive Transport of Injected CO₂ on the Colorado Plateau, Utah, USA. *Chemical Geology*, 217, 387-405.

- Wollenweber, J., Alles, S., Busch, A., Kroos, B. M., Stanjek, H., & Littke, R. (2010). Experimental Investigation of the CO₂ Sealing Efficiency of Caprocks. *International Journal of Greenhouse Gas Control*, 4, 231–241.
- Wu, J., Farouk, T., & Ward, C. A. (2007). Pressure Dependence of the Contact Angle. *The Journal of Physical Chemistry B*, 111, 6189-6197.
- Wu, S., & Firoozabadi, A. (2010). Permanent Alteration of Porous Media Wettability from Liquid-Wetting to Intermediate Gas-Wetting. *Transport in Porous Media*, 85, 189-213.
- Xu, C., Torres-Verdin, C., Yang, Q., & Diniz-Ferreira, E. L. (2013). Connate Water Saturation - Irreducible or Not: the Key to Reliable Hydraulic Rock Typing in Reservoirs Straddling Multiple Capillary Windows . *the SPE Annual Technical Conference and Exhibition*. Louisiana, USA, 30 September–2 October .
- Xu, T., Apps, J. A., Pruess, K., & Yamamoto, H. (2007). Numerical Modeling of Injection and Mineral Trapping of CO₂ with H₂S and SO₂ in a Sandstone Formation. *Chemical Geology*, 242, 319–346.
- Yamasaki, A. (2003). An Overview of CO₂ Mitigation Options for Global Warming— Emphasizing CO₂ Sequestration Options. *Journal of Chemical Engineering of Japan*, 36, 361-375.
- Yamasaki, A. (2003). An Overview of CO₂ Mitigation Options for Global Warming— Emphasizing CO₂ Sequestration Options. *Journal of Chemical Engineering of Japan*, 36, 361-375.
- Yan, J., Plancher, H., & Morrow, N. R. (1997). Wettability Changes Induced by Adsorption of Asphaltene. *SPE Production & Facilities*, 12, 259–266.
- Yusof, M. A., Neuyam, Y. A., Ibrahim, M. A., Saaid, I. M., Idris, A. K., & Mohamed, M. A. (2022). Experimental Study of CO₂ Injectivity Impairment in Sandstone due. *Journal of Petroleum Exploration and Production Technology*, 12, 2191-2202.
- Zhang, H., Al Kobaisi, M., & Arif, M. (2023). Impact of Wettability and Injection Rate on CO₂ Plume Migration and Trapping Capacity: A Numerical Investigation. *Fuel*, 331, 125721.
- Zhao, X., Blunt, M. J., & Yao, J. (2010). Pore-scale Modeling: Effects of Wettability on Waterflood Oil Recovery. *Journal of Petroleum Science and Engineering*, 71, 169–178.

- Zhou, Q., Birkholzer, J. T., Tsang, C., & Rutqvist, J. (2008). A Method for Quick Assessment of CO₂ Storage Capacity in Closed and Semi-closed Saline Formations. *International Journal of Greenhouse Gas Control*, 2, 626-639.
- Zuluaga, E., & Monsalve, J. C. (2003). Water Vaporization in Gas Reservoirs. *SPE Eastern Regional/AAPG Eastern Section Joint Meeting*. 6-10 September. Pittsburgh, PA, USA.

Appendix A Official Permissions and Copyrights

 ? Help Live Chat

SPRINGER NATURE

Simulation Study of sc -CO₂ Based Silylation for Decreasing Severity of Water Blockage and Salt Precipitation during Geological CO₂ Storage in Deep Saline Aquifers

Author: Egl A. Pratama et al
Publication: Transport in Porous Media
Publisher: Springer Nature
Date: Aug 17, 2023

Copyright © 2023, The Author(s)

Creative Commons

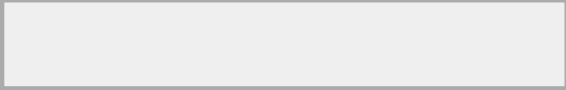
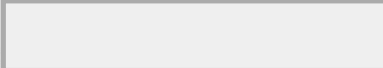
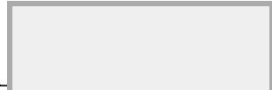
This is an open access article distributed under the terms of the [Creative Commons CC BY](#) license, which permits unrestricted use, distribution, and reproduction in any medium, provided the original work is properly cited.

You are not required to obtain permission to reuse this article.
To request permission for a type of use not listed, please contact [Springer Nature](#)

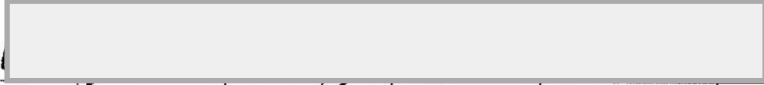
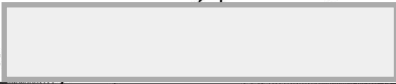
© 2023 Copyright - All Rights Reserved | [Copyright Clearance Center, Inc.](#) | [Privacy statement](#) | [Data Security and Privacy](#) | [For California Residents](#) | [Terms and Conditions](#)
Comments? We would like to hear from you. E-mail us at customer-care@copyright.com

Appendix B Attribution of Co-authors

Paper title “Simulation Study of sc-CO₂ Based Silylation for Decreasing Severity of Water Blockage and Salt Precipitation during Geological CO₂ Storage in Deep Saline Aquifers”,
Transport in Porous Media, 2023, 150, 131-155.

	Conception & Design	Acquisition of Data & Method	Data Analysis	Interpretation & Discussion	Proof-reading & Approval
Matthew Myers (Co-author 1)			✓	✓	✓
I acknowledge that these present my contribution to the above research output.					
Signature:					
Asep K. Permadi (Co-author 2)		✓		✓	✓
I acknowledge that these present my contribution to the above research output.					
Signature:					
Ali Saeedi (Co-author 3)	✓			✓	✓
I acknowledge that these present my contribution to the above research output.					
Signature:					

Paper title “Wettability Impacts on Multiphase Flow and Capillary Residual Trapping in Underground CO₂ Storage: Review and Simulations”, being prepared for publication.

	Conception & Design	Acquisition of Data & Method	Data Analysis	Interpretation & Discussion	Proof-reading & Approval
Matthew Myers (Co-author 1)			√	√	√
I acknowledge that these present my contribution to the above research output.					
Signature:					
Asep K. Permadi (Co-author 2)		✓		√	√
I acknowledge that these present my contribution to the above research output.					
Signature:					
Ali Sacedi (Co-author 3)	√			√	√
I acknowledge that these present my contribution to the above research output.					
Signature:	